ENVIRONMENTAL AND MEDICAL APPLICATIONS OF MOLECULARLY IMPRINTING POLYMER SENSOR FOR THE DETECTION OF PROGESTERONE

A Dissertation

presented to

the Faculty of the Graduate School

at the University of Missouri-Columbia

In Partial Fulfillment

of the Requirements for the Degree

Doctor of Philosophy

By

SALLY M QASIM

Dr. Maria Fidalgo, Dissertation Supervisor

MAY 2022

CIVIL AND ENVIRONMENTAL ENGINEERING DEPARTMENT

The undersigned, appointed by the dean of the Graduate School, have examined the dissertation entitled

ENVIRONMENTAL AND MEDICAL APPLICATIONS OF MOLECULARLY IMPRINTING POLYMER SENSOR FOR THE DETECTION OF PROGESTERONE

presented by Sally M Qasim,

a candidate for the degree of doctor of philosophy,

and hereby certify that, in their opinion, it is worthy of acceptance.

Professor Maria Fidalgo

Professor Baolin Deng

Professor Luis Polo-Parada

Professor Martha Sofia Ortega

Professor Binbin Wang

DEDICATION

I dedicate this thesis to the memory of my dear brother, beloved mother and beloved father, my loving husband, my dear sisters and my four heroes Ali, Hussein, Lana and Youssef for supporting me along the way.

ACKNOWLEDGEMENTS

I would first like to thank my advisor, Dr. Maria Fidalgo, for her continued support, patience, humor, guidance, and encouragement during my program at the University of Missouri-Columbia. I would also like to thank my thesis committee, Dr. Baolin Deng, Dr. Enos Inniss, Dr. Luis Polo Parada, Dr. Martha Sofia Ortega, and Dr. Binbin Wang for their supports, comments and suggestions throughout my research. Thanks to Dr. Chung-Ho Lin for his support and supplying my research materials .

I thank all my friends who always believed in me and encouraged me to do my best especially, Mohammed Bayati, Mohammed Numaan, Abbas Khadem, and Zahara Salahshoor. You guys made this far away land feel like a home away from home and you were there with me through some of the toughest times in my life

I am grateful to my beloved parents, my Dad and Mom for their love, endless support from day one all the way to this very moment. My Mom, I will always remember, you and Dad giving me anything and everything I need to succeed in my life, without your support I would never be where I am today.

Then last but not least to my loving husband Adel Al-khafaji who stood by me through thick and thin and gave me the strength to be myself. Your unconditional love and faith never cease to amaze me. I am so thankful that I have you in my corner pushing me when I am ready to give up. Finally, I am thankful to my wonderful kids: Ali, Hussein, Lana and Yousef who filled my life with joy and love. The lovely ones stood by me through tough and good times with patience.

Table of Contents

LIST OF FIGURES

LIST OF TABLES

ABSTRACT

Molecularly imprinted polymers are spatial technique with artificial recognition sites compatible to the template size, shape, and functional groups arrangement. The MIPs have shown high selectivity and affinity for the target molecules with a substantial potential for the hormones detection as an environmental sensor. The objective of this research is to fabricate a label-free molecular imprinted polymer (MIPs) sensor and investigate the sensing ability for progesterone detection in aqueous solutions and blood. The Progesterone (PGN) is a cholesterol-long biosynthetic endocrine disruptor steroid and is naturally occurring estrogenic compound with a majority effect to alter the vital functions of the human body. The MIPs detection was based on the reflectance mechanism of inverse opal film, after the PG attachment into the photonic MIP binding sites modified the Bragg diffraction spectra of the films due to swelling and refractive index changes, producing the optical signal. MIPs were investigated by equilibrium binding, kinetics experiments, and UV- visible spectra that occurs with the rebinding at different progesterone concentrations in deionized water and 150 mM NaCl solutions. The MIPs response were investigated with progesterone concentration in the 1–100 $\mu g\ L^{-1}$ range; with LOD of 0.5 $\mu g\ L^{-1}$, reaching the detected range of hormone in natural waters. Furthermore, hydrogel MIP films were successfully tested in various real water matrices, they revealed satisfactory recognition ability towards the analyte, and a promising performance in challenging, unknown natural water samples. Moreover, the MIPs film exhibited good selectivity towards the progesterone hormone when exposed to structurally similar molecules, evidenced by a larger response than non-imprinted films (NIPs) due to the specific adsorption provided by molecular imprinting. Computational studies suggested that size along with surface

potential influenced the binding of analog compounds. The molecularly imprinted polymer (MIP) were applied to whole blood and plasma samples of three different animals, the levels of free and total PG were analyzed along with different days of the estrous cycle of the cows. The commercial PG kits test results followed the same trend with MIPs test results for the non-bound PG in the blood samples. The measurements revealed the minimum concentration at day 0, and highest level between day 10 and 14. Both MIPs and commercial PG kits test results were in agreement in evaluating the PG levels trend during the estrous cycle, however, there was some variance in evaluating the exact concentrations of PG hormone during the cycle, but no discrepancy in determining the cow's pregnancy profile.

Chapter 1. Introduction

1.1. Background

Progesterone is a naturally occurring steroid produced as a result of a long biosynthetic pathway. Many reproductive-related activities controlled by progesterone hormones, such as mammary glandular development, the endometrial cell regulation, pregnancy establishment and maintenance. However, progesterone's carcinogenic effects are possible at enhanced levels and are confirmed as an animal carcinogen(Ričanyová et al., 2010) . In humans, progesterone's disturbed release can harm the healthy physiological activities in the body, which makes its detection essential.

Over the last years, many methods have been dominated to analyze the progesterone as adsorption or concentration media using analytical techniques, mostly were liquid chromatography (LC-APCI/APPI-HRPS-SPE)(Golovko et al., 2018), LC-MS(Tomšíková et al., 2012),(HPLC-DAD) (X. Huang et al., 2008), immunoassays (Samsonova et al., 2018), and gas chromatography/mass spectrometry(GC/MS)(Yang et al., 2006), all the over mentioned methods are still expensive, time-consuming, and sample preparation is required. Consequently, progesterone levels assessment's challenge was to develop fast, sensitive, and reliable analytical methods for detection and quantification together with the complexity of the low concentration of progesterone(Chang et al., 2011).

Molecular imprinting is one of the most popular techniques for creating artificial sensors for biomolecules to recognize and binds to their molecular targets such as antibodies, hormones, and enzymes(C. He et al., 2008; Katz & Willner, 2004). Initially, during the synthesis process of molecular imprinting polymers (MIPs), a complex formed first between the target molecules and one or two monomers in an appropriate solvent. A

copolymerization between the polymeric materials with molecular recognition abilities against a target molecule (template) is motivated in the presence of UV light, initiator, and crosslinker (Dai, 2017). As a result, specific binding sites created after the template removal from the polymer matrix after polymerization (García-Calzón & Díaz-García, 2007). Over the last years, great attention has been endowing to the colloidal crystal templating as optical sensors based on molecular imprinted polymers MIPs. The improvement in optoelectronic devices and imaging techniques combined with low cost of light sources and detector (Abdin et al., 2015). An approach was proposed based on combining molecular imprinting and colloidal crystal to prepare imprinted photonic polymers with 3D, highly ordered, specific binding, and microporous structures with high sensitivity and specificity (Griffete et al., 2012; Wu et al., 2008). Therefore, optic sensor technology was used to detect progesterone by many researchers. The challenge of progesterone levels assessment was to develop fast, sensitive, and reliable analytical methods for detection and quantification and the complexity of the low concentration of progesterone.

In this work, the projects are a mixture of three techniques to detect progesterone hormone in water and blood. The first project is to optimize the colloidal crystal formation and molecular imprinted sensors fabrication via different parameters. The second one is to detect the progesterone in water with a very low concentration with optimized MIPs, involving testing various sets of experiments to explore the equilibrium, kinetics binding of the PG in water, and investigating the affinity of the prepared MIPs of target molecule binding under the effect of interferences. The third one is to detect the progesterone in blood samples with a very low concentration using the optimized MIPs as the veterinary

progesterone measurements can help improve fertility and assess the cow's reproductive status and diagnose pregnancy.

Another research project is a work that deals with the fabrication characterization and modeling of interparticle interactions of a controllable and environmental benign of uniform, porous, and high surface area Iron and Aluminum oxide ceramic membranes.

1.2 Research Objectives

The overall objective of this work is to apply novel types of nanomaterials in different fabrication techniques to internalize the precursors, employing either physical compaction or chemical reaction, incorporate the nanomaterials into the final nanoporous structures in order to get better materials either in environmental or biomedical applications. After the introductory chapter, the second chapter is a literature review covering nanomaterials in general (definition), physical interaction theories, properties, applications, and characterization techniques.

In chapter three, the objective was to develop a controllable and environmental benign fabrication of uniform, porous, and high surface area ceramic membranes using carboxylate-alumoxane (AA) and ferroxane (Fe) nanoparticles, using DLS, BET, and XRD for characterization, employing the DLVO aggregation to describe the thermodynamic interactions, and investigate different pH levels.

In chapter four, the fabrication of molecular imprinted polymers MIPs for selective detection of progesterone in an aqueous solution is optimized. A novel manufactured costume-made experimental chamber was used for the fabrication of colloidal crystal template by self-assembly technique. The optimization study included optimizing parameters for colloidal crystal formation and the optimization of the polymerization

parameters. The material was characterized by SEM microscopy, and DLS. Optical properties were investigated by UV-vis reflectance spectroscopy.

In chapter five, MIPs were investigated by equilibrium binding, kinetics experiments, and UV- visible spectra to investigate Bragg diffraction peak shift that correlated with different progesterone concentrations in water, as well as investigating the binding affinity of progesterone in 150 mM NaCl solutions and characterizing the MIPs films with FTIR and SEM. Additionally, the competitive recognition ability of the MIPs, to hormones that have a similar chemical structure to progesterone was studied. A group of selected compounds: estradiol, hydrocortisone, and dehydroepiandrosterone-sulfate are compared to the response to progesterone.

In chapter six, the optimization factors study in (Ch.4 and Ch.5) on the fabrication of MIPs, were applied for improved understanding of progesterone variability profiles, the sensors are applied to serum and blood samples during estrous cycles of cows with the objective of measuring progesterone levels with a MIP sensor. Additionally, the total progesterone was measured using Na Acetate buffer solution, in order to release the protein- bound progesterone. The information provided by the sensor can enhance the productive performance of dairy cattle and anticipating the pregnancy profile of the cows breed.

Chapter 2. Literature review

2.1. Introduction to Nanomaterials

In the past few years, the nanostructure technology has been growing widely in interdisciplinary areas of research and development activity. The nanomaterials are the building blocks of the nanotechnology and nanoscience for creation a new nano sized materials (Siegel et al., 1999). Nanomaterials were first known as early as 1857 when Michael Faraday wrote his first scientific report about the colloidal gold particles synthesis. In 1940's the fumed silica nanoparticles were fabricated and used in rubber reinforcements in USA and Germany as substitutes for ultrafine carbon black. The scale of a nanometer is one millionth of a millimeter – approximately 100,000 times smaller than the diameter of a human hair. At this scale a vast interest of nanomaterials has been emerged due to their unique optical, magnetic, electrical, and biological properties, which have a potential impact in electronics, medicine, and other fields(A, Alagarasi, 2011).The feature of high surface area-to-volume ratio of nanomaterials has evolved the treatment quality and reactivity with environmental pollutants, viz., adsorption, photocatalysis, membrane processes(Zekić et al., 2018),(D. Singh et al., 2020).The nanomaterials structure can be classified into one dimension (eg. surface films), two dimensions (eg. strands or fibres), or three dimensions (eg. particles) **(Figure 2.1).** Nanomaterials can exist in different forms, single, fused, aggregated or agglomerated forms with spherical, tubular, and irregular shapes **(Figure 2.2)**,(A, Alagarasi,. 2011). The most common nanomaterials used in water and wastewater treatment are Zero-valent metal nanoparticles (nZVI), metal oxides nanoparticles, carbon nanotubes (CNTs) and nanocomposites (Lu et al., 2016),which have numerous of advanced features as :-

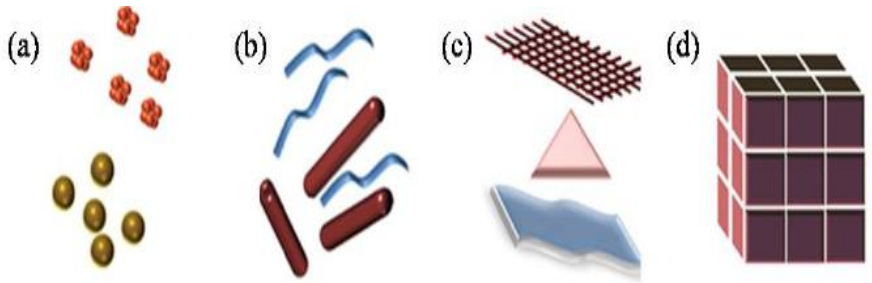

Figure 2. 1 Nanomaterials structure classification: (a) 0D spheres and clusters; (b) 1D nanofibers, nanowires, and nanorods; (c) 2D nanofilms, nanoplates, and networks; (d) 3D nanomaterials(Sajanlal et al., 2011)

Zero-valent metal nanoparticles (nZVI) is used as a reducing agent to convert the toxic materials into safer forms(Fu et al., 2014).The nZVI have been applied widely for removal various organic and inorganic pollutants such as heavy metals (Arancibia-Miranda et al., 2016), polychlorinated compounds (Amin et al., 2014),and phenols(Z. Sun et al., 2017).Metal oxide nanoparticles (MNPs) as titanium, zinc, aluminum, and iron oxide have many of prodigious properties such as a high specific surface area with more specific sites, with adsorption efficiency superior to activated carbon (Corsi et al., 2018), and multiple heavy metals removal potential (S. Singh et al., 2019). Iron oxide nanoparticles with a specific chemical reaction, low toxicity, and biocompatibility, all of that facilitate their adaptability in synthesis ,modification ,and coating(Ali et al., 2016).

In the field of nanotechnology, a great interest of CNTs have drawn due to their excellent conductivity (Guzmán-Verri & Voon, 2007), mechanical strength ability (Esawi et al., 2010), high chemical stability, and high thermal isolation (Kundu et al., 2008).

In addition to the aforementioned nanomaterials, the TiO2 photocatalyst had a high degradation efficiency of organic contaminants and inactivation of pathogenic bacteria ceramic and polymeric membranes merged with UV-A irradiation, thus adding various of

photoactive nanomaterials to nanocomposite membranes can reduce the fouling(Rodrigues et al., 2017).

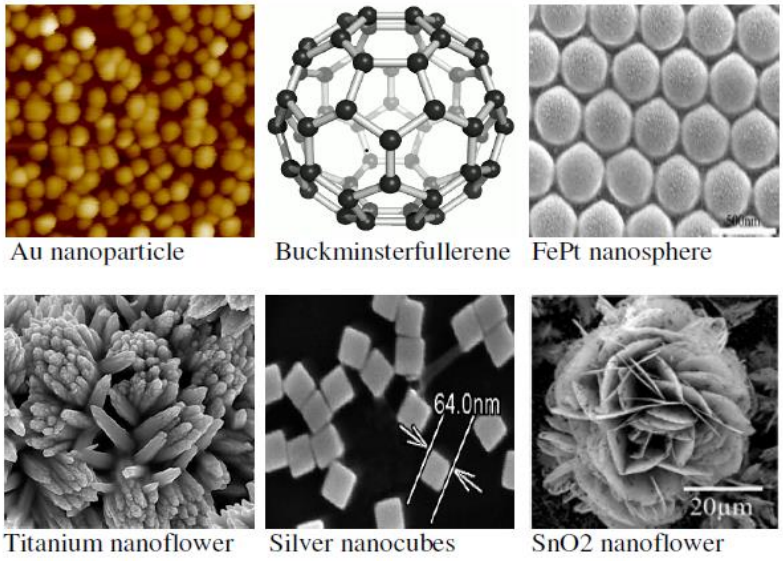

Figure 2. 2 Different forms of nanomaterials (A, Alagarasi,. 2011)

2.2. Particle interactions

2.2.1. Interaction forces

The interparticle interaction between the nanoparticles in aqueous phases is forming the "self-assembling" molecular aggregates. The size and shape of these formations are regulated by the interfacial chemical reactions via two types of forces: first, the short-range interactions between the molecules, which is influenced by the NPs size and shape, electrolyte type and concentration, pH, temperature, and usually happens at very close contact (<1 nm); second, the long-range interactions-those are controlled by the attraction and repulsion forces between the aggregates at distances between (1-100 nm). The two types of aggregation formation, the diffusion-limited cluster aggregation (DLCA), and reaction-limited cluster aggregation (RLCA) are determined based on the fractal

dimension, which describe the aggregate structure (dendritic or compact).These types are characterized by the collision efficiency (α), ranging from 0 to 1, representing the successful attachment prospect. The value of (α = 1), when the particles attaching is successful from the first time and leads to form large dendritic aggregates, whereas (α < 1), when particles sticking after several collisions and the forms denser and less dendritic aggregates (Israelachvili, 2011; W. Zhang, 2014) . **Figure 2.3.** shows the difference between monodisperse, dendritic, and compact clusters of aggregated NPs.

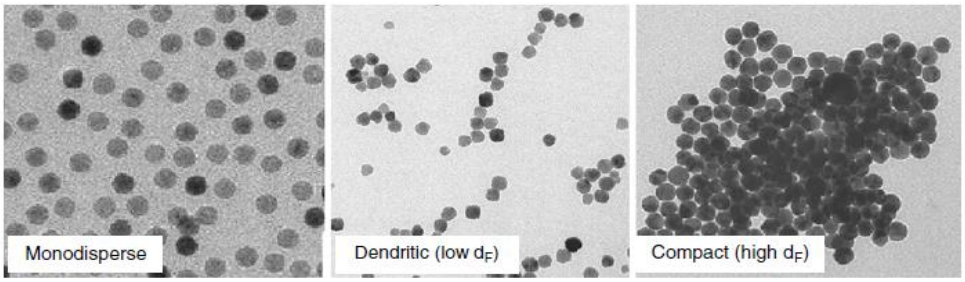

Figure 2. 3 The comparison of various types of NPs aggregation clusters (W. Zhang, 2014)

2.2.2. Factors influencing aggregation in aquatic environments

2.2.2.1. Size and Shape Effect

The smaller sizes of NPs have higher surface energy than larger particles, accordingly, this will increase the attachment efficiency(α) , and the interaction energy barrier screening, as a result, a higher tendency to aggregate (Y. T. He et al., 2008). Meanwhile, the shape of the particles determine the interaction energy between the NPs like van der Waals and repulsive electrostatic forces and are modeled based on as plate-plate, sphere-sphere interaction expressions (N. Sun & Walz, 2001).

2.2.2.2. Solution pH and Ionic Strength Effect

The solution pH and dissolved ionic species are the key factors affecting the electrostatic stabilization of NPs in water by influencing the surface charge (type, density, and accumulation), via the (protonation or deprotonation of a high density of oxygen-containing functional groups).The NPs affinity of destabilization and aggregation are promoted at surface charge neutralization (pH of zero surface charge), and the electrical double layer (EDL)screening. Meanwhile, at low pH values, the surface of NPs will be positively charged where an excess of H^+ protons, whereas negatively charged at high pH and excess of OH^-. As a result of the exchangeable reactions between the NPs surface functional groups (e.g., hydroxide, carboxyl, and oxide groups) with the aqueous H^+ or OH^- (R. Lee et al., 2012).The high tendency of an opposite charge ionic species of accumulation at the charged interface can compress the electrostatic double-layer EDL and decrease the Debye length (κ^{-1}) between the colloids, and effectively results in the attractive van der Waals interactions become dominant over electrostatic repulsion and enhance the particle aggregation. The degree of electrostatic destabilization is highly influenced by the electrolyte concentration, valence of counter-ions, and proximity between the electrolyte and colloids (Mukherjee & Weaver, 2010).

2.2.2.3. Temperature Effect

The aggregation kinetics can affect directly by temperatures as they are influencing on random Brownian motion of particles and thus the collision frequency. Consequently, a higher temperature can effectively increase the aggregation rate(Garciagarcia et al., 2009).

2.2.3. Modeling of particle interactions: DLVO theory

The DLVO theory was first developed by Derjaguin and Landau (1941) and Verwey and Overbeek (1948) to explain the colloidal stability and their aggregation in aqueous solutions quantitatively. The classic DLVO was initiated based on the total interaction energy (V_{TOTAL}), which integrates (attractive van der Waals V_A and repulsive electrostatic forces V_R), that results from the interplay of electrical double layers of particles surfaces (Butt & Kappl, 2018). Essentially, the total interaction energy of van der Waals interactions (V_A) and electrical double layer interactions (V_R), as a function of separation distance, is the crucial factor in determining the colloidal electrostatic stabilization.

$$V_T = V_A + V_R \qquad \text{Equation(2.1)}$$

In general, three profiles of the interaction energy versus the distance between two particles can be described by a very weak attraction at large distances (secondary energy minimum), an electrostatic repulsion at intermediate distances, and a strong attraction at short distances (primary energy minimum) (Butt & Kappl, 2018). Numerous of mathematical expressions were deduced to explain the experimental interaction of particles as the linear superposition approximation (LSA), in order to express the electrical double layer and Van der Waals interaction of Sphere-Sphere particle, which based largely on the separation distance validity as shown in tables 2.1 and 2.2.

Table 2. 1 Table 2.1 Sphere-sphere double-layer interaction energies (Elimelech et al., 1998).

Expressions	Method	Validity	Source
$\frac{128\pi a_1 a_2 n_\infty kT}{(a_1+a_2)\kappa^2}\Upsilon_1\Upsilon_2\exp(-\kappa h)$	LSA DIM	$h \ll a_i$ $\kappa a_i > 5$	(Gregory, 1975)
$\frac{128\pi a_1 a_2 n_\infty kT}{r\kappa^2}\Upsilon_1\Upsilon_2\exp(-\kappa h)$	CPA LPB LSA	$\kappa r \gg 1$ $\kappa a_i \geq 10$	(Bell et al., 1970)
$\frac{128\pi a_1 a_2 n_\infty kT}{(a_1+a_2)\kappa^2}(\phi_1^2+\phi_2^2)[\frac{2\phi_1\phi_2}{\phi_1^2+\phi_2^2}\ln(\frac{1+e^{-\kappa h}}{1-e^{-\kappa h}})+\ln(1-e^{-2\kappa h})$	CPA LPB DIM	Small ϕ_i $h \ll a_i$ $\kappa a_i \gg 1$	(Hogg et al., 1966)
$\frac{128\pi a_1 a_2 n_\infty kT}{(a_1+a_2)\kappa^2}(\phi_1^2+\phi_2^2)[\frac{2\phi_1\phi_2}{\phi_1^2+\phi_2^2}\ln(\frac{1+e^{-\kappa h}}{1-e^{-\kappa h}})+\ln(1-e^{-2\kappa h})$	CCA LPB DIM	Small ϕ_i $h \ll a_i$ $\kappa a_i \gg_1$	(Wiese & Healy, 1970)
$\frac{\pi a_1 a_2}{a_1+a_2}[(\frac{2\varphi\sigma}{\kappa})](\frac{\pi}{2}-tan^{-1}\sin(\kappa h)-\left(\frac{\sigma^2}{\varepsilon\kappa^2}-\varepsilon\varphi^2\right)\ln(1+e^{-2\kappa h})$	CPA and CCA LPB	$h \ll a_i$ $\kappa a_i \gg 1$	(Kar et al., 1973)

Table 2. 2 Retarded sphere-sphere van der Waals interactions (Elimelech et al., 1998)

Expressions	Validity	Source
$-\frac{A\lambda}{237h^3}$	$2\pi h/\lambda \gg 1$	(Overbeek & Jonker, 1952)
$-\frac{2Aa}{12\pi h}\left[\frac{2.45}{10}\left(\frac{\lambda}{h}\right)-\frac{2.17}{60\pi}(\frac{\lambda}{h})^2+\frac{0.59}{280\pi^2}(\frac{\lambda}{h})^3\right]$	$h \gg \lambda/6$	(Schenkel & Kitchener, 1960)
$-\frac{Aa_1 a_2}{6(a_1+a_2)h}\left[\frac{2.45}{10\pi}\left(\frac{\lambda}{h}\right)-\frac{2.17}{60\pi}(\frac{\lambda}{h})^2+\frac{0.59}{280\pi^3}(\frac{\lambda}{h})^3\right]$	$h > 4/\pi$, $h \ll a_i$	(Ho & Higuchi, 1968)
$-\frac{Aa_1 a_2}{6h(a_1+a_2)}\left[\frac{1}{1+11.2h/\lambda}\right]$	$h < \lambda/\pi$, $h \ll a_i$	(Schenkel & Kitchener, 1960)
$-\frac{Aa_1 a_2}{6h(a_1+a_2)}\left[1-\frac{bh}{\lambda}\ln(1+\frac{\lambda}{bh})\right]$	$h \ll a_i$, b=5.32	(Gregory, 1981)

2.3. Nanoparticles as building blocks for nanostructured materials

In nanotechnology, the objects can't be described as "phase" or "particles", it must refer to them as "structures", organized in particular arrangement ways(Berg, 2010). Many of strategies are utilized in synthesis and assembly nanomaterials: using liquid, solid, or gas phase to internalize the precursors; employing either physical compaction or chemical reaction to incorporate the nanomaterials into the final material structure format. Basically, any type of nanostructured materials (metal, ceramic, polymer, semiconductor, glass, composite) are fabricated from controlled synthesis and subsequent assembling of nanoscale building blocks like (clusters or nanoparticles, nanotubes, nanolayers, etc.). Four major challenged areas that engineered nanostructure applied in are, dispersions and coatings, high surface area materials, functional nanodevices, and consolidated materials (Siegel et al., 1999).

Superstructures (**monoliths**) with a micro-or nano- composites can be produced by dispersion in a medium or (self-assembled) and can have unique and significant properties, such as heat resistant ceramics or high strength material with low weight as polymer. One of these extraordinary structures are the **sintered arrays** which can produce nano-filters, membranes, or materials with high thermal insulation. The other unique configuration is **LOC("lab-on-a-chip")** an assembly of nano-or micro-sized channels, tubes, etc. on special surfaces, which are exploited as a basis for chemical sensors with high accuracy and efficiency (Berg, 2010).Similar to the atoms and molecules the nanoparticles assembly can be manipulated to be in one, two, or three dimensions in order to create a patterned surface. Fabrication a sensing template will require arranging the nanoparticles in a specific

inter- particles separation. For example, this approach can be applied to many disciplines such as direct polymer and silica nanoparticles to specific surface locations in optical sensors(Zhou et al., 2012), assembling of metallic particles on the copolymer nanostructures templates to create metal nanofoam materials (Vukovic et al., 2013), and the molecular recognition methods to control the assembly of nanoparticles and enhance the molecule affinity to bound to their surfaces (Deng et al., 2018) (Nagarajan& Hatton, 2008).

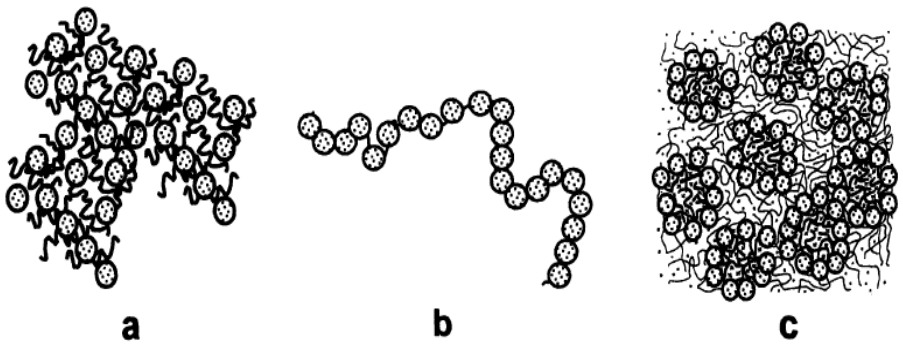

Figure 2. 4 Nanoparticles assembling methodologies. (a) porous nanoparticle assembly for catalytic or adsorption, (b) Nanoparticles assembly on a DNA as a nanoelectrical wire, (c) Nanoparticles assembly on a copolymer surface for a sensor application(Shenhar et al., 2005) .

2.3.1 nanoparticles as precursors for porous Ceramic membranes fabrication

Over the past decades, many of researchers have focused to incorporate many types of nanomaterials as a precursor of porous ceramic membranes in order to improve a diverse of membrane properties such as permeability, hydrophilicity, selectivity, microstructure (porosity and pore size), mechanical strength, and other features for water treatment and fouling limiting. The pore sizes of porous ceramic membranes are related to the sizes of ceramic precursors and sintering temperatures. The most applied nanomaterials in porous

ceramic membrane fabrication are metal oxides including, alumina (α-Al_2O_3), silica (SiO_2), zirconia (ZrO_2), titania (TiO_2), and zeolite (Li et al., 2020).Titania nanoparticles have been used widely in porous ceramic membranes due to their distinctive properties, as particular chemical resistance, high water flux, photochemical and catalyze reactions initiator. The TiO_2-doped ZrO_2 (hereafter denoted as TDZ) nanofiltration (NF) membranes (Y. Lu et al., 2016), have showed good stability and reproducibility. The phase transition of Ti^{4+} have decreased the crystallite size, and increased surface area. The membranes have exhibited high water permeability reached 35~40 L m^{-2} h^{-1} bar^{-1}, and low MWCO of 500 Da.

Alumina (Al_2O_3) has different phases such as γ, η, and θ. The most common phase used in ceramic membrane fabrication is α-alumina. Alumina membranes are widely utilized in separation membranes of water and wastewater treatment, due to the wide pore size range, thermodynamic stability, and durability. Alumina UF membranes in dye wastewater treatment(Zou et al., 2017).In this report, a co-sintering process was used to control the activators contents of boehmite sols and produce bilayer α-alumina membranes. The fabricated membranes have reached 10 kDa molecular weight cut off (MWCO), 99% rejection performance, and water permeance up to 70 Lm $^{-2}$ h^{-1} bar^{-1}

2.3.2 Coatings of ceramic membranes

The ceramic membrane can be modified via coating and attach of the nanoparticles on the ceramic surface or inside the pore walls. This incorporation can enhance different characteristics, either physical (particle size, pore size and porosity), chemical (hydrophilicity and stability),or functional as(photoactive, bacteria killing, etc.)(Z. He et al., 2019).For example, iron oxide based ceramic membrane has been employed as a catalyst combined with ozonation to degrade the natural organic matters (NOM) in the

water and stop the reaction with disinfection by-products (DBPs). In another approach the Fe_2O_3 nanoparticles incorporated onto different alumina-zirconia–titania (AZT) ceramic membranes(Karnik et al., 2006). He was able to modify the membrane structure to be more uniform, coarse-grained surface with nano-sized interconnected pores. These membranes were usefully improved the water quality and reduced the concentration of the DBP precursors. Furthermore, γ-Al_2O_3/α-Al_2O_3 hollow fiber NF membranes with different MWCO (Z. Wang et al., 2016).Using the sol-gel, dip coating and sintering processes. The fabricated membrane with pore size of 1.61 nm, had water permeance of 17.4 L m^{-2} h^{-1} bar^{-1}, and compatible quality for industry applications.

2.3.3 Characterization techniques for ceramics

Various characterization techniques are required to understand optimal functioning of ceramic membranes, either chemical, physical, surface complexes, morphology, etc. These techniques methods can be categorized into several groups according to the information type, whether related to (structure and composition), (morphology, mechanical properties, charge, etc.),or(bulk characteristics and porosity), (Bernstein et al., 2013). The chemical characteristics of ceramics can be identified using the vibrational spectroscopies techniques as surface- FTIR techniques, in particular, attenuated total reflection (ATR).In ATR–FTIR an infrared (IR) spectroscopy is utilized to make transition combination between vibrational states of chemical bonds and some collective vibrations, that has specific relevant to the aromatic rings, polymers, or crystals. This technique is preferable to analyze the thickness and chemical reactions in the top layer (Mohamed et al., 2017).

The physical characteristics and morphology of ceramics are assessed using different techniques as Electron Microscopy. In scanning electron microscopy (SEM) an

interaction between the focused beam electrons and the atoms of sample can produce images of ceramic surface topography,focus on wide, large areas and irregular shaped objects, with a high magnification range, and resolution (Tamime et al., 2011).

The bulk characteristics as pore size, pore size distribution and surface area of ceramic membrane for pressure-driven separations are measured using the Brunauer–Emmett–Teller (BET) method. In this method usually, nitrogen gas is used to fill the primary monolayer pores, this result is fitted to BET isotherm which represent the total number of nitrogen molecules inside pores, using the known area per nitrogen molecule, the total pore area will be determined, pore radius, and pore volume. Besides, the adsorption–desorption hysteresis, are used to evaluate the pore geometry and pore sizes uniformity (Prádanos et al., 1996).

2.4. Nanoparticles as templates for optical active films

The unique optical properties are particularly associated with nanoparticles as templets comprised of materials with high-or low refractive index, transparency, photoluminescence, and photonic crystal characteristics. It is important to precise the nanoparticles synthesis methods as they have a conclusive effect on the nanoparticles fingerprints, including size distribution, morphology, crystallinity, purity, and composition(Iskandar, 2009).Various of nanoparticle were fabricated and used as templets of optical sensor for different environmental pollutants. An optical sensor technique was fabricated (Xue et al., 2013),based on the surface–imprinted core-shell Au nanoparticles using Surface-enhanced Raman scattering (SERS), to detect the bisphenol A in surface and Gatorade drink water. In this report the signal of SERS was enhanced due to a specific

binding of the target molecule on the core-shell of MIP on the Au nanoparticles surface. This approach considered very efficient and fast way to detect the bisphenol A in water.

Also, a new collaboration between the nanoparticles and optical sensors application was represented in a chitosan/graphene oxide - magnetite - molecularly imprinted polymer (Cs/GM-MIP), combined with the CdTe quantum dots@luminol nanoparticles to detect the chrysoidine, an industrial dye used for paper, fiber, and leather. The Chemiluminescence method was used for detection, via prompting the adsorption affinity of the Cs/GM on the surface of MIP with increased concentration of chrysoidine. In this approach, the CdTe QDs@luminol-Cs/GM-MIP-CL sensor showed high sensitivity in target detection with a detection limit of 32×10^{-9}M (Duan et al., 2016).

2.4.1 Colloidal crystals and opals

In general, the crystalline structures assembled from colloid-sized particles are called (“colloidal crystals”), that reveals some of the basic principle interaction in the colloidal systems. The remarkable optical property of the colloidal crystals, is related to diffraction and interference of light in their ordered arrays (Velev et al., 1998).Highly ordered crystalline structures of photonic crystals can possess a periodic modulated dielectric constant, with a range on the scale of visible light wavelengths (380–750 nm).These periods can be affected by the spreading of electromagnetic waves due to Bragg reflections on lattice planes of materials(Waterhouse & Waterland, 2007).Two approaches are used in photonic crystal fabrication: nanolithography and self-assembly. Nanolithography is called the (‘‘top-down’’ approach), was used to etch small particles into different solid substrates. This method had some drawbacks as high cost, slowness and limited layers thickness. In contrary, the self -assembly approach (‘‘bottom-up’’ approach),

is used widely by the researchers to form a three-dimensional (3D) periodic structures of colloidal crystals particles, which known as opals. A crystallization of various monodisperse spheres of silica, polystyrene or polymethylmethacrylate (PMMA) are employed to form face-centered cubic (fcc) arrays, and the experimental work have exposed that pseudo photonic band of silica or polymer spheres gap exists in the plane [111] direction for fcc arrangements (Busch & John, 1999). Recently, the colloidal crystals have demonstrated to be an ideal premises blocks for creation different polymeric and inorganic materials with highly porous structures, can be applied in catalysis and separation technologies. The colloidal crystals are used as precursor in the preparation of heterogeneous of well-defined structures for catalyst materials via investigation the effect of size, shape, composition, and support chemistry in catalyzed reactions, and their application in microscopy and spectroscopy domains (Cargnello, 2019).

Many of new methods developed in this field are consider the flow and solvent evaporation, but the most applied method for opal films fabrication is the CDM (capillary deposition method, a (special flow induced technique).In (CDM) method the colloidal crystals are start to self -assembly from the liquid meniscus at the cell edge and propagates inward into the center of the substrate. The crystal orientation is highly controlled by the substrate and the growth direction. The transmission spectra with a long wavelength scattering background in CDM as a result of homogeneous defect distribution (Muldarisnur & Marlow, 2010). The thickness of opal films from a few layers to hundreds of layers is precisely dominated by the sphere size and solution concentration. Furthermore, the resulting no. of layers can be determined based on a model developed by(Dimitrov & Nagayama, 1996) for the self-assembly of *monolayer* colloidal films (P. Jiang et al., 1999).

2.4.2 Inverse opals

The photonic inverse opals are three-dimensional structures elaborated from the self -assembly of photonic colloidal crystals(opals) templates, using a nano-spheres with a dielectric properties, thus removing this material from the original opal template either by wet chemical etching(SiO_2),or calcination method (polymer spheres) (Waterhouse & Waterland, 2007).

A photonic crystal heterostructures using TiO2 and ZnO inverse opals was fabricated (Y. Zhang et al., 2012).The researcher used the electrochemical deposition method to deposit the colloidal crystal template, thereafter, sol–gel method was used to prepare the TiO_2 inverse opal structure by filling into the gaps of the prepared ZnO-filled colloidal crystal template. The reflection signal of invers opal at 570 nm, have implied the heterostructures as an excellent filter or selector. Furthermore, the reflection stop band of the fabricated heterostructure have confirmed ideal properties of ordering and internal structure in terms of narrow, deep and sharp-shaped. The researcher can work in future to enhance the features of photonic crystal heterostructures to be fitted into the optical domain.

An inverse opal films of molecularly imprinted polymers (MIP)were fabricated using the colloidal crystal template method (Griffete et al., 2012), for the detection of Bisphenol A and pH sensing. In this article, the Langmuir_Blodgett (L_B)technique was used to control the number of colloidal crystal layers ,and the thickness of the resulting inverse opal hydrogel (IOH).the swelling behavior of IOH films was studied at different pH and different concentration of BPA with various thicknesses.

2.5. Applications of colloidal crystal templating in sensors: molecular imprinted polymers (MIP)

Over the last years, high attention has been endowing to the **colloidal crystal** templating as optical sensors based on molecular imprinted polymers MIPs, since of the improvement in optoelectronic devices and imaging techniques combined with low cost of light sources and detector (Abdin et al., 2015).An approach was proposed based on combining molecular imprinting and colloidal crystal in preparation of imprinted photonic polymers with 3D, highly ordered, specific binding, and microporous structures with high sensitivity and specificity, due to the porous structure of these materials (inverse opals), the exhibition of fascinating optical property (Bragg diffraction), in addition to a bright structural color. Particularly, the fabrication of highly ordered microporous materials from a responsive polymer hydrogel, will generate their ability to swell or shrink in aqueous solution as a consequence to a molecular recognition, leading to a periodic spacing change and reflection in optical properties (Wu et al., 2008) (Griffete et al., 2012) ,Accordingly, numerous of researchers have employed the colloidal crystal templating with great potential to be environmental sensors for the detection of specific contaminant.

The colloidal crystal template (monodisperse SiO_2 nanospheres, and molecularly imprinted photonic polymer have fabricated as an optical sensor to detect chloramphenicol. Precursors with different compositions (the template molecule chloramphenicol (CAP), methacrylic acid (MAA) as the monomer, ethylene glycol dimethacrylate as the cross-linker, 2,20-azobisisobutyronitrile as the initiator, and different solvents, were infused into

the void spaces of the respective templates and aggregated. Numerous nanocavities derived from were prepared by removing the SiO_2 template and the imprinted CAP. The MIPP had a specific recognition of the target CAP. The results showed that the embedding and transporting of CAP could change the reflection peak intensity of the MIPP. The MIPP exhibited good responsiveness, reached to minimum detection range from 1 ng mL^{-1} to 1 μg mL^{-1} of CAP. Short response time at 8 min was reported upon the addition to CAP at a concentration of 10 ng mL^{-1}. The results proved that MIPP had shown good performance and detection capacity after many cycle times. Thus, the molecularly imprinted photonic polymer sensors could specifically detect CAP in a simple, time-saving, and low-cost manner (Zou et al., 2017).

The amino-functionalized carbon dots (AC-dots) have elaborated to molecularly imprinted polymer (MIP) for fluorescent determination of 2,4-dinitrotoluene. Colloidal crystals were fabricated by vertical self-assembly with a 0.5% volume fraction. The MIPs have exhibit higher adsorption than NIPs, with imprinting efficiencies ranging from 2 to 2.5. The detection technique was to capture the DNT specifically by the cavities in the MIP and interact with AC-dots on the surface. This interaction results in quenching of the fluorescence of the AC-dots. The results demonstrated DNT a response time reached equilibrium within ~30 min. Also, the researcher has proved a high selective recognition of DNT in aqueous solutions (Dai, 2017).

2.6. Biomedical applications of MIP sensors

Various of molecular imprinted photonic polymers MIPPs, were fabricated and applied in the biomedical applications field ,for example, a magnetically imprinted surface enhanced Raman scattering (MI-SERS), has been used for determination ciprofloxacin,

typing of fluoroquinolone antibiotic by (an et al., 2015).A sandwich nanostructure of molecular imprinting polymers used ultrasensitive SERS techniques for propranolol detection by (liu et al., 2018).

The hexagonally packed macroporous molecularly imprinted polymer films have prepared via optimizing colloidal crystals templates for detection the follicle-stimulating hormone protein (FSH). A precise assembling of colloidal crystals beads was promoted by adding a heating step after assembling(Kalecki et al., 2020). This step has supported the imprinting of colloidal crystal and retain hexagonal packing structure. The colloidal crystals were imprinted on the Au-glass slides in multilayers. An electrochemical transducer was combined with the prepared nanostructured molecular recognition films to design a chemosensing system. The prepared hexagonally packed macroporous molecularly imprinted polymer films were tested for the determination of FSH in the range from 0.1 fM to 100 pM. The results revealed high selectivity of chemosensor in terms of the interference with other analogue protein hormones and detection limit of the 0.1 fM.

In report a surface plasmon resonance was used for determination of histamine by employing MIP films. The MIP film was prepared by dissolving of MAA and EGDM in DMSO with the target molecule histamine and then degassed this polymerization solution under ultrasound. Next, the thin film gold chip was coated with the spin-coating solution. The optic MIP have approved high selectivity, sensitivity, and reproducibility toward histamine as a compared with the NIP sensor. The measured resonant angle shift increased with the increase of histamine concentration in the range of 25-1000 μg L^{-1}, and the detection limit for the sensor was 25 μg/L(S. Jiang et al., 2015).

Another biomedical application of MIPs was investigated(Casis et al., 2014). During his study on the MIP, he fabricated a new nonporous material based on MIP to detect the progesterone in water using new method for the colloidal crystals templating. This templating led to highly organized porous structures without any distortion. Also, swelling ratio was examined to determine the efficiency and specificity of the MIP, which is considered a mentioned measurement on the cross-linking. Also, FTIR and HPLC were used to assess the ability of the MIPs to capture the target molecule. Eventually, the capacity and selectivity inference were evaluated by incubation of the MIPs in solution with the template and another contaminant for 24 hr. The maximum imprinting capacity was found equal to 3.15 at a ratio of 1:0.1 molar between monomer/cross linker. More future work will be needed to examine the selectivity of the MIPs in terms of interference with other resembling molecules.

An efficient molecularly imprinted polymers (MIPs) was fabricated for bisphenol A (BPA) and progesterone (PG) detection(Cáceres et al., 2018). Radical polymerization was used to synthesize multiple of MIPs, and high yields up to (96.6%) was obtained. In this study different parameters are optimized as solvent type, cross-linker, and template ratio. Two different assays were employed for the adsorption mechanism. The kinetic test results showed a high retention within 15 min of contact, with limits of detection LOD reached 0.015 mg/mL, and 11.3 mg/mL for BPA and PG, respectively. Upon testing MIPs the results appeared no significant interference observed with other endocrine disruptors. In future, the researcher will need to work more on the binding efficiency of imprinted polymers and enhance via decreasing the solutions polarity and testing different mobile phases.

A polypyrrole molecularly imprinted polymer for the selective extraction of progesterone hormones from environmental and biological samples using gas chromatography (Nezhadali et al., 2016).A chemical oxidation of pyrrole using $FeCl_3$ based on molecularly imprinted polymer (MIP) are examined in (urine, blood, hospital waste water and tap water) .Gas chromatography coupled with Flame Ionization Detector (GC-FID) analysis was applied for quantitative determination. The limit of detection (LOD) and limit of quantification (LOQ) of the method were obtained to be 0.625 and 1.875 ng mL^{-1} respectively. In this study different parameters were optimized for the application of the MIP for separation and preconcentration like desorption solvent, amount of sorbent, pH, and ionic strength. the recoveries for the spiked tap water, hospital wastewater, urine and blood serum samples were 96.6, 86.2, 101.32 and 88.25%, respectively. This method can be suitable for the extraction of trace amounts of PGN in the complicated biological and environmental samples.

A novel bifunctional group monomer based molecularly imprinted polymers for the biomimetic detection of progesterone(Nawaz et al., 2020).In this work the molecularly imprinted polymers (MIPs) was prepared based on bifunctional group monomer itaconic acid (IA) with hydrogen bonding interactions by applying a combination of a reversible addition chain transfer mechanism (RAFT) and surface plasmon resonance (SPR).UV photopolymerization in synergy with 2-methyl 2[(dodecylsulfanylthiocarbonyl) sulfanyl] propanoic acid (TTCA) as a chain transfer reagent was employed for MIP film synthesis on an SPR sensor chip for the detection of progesterone. In addition, the biosensor was characterized by contact angle measurements, frontier transfer infrared spectroscopy

(FTIR) and scanning electron microscopy (SEM). The researcher revealed that a high adsorption capacity and excellent selectivity of the itaconic acid-based MIP (IA based MIP) biosensor showed in comparison to other analogues and non-imprinted polymer (NIP) film. The author suggested that IA based MIPs are ideal candidates for biosensor use owing to the bifunctionality of the monomer with limit of detection (LOD) and limit of quantification (LOQ), i.e., 0.28 $\times 10^{-19}$ mol L^{-1} and 0.92 $\times 10^{-19}$ mol L^{-1}, respectively. Furthermore, more improved methods are needed to enhance the selectivity of bifunctional group monomer-based MIPs and their commercial utilization to imprint various analytes.

Electro fabrication of molecularly imprinted sensor based on Pd nanoparticles decorated poly-(3 thiophene acetic acid) for progesterone detection was reported by (Cherian et al., 2022).In this research an electrochemical composite film comprising of palladium nanoparticles with 3-thiophene acetic acid (3-TAA) coupled with molecular imprinting technology was proposed for the detection of progesterone. Electrochemical impedance spectroscopy (EIS) and cyclic voltammetry were used to analyse the various modified working electrodes (CV). The material was characterized by field emission scanning microscopy, energy dispersive X-ray spectrometry, optical profilometry, and X-ray photon electron spectroscopy. The researcher reported that Pd nanoparticles resulted in enhanced sensitivity and molecular imprinting technology contributed to its specificity. The results revealed that the MIP/Pd/CFP electrode had the lowest charge transfer resistance compared to other control electrodes because of the molecular cavities.

A comparison of features of the molcular imprinted polymer sensors for the detection of progesterone between this work and others are reported (Table 2.3). For example, MIP

based sensors for progesterone combined with surface plasmon resonance, gas chromatography-flame ionization or HPCL achieved LODs of 8.8×10^{-12} ng/mL(Nawaz et al., 2020), 1.1×10^{-4} ng/mL (Nezhadali et al., 2016) (Cáceres et al., 2018) for the first, and second, third case respectively. These values are lower than the one reported in this work; however, our method has many of pros over other proposed methods. Optical and in particular photonic sensors, have the advantage of being simpler, since they are label-free and do not require complex analytical equipment to read their responses, which can be particularly important for in situ measurements.

Table 2. 3 Features of reported molcular imprinted polymer sensors for the detection of progesterone

Monomer	Polymerization Method	Cross Linker	Initiator	Analytical Method	LOD (ng mL^{-1})	Ref.
Acrylic Acid	RAFT(UV-light)	EGDMA	AIBN	Photonic Reflectance	5×10^{-1}	This work
Itaconic acid	RAFT(UV-light)	EGDMA	TTCA	SPR	8.8×10^{-12}	(Nawaz et al., 2020)
pyrrole	Chemical polymerization	EGDMA	____	GC-FID	_____	(Nezhadali et al., 2016)
3,4-Ethylenedioxthiophene	Electrochemical preparation	____	____	Voltammetry	1×10^{-3}	(Luo et al., 2017)
Acrylic Acid	Thermal polymerization	DVB	AIBN	HPLC	1.1×10^{-4}	(Cáceres et al., 2018)

High performance liquid chromatography: HPLC; gas chromatography coupled with flame ionization detection: GC-FID; 1,4-divinylbenzene: DVB;2,2-azobisisobutyronitrile: AIBN; 2-methyl-2-[(dodecylsulfanylthiocarbonyl)sulfanyl]propanoic acid :TTCA.

2.7 Characterization techniques for Molecular Imprinted polymers (MIP)

Different of analytical techniques are applied for the chemical and morphological characterization of Molecular Imprinted polymers (MIP), such as solid-state NMR techniques (Annamma & Mathew, 2011), Fourier-Transform Infrared Spectroscopy (FT-

IR) (Sole et al., 2007),as more information can be acquired about the chemical composition of the polymer. Exhaustively, FT-IR studies are used in MIPs characterization via investigating the polymer surface functional groups and compare between polymer and functional monomer spectra to explore the change of some signals, as an indication of polymerization of the polymerizable group of the monomer, such as the stretching in carbon double bond of a vinyl functional monomer (Sole et al., 2007; Vasapollo et al., 2011).

The morphological characteristics of MIPs are investigated using microscopy techniques as light microscopy for different light magnification and resolution of polymer surface ,and scanning electron microscopy (SEM) to macro-pores images (Cacho et al., 2004). Whereas, the specific surface area, specific pore volume, pore size distribution and average pore diameter values of the polymer particles are characterized using BET (Brunauer, Emmett and Teller) analysis, the nitrogen sorption porosimetry technique. In addition, the main tests to characterize the molecular recognition behavior of MIPs are the binding capacity and selectivity, and these characteristics can be evaluated via the batch rebinding experiments, or another approach of characterization can be done directly is to use the MIPs as chromatographic stationary phases, and thus quick and easy results will reveal analyzing the binding properties (Cacho et al., 2004; W.-C. Lee et al., 2008).

Chapter 3. Optimization Factors of Molecularly Imprinted Polymer Fabrication for the Detection of Progesterone

3.1 Introduction

In the last 20-30 years, the research concerning progesterone has significantly grown, leading to significant progress in pregestational therapy (Cáceres et al., 2018). Progesterone hormone is secreted and controlled by the adrenal glands.PG regulates the activity of cells and organs (Zhao et al., 2010). Recently, synthetic progesterone has been widely used in human and veterinary therapies as growth promoters in livestock (Fent, 2015). The primary source of these disrupting compounds is an inefficient removal from the wastewater plants (WWTPs)(Kumar et al., 2015).

Typically, the progesterone levels in wastewater treatment plant (WTP) effluents are found at concentrations of up to 50 ng/L. In surface water, the concentrations were similar as in treated wastewater, the levels varied between 1 ng/L to up to 100 ng/L, but even higher sometimes (Fent, 2015). HPLC coupled with detectors such as spectroscopic ultraviolet−visible (UV−visible), diode array, fluorescence, and mass spectroscopy offers the determination of progesterone up to a limit of detection of 0.04−2.01 ng L–1 in environmental waters, 0.08−2.84 ng g–1 in soils, 26−175 ng g–1 in sewage sludge and 140−410 ng L–1 in wastewater (Tomšíková et al., 2012).

Molecularly imprinted polymers (MIPs) represent a competitive alternative technique, as this detection technology consider a combination between the molecular imprinting and photonic crystal technique (Zhou et al., 2012).In the process of fabrication of those MIP films, the following steps are: the colloidal crystals are created; the imprinted

Polymer is polymerized; the silica particle is removed by immersion in HF, and the elution of the target with a suitable solvent ratio creates the film. The Molecular Imprinting (MI) technology allows two photonic characteristics: first, the fabrication of specific sites with high selective adsorption of the target molecule within the polymer films; second, the photonic crystals can reflect a light signal upon the target molecule adsorption(Lee et al., 2016),(Zhou et al., 2012).

Many researchers have reported the MIPs for the detection of hormones in the water. A molecularly imprinted polymer (MIP) photonic film has fabricated for the detection of testosterone in water (Kadhem et al., 2018). A nanoporous materials based on molecularly imprinted polymers (MIPs) was used, which combines the non-covalent imprinting method with the colloidal crystal template technique to produce membranes with pre-specified morphology capable of selectively recognizing progesterone (Casis et al., 2014).

However, a major drawback of their technique is the lack of producibility; most of the fabricated mips were on a lab-scale, few sensors were reported, and slow fabrication process. In this study, an improvement of the fabrication process is proposed and contributed to achieving commercial fabrication standards on a large-scale under controlled conditions. Multiple parameters are optimized, such as colloidal crystal formation, the polymerization reaction time, the time in Hydrofluoric Acid bath, and the target elution.

3.2 Methods and Materials

3.2.1 Reagents and Apparatus

Ethanol (99.5%, 200 proof), acrylic acid (AA) (99%), ethylene glycol dimethacrylate (EGDMA) (98%), and 2,2'-azobisisobutyronitrile (AIBN) (98%) were purchased from Sigma-Aldrich (St. Louis, MO, USA). Monodispersed silica particles with a diameter of 300 nm were obtained from Pinfire - Gems & Colloids (Frankfurt, Germany). Progesterone (98%) was purchased from Cayman Chemical (Ann Arbor, MI, USA). Hydrofluoric acid (HF) (49%) and acetic acid (96%) were supplied by Fisher (Fair Lawn, NJ, USA). Ultra-pure water (18.2 MΩ.cm at 25 0 C) was obtained from a Thermo Scientific™ Barnstead™ E-Pure™ Ultrapure Water Purification System (Waltham, MA, USA). Methanol (99%) and HPLC- grade progesterone standard were supplied by Sigma-Aldrich (St. Louis, MO, USA). A poly (methyl methacrylate) PMMA Plexiglass plastic slides and glass microscope slides, both with dimensions (1 X 13 X 76) mm, were purchased from ePlastics (San Diego, CA, USA) and Fisher Scientific (Pittsburgh, PA, USA), respectively. All chemicals were reagent grade and used as received without further purification. Colloidal crystals were obtained with SiO_2 nanospheres through self-assembling in a custom-made experimental chamber (Fig 3.1). The machine allows for the control of several conditions during the deposition: stepper motor velocity, slide level height, type of deposition beaker, and heating element location. The system is based on the use of CNC linear actuator stage led screw (8 mm) slide rail guide with a 42-steeper motor. The stepper motor has a resolution of 1.8°, this represents 200 steps/turn. The linear actuator was 300 mm long. The stepper motor was supplemented by a stepper-motor gear reduction combo unit (100:1, suggesting 20,000 steps/turn)

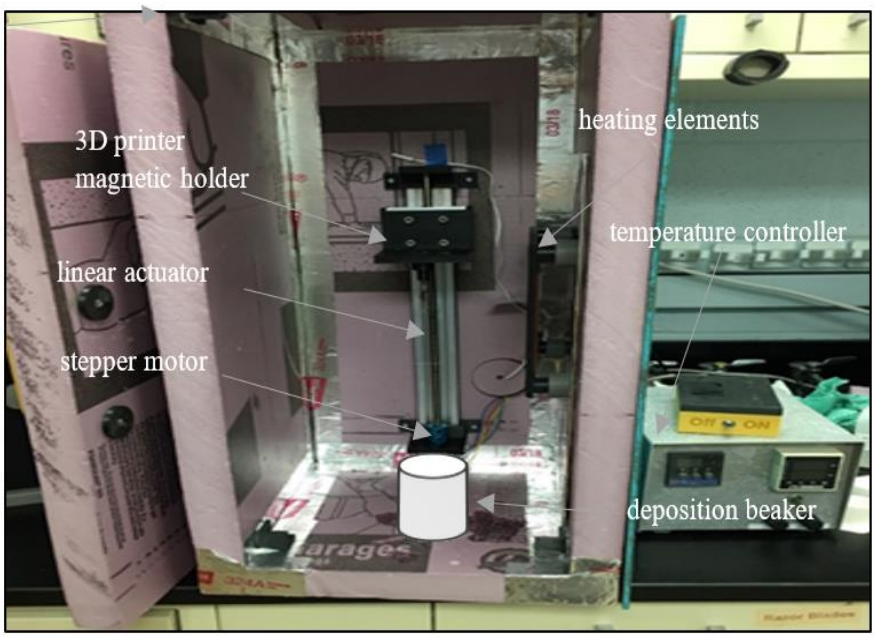

Figure 3. 1. The SiO_2 colloidal crystals assembling deposition-controlled instrument

This combination allows for (8 mm/20,000 steps) 400 µm/step resolution. The stepper motor was controlled by a microcontroller (ESP-32) using an LV8729 stepper driver with a maximal resolution of 1/256/step. Thus, the final resolution of the entire system combo was 1.5625 µm/step. The ESP-32 was programmed in-house using Arduino IDE. The ESP-32 human interface was using a resident Webserver in the ESP-32. Under this configuration, any computer, phone, or tablet with internet capabilities could establish point-point communication with the ESP-32, which was password protected. Alternatively, we use a Nextion Oled TFT screen 340 x 200 to directly control the ESP-32 and the parameters. The developed software allows for full control over the speed, ramping, acceleration, delays for the stepper motor. In the holder of the CNC linear actuator, the 3D printer magnetic holder kept the glass slides in a vertical position. These were submerged or retrieved into the SiO2 particle suspension. The container containing the bath solution was heated by a homemade heated plated, using a silicon heather patch. The temperature

plate was controlled by an OMEGA PID temperature controller CND3. This configuration allows for a temperature control +/- 0.1 °C. Different container materials were used as a recipient for suspension: glass, polyethylene, and Teflon beakers were tested. The entire system was placed inside of thermal isolation box, homemade with 1" XPS (Extruded polystyrene) sheet. A Digital humidity (AcuRite) and temperature monitor was placed into the box to monitor both conditions inside and outside the box.

3.2.2 MIPs Sensors Fabrication

The MIP fabrication process involves the following steps: the deposition of silica nanoparticles to form colloidal crystals, conducted using the machine that described in the previous, and shown in (Fig 3.2.); addition of PMMA support slides on top of colloidal crystals; infiltration of the crystal structure by the pre-polymerization solution; UV polymerization; silica particle removal by immersion in HF; and elution of the target with a suitable solvent. The steps are described in more detail in the following paragraphs.

In order to obtain a stable suspension to be used in the colloidal crystal fabrication, 4 g of SiO2 particles were suspended in 150 ml of ethanol, mixed, and stirred at 300 rpm at approximately 24 h. The colloidal crystals were created by dipping a batch of 4 clean microscope glass slides with dimensions 1x13x76 mm vertically into different container vials that were explained before in the previous part, containing a determined volume fraction of SiO2 particles suspension in ethanol; the controlled velocity motor was used to remove the slides from the suspension. The photonic crystal templates were fabricated under different controlled temperatures 35±0.1°C and 60±0.1°C; the relative humidity was monitored during deposition. The slides were moved upwards from the suspension with a specified motor velocity of 0.139 mm/min for approximately 3-4 h, accompanied by the

volatilization of ethanol, resulting in the self-assembling of the particles forming crystals (0.104 mm/min) on both sides of the glass slides.

The pre-polymerization solution was prepared as follows: 62.9 mg of progesterone as the target was dissolved in 1 ml ethanol; the functional monomer AA (439 µl) was added, and the mixture was left for 12 h at controlled temperature 4 oC to allow the complexation with monomer via hydrogen bonding to proceed. Then, 302 µl of the crosslinker EGDMA was added, which corresponds to a molar ratio of target: functional monomer: crosslinker of 1:32:8. Finally, 12 mg of AIBN was added as an initiator. Poly (methyl methacrylate) (PMMA) plexiglass plastic slides were placed on both sides of the glass slide with colloidal crystals, holding them together firmly, forming a “sandwich”-type structure. The polymerization solution was allowed to rise by capillary forces, dipping one end of the "sandwich”-type structure until the solution penetrated all the void volume of the colloidal crystals. The polymerization reaction proceeded inside the colloidal crystal voids under UV light at λ= 365 nm for 4 h at room temperature. The non-imprinted polymers (NIPs) were fabricated as a control with the same steps as MIPs except for the addition of progesterone. The silica particles were eliminated by immersion in 5% HF for 24, 36, or 48 hours, followed by rinsing with deionized water exhaustively. In the last step, the target was eluted by washing the inverse opal film with different ratios 1:9,1.5:8.5, and 3:7 (v:v) of acetic acid: ethanol solutions, with the replacement of solution every 30 min for a total of 3 hours or 4 hours, and the final wash was with ethanol solution only, in order to remove the acetic acid residues from the slides.

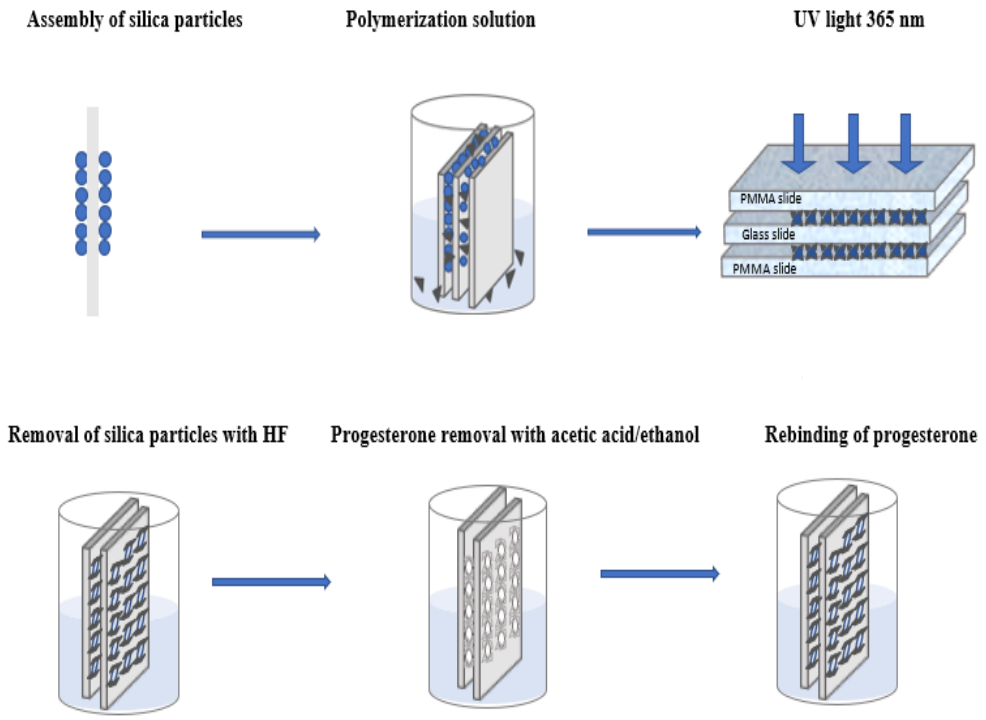

Figure 3. 2 Schematic representation of the MIPs fabrication process

3.3. Characterization of Silica NPs

3.3.1. Scanning Electron Microscope (SEM)

The colloidal crystals were imaged to investigate their morphology and size of the silica nanoparticles by a FEI Quanta 600 FEG (Thermo Fisher Scientific, Hillsboro, OR, USA) Environmental Scanning Electron Microscopy (ESEM). The slides were fixed firmly on a metal rack using carbon tape, and to get a conductive surface layer, a thin layer of gold (1.5–3.0 nm) was coated using an Emitech K575x sputter coater (Quorum Technologies Ltd., Ashford, Kent, UK). The images were analyzed, using ImageJ software version 1.50 (National Institutes of Health, NIH). At least 3 different images for over 300 particles were measured.

3.3.2. Dynamic light scattering (DLS)

A Zetasizer Nano ZS instrument (Malvern Instruments) was used to investigate the silica particle size distribution in the suspension by Dynamic Light Scattering (DLS). At least 3 suspensions of silica nanoparticles were prepared independently with a concentration of 10 mg/L.

3.4. Optimization of the Fabrication Parameters

The objective of the optimization is to achieve the uniform formation of opal films with narrow peaks and consistent peak wavelengths, as needed for susceptible, reproducible sensors. The quality of the material was evaluated by comparison of the optical properties of the 3 spots tested and between different samples. The optical property is assessed in terms of λmax values of diffraction peak of the crystals; it is desirable that the distribution of λmax for all spectra collected have a low standard deviation, high peak reflectance value, and narrow, well-defined peak.

3.4.1. Optimization of parameters for colloidal crystal formation

Since the packing structure of a colloidal crystal is considered the crucial factor that determines its functioning in the optical application, various parameters are investigated influencing the close packed-layers and thus the diffraction properties of the opal films.

3.4.1.1. Effect of Temperature

The interparticle capillary forces between the colloids depend on the evaporation rate of the solvent in suspension. Furthermore, a balance must be achieved between the solvent evaporation and the colloid influx rate to the meniscus region on the substrate(Jiang et

al.).The homemade heated plated, using a silicon heather patch was adjusted for different controlled temperatures between 50 and 70 °C with a deviation of ±0.1 degree, for the fabrication of photonic crystal templates in order to investigate the effect on the uniformity and the film thickness.

3.4.1.2. Effect of type of container material

Different container vial materials considered were polyethylene, glass, and Teflon; at temperature 60 °C; containing volume fraction 1.3 % suspension of SiO_2 particles in ethanol, were used for the fabrication of photonic crystal templates in order to explore the effect of any interaction between the colloids in suspension and the vial walls, and investigate the uniform formation of the films represented by the diffraction optical response of the colloidal films by evaluating the peak wavelength and reflectance value.

3.4.1.3. Effect of the arrangement of the heating elements

Two different heating configurations, using a heating plate and patch, were employed to heat the particle suspension to investigate the effect of the heat distribution on the colloidal crystal formation. Both configurations allowed for temperature control +/- 0.1 °C. Type 1 heater was regular lab-made, while type 2 was a flat heater made of silicon rubber material, it was purchased from Watlow company (Columbia, MO, USA).

The colloidal crystals were created by dipping a batch of 3 clean microscope glass slides into Teflon container vials. The film's quality was investigated by the diffraction optical response, evaluating the peak wavelength and reflectance value for each one, as shown in (Fig. 3.3).

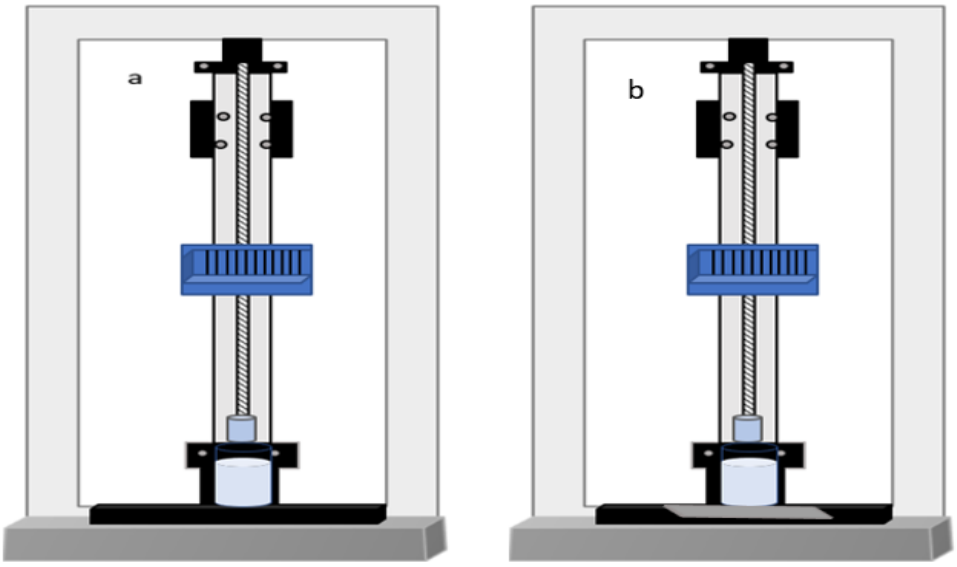

Figure 3. 3. The arrangement of the heating elements:(a)Type 1(the bottom heater),(b)Type 2(the flat heater).

3.4.2. Optimization of the polymerization: reaction time

The MIPs were fabricated via bulk polymerization, as it can help to create more binding sites in the configuration arrangement of colloidal crystal structure during the imprinting process (Nezhadali et al., 2016). The polymerization reaction proceeded inside the colloidal crystal voids under UV light (λ= 365 nm). The reaction occurred in three steps: initiator to form active radicals; the chemical reaction chain by an active monomer; and the termination reaction (Xiao et al., 2018). The films were placed under UV lamps for 3 h or 4 h at room temperature; the temperature of the film was controlled using cooled ice packs. The effect of the time of UV irradiation was studied, looking at the optical response of the colloidal films by evaluating the peak wavelength and reflectance value. After the polymerization reaction, visual inspection was conducted for each film in order to check whether the film was created, damaged, or detached from the slide. Faulty films are discarded and not used in future tests.

3.4.3. Optimization of the silica particle etching step: time in Hydrofluoric Acid bath

The creation of substantial macropores in molecularly imprinted films as molds is highly favorable for mass transportation and fast accessibility to recognition sites. These highly ordered 3D films can be formed by the removal of silica particles and making interconnected pores in an inverse opal structure (Casis et al., 2014, Chen et al., 2019).

The silica particles were eliminated by immersion in a 5% HF bath. The effect of etching time was investigated by soaking the films in the acid solution for 24 hrs, 36 hours, and 48 hrs, followed by exhaustive rinsing with deionized water. The resulting porous films were characterized by their reflectance spectra in the UV-visible range, identifying the peak wavelength and determining the shift of the Bragg's diffraction peak after each etching time

3.4.4. Optimization of the target elution step

3.4.4.1 Effect of the solvent composition (Acetic Acid: Ethanol ratio)

The analyte is removed to create specific binding cavities, compatible in shape, size, and functionality group in the imprinted films (Chen et al., 2019),(Li et al., 2012). The elution of progesterone was conducted with a solution of acetic acid in ethanol, by soaking the film and replacing the solution every 30 min, for 3 h. Different volume ratios of acetic acid to ethanol were investigated: 1:9 (1 mL AA + 9 mL ethanol), 1: 5.67 (1.5 mL AA + 8.5 mL ethanol), and 1:2.33 (3 mL AA + 7 mL ethanol). The effect of each elution solution was evaluated by measuring the peak wavelength shift in their UV-Vis reflectance spectra, in accordance with the properties of the photonic molecular imprinted films. After the treatment, a visual inspection was conducted for each film, in order to check whether the

film was damaged or detached from the slide. Thus, the faulty films were discarded and not used in future tests.

3.4.4.2 Effect of the washing time

The optimization of the target removal process from the MIPs was also conducted with respect to the washing time, as a shorter time for target removal is more desirable for the entire process (Nezhadali et al., 2016). The elution was carried out by washing the film with 1:9 (v: v) acetic acid: ethanol solutions, for 3 hours and 4 hours, both with the replacement of clean solutions every 30 min. The shift in peak wavelength was measured every 30 min during the experiments. A visual inspection of the film quality was conducted to observe if the film was either damaged or detached; the films showing obvious signs of damage were discarded.

3.5. Results and Discussion

3.5.1. Characterization of Silica NPs

Figure 3.4. shows the morphology of the colloidal crystals at 4 different magnifications, fabricated from a 1.3 % volume fraction silica particle suspension to attain the desired number of silica particle layers. Fig. 3.4 a,b shows SEM images of the cross-section and the top view of the obtained colloidal crystals. The measurements of the representative images showed that the colloidal crystal film thickness is about 3.7 μm. Particle size measurements from the SEM images (top views only) showed a size distribution of the particles, with an average radius of 232 nm and a standard deviation of 27 nm (Fig. 3.4 c).

The size of the silica particles was measured by DLS measurements. The results showed that the Z- average hydrodynamic diameter was 375±7 nm, and the standard

deviation of the uniformity of dispersion (polydispersity index) equals 0.012. Although, the DLS commonly overestimates size due to the effect of the solvent on the hydrodynamic diameter.

The arrangement of the SNPs in the photonic crystal films revealed several face-centered cubics (FCC). This (FCC) with hexagonal structures is related to a complementary optical property and refractive index of the photonic crystal (CC) films in all directions. Fig.3.4 d showed the backscatter image of the silica nanoparticles (SNPs), which demonstrates that the 3D ordered opal structure remains close-packed in a hexagonal lattice (Li & Sun, 2009).

The optimal film thickness was determined to be 13 to 15 layers of silica particles in the colloidal crystal, based on previous work (Kadhem et al., 2018). This thickness produced an adequate number of binding sites, acceptable diffusion rates, and consequently faster equilibrium than thicker films. As the number of layers in the colloidal crystals increases and consequently the thickness of the produced polymer film, diffusion of target molecules into the cavities becomes slower, and there may be a partial detachment of the colloidal crystals and films from the surface.

The desirable thickness of the colloidal crystals film thickness was achieved by controlling the particle concentration in the suspension. A relationship was established between the thickness of the crystals and the volume fraction of particle suspension (Jiang et al.) as shown in Equation 3-1 :

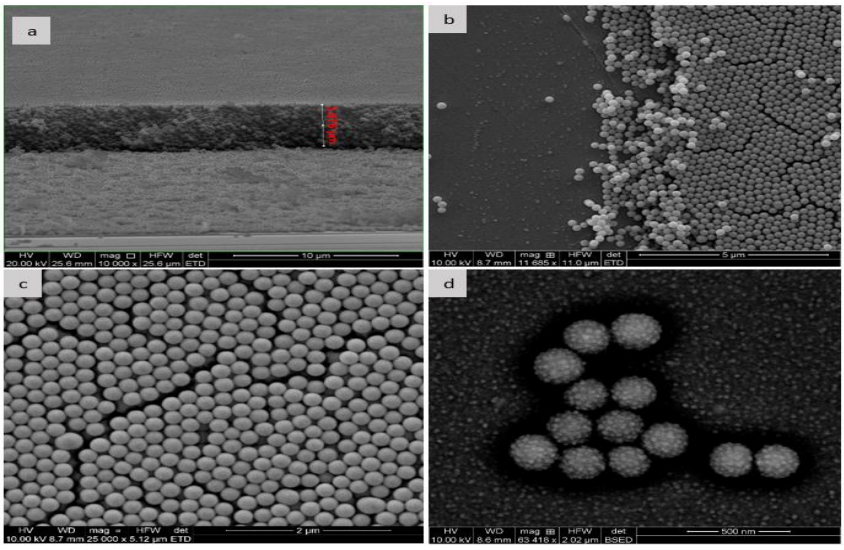

Figure 3. 4. SEM images of (a)colloidal crystal showing cross-section ;(b) colloidal crystal top layer ;(c) the face-centered cubic array of colloidal crystal; (d) backscatter internal morphology of the colloidal crystal.

$$K = \frac{\beta L \emptyset}{0.605 d(1-\emptyset)} \qquad (3\text{-}1)$$

where K is the number of layers, β is the ratio between the velocity of a particle in solution and the fluid velocity and is taken to be 1, L is the meniscus height, d is the particle diameter, and Ø is the particle volume fraction in solution. The calculated number of layers according to equation 1, with L = 3500 μm =0.013,β= 1, and d =232 nm, was 328 layers. However, the number of layers observed from SEM images was about 13-15 layers. However, equation 3-1 reported by (Jiang et al.), can only be applied to the vertical self-assembly method of colloidal crystal deposition and cannot be applied to the situation in our study and the deposition set-up, as it overestimated the no. of layers. However, the inverse relationship between the particle volume fraction Ø and the number of layers K is still valid.

3.5.2. Optimization Factors Study

3.5.2.1. Optimization of parameters for colloidal crystal formation

3.5.2.1.1. Effect of Temperature

The variation of ambient temperature during colloidal crystal formation between 50°C and 70 °C showed a fluctuating effect on the colloidal crystals arrays arrangement, determined by the peak wavelength (λmax) values of reflectance spectra of the fabricated crystals. Spectra were collected at three positions for each colloidal crystal fabricated: an upper spot near the top border, a middle spot, and a lower spot close to the bottom side of the deposition, as shown in (Fig.3.5).

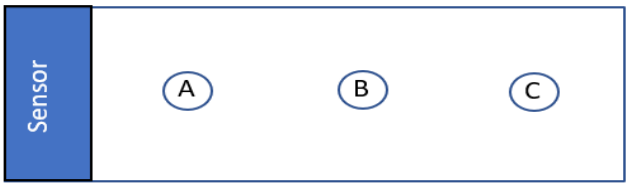

Figure 3. 5. The spectra spot positions.

The values of upper, lower, and general spots areas were 543±2,542±3, and 542±3 nm, respectively at 50 °C; 548±4, 544±2, and 546±3 nm at 55 °C; 551±13,543±3, and 547±10 nm at 60 °C; 550±14,548±13, and 549±13 nm at 65 °C; and 542±2, 541±3, and 541±2 nm at 70 °C **(**Figure 3.6)(Figure 3.7). The results didn't demonstrate the effect of temperature extreme limits, nor a balanced relationship between the evaporation rate and particles influx rate to the meniscus region. Both the highest and lowest temperatures tested showed good results, but the in-between results didn't show a trend with increasing temperature. Another situation that may have caused this effect was the fact that the intermediate temperature experiments have recorded lower ambient humidity levels than

the highest and lowest temperatures. The high humidity level in the lab can affect the fabrication process. The water equilibrium between liquid-gas phase and the hygroscopic nature of ethanol solvent to attract and adsorb water molecules that can form a hydrogen bonding between the hydroxyl group(-OH) on ethanol surface and the oxygen in water, all of that has motivated the driving force to water vapors to condense and dissolve in solvent suspension in higher concentrations at 50, 55, and 70 °C temperatures than 60, 65 °C. Furthermore, these water concentrations can be considered as low ionic strength solutions that can affect and lower the interaction forces between the particles, and thus favor net repulsive forces in suspension and induce the individual approach of colloids to the glass substrate to form the deposits (Cortalezzi et al., 2005; Hiemenz, 1997), as shown in (Eq.3.2).

$$\phi R = \frac{64\,\pi R n_0\, kT \gamma_0^2}{k} \exp\left(-\sqrt{\frac{2N_A\, e^2 1000\, I}{\varepsilon\, \varepsilon_0 k_B T}}\, h\right) \qquad (3\text{-}2)$$

Where R (nm)is the radius of the particle, h(nm) is the spacing between two particles surfaces, n_o the bulk ionic concentration, γ_o is the reduced surface potential of the particle, k_B is Boltzmann constant, T is absolute temperature, I is the ionic strength, ε is the dielectric constant of the solvent, ε_o is the permittivity of vacuum, e is the electron charge, and N_A is the Avogadro's constant.

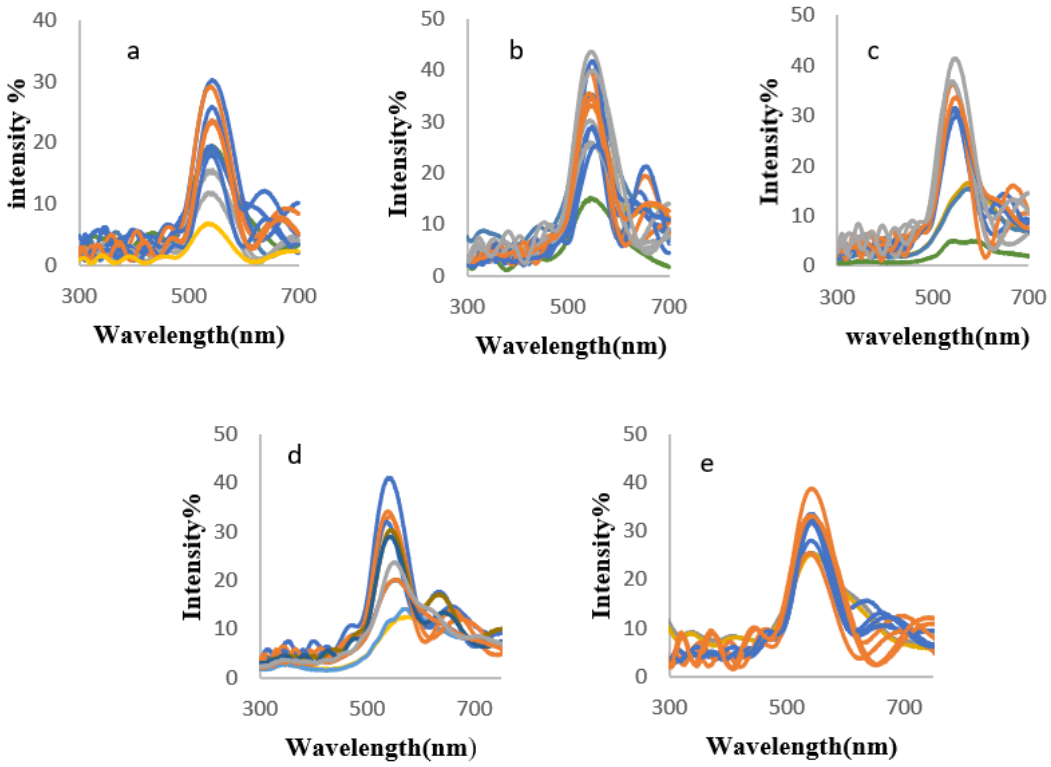

Figure 3. 6. The reflective spectra of colloidal crystal obtained at different deposition temperatures: (a) 50°C,(b) 55°C,(c) 60°C, (d) 65°C, (e) 70°C.

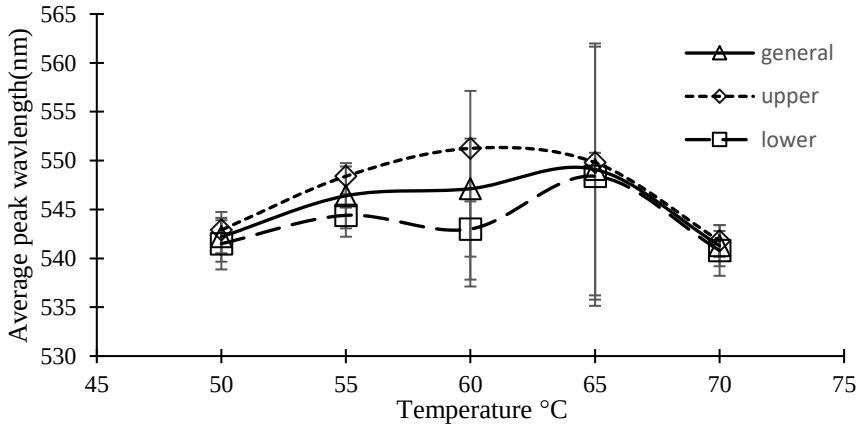

Figure 3. 7. The average peak wavelength of colloidal crystal versus the temperature of the deposition chamber.

The results revealed that there is no substantial difference effect of the temperature at highest and lowest values, both were good in terms of the low standard deviation of the average peak wavelengths of the material deposits and consistently produced high-quality

crystals. However, the crystal deposition at temperature 70°C was preferred more than others for lower standard deviation values.

3.5.2.1.2. Effect of Suspension Container Type

The effect of the interaction between the colloidal particles in suspension and the vial walls on the fabrication of photonic crystal templates was investigated using different container types.

The results showed that the polyethylene vial type is slightly better than the glass and Teflon containers with an average λmax of 539±3.34 nm, high reflectance value up to 45%, narrow peak shape with no shoulders, and a low noise to signal ratio. The average λmax when a Teflon container was used were 543±3.59 nm, while a λmax of 547±4.44 nm was observed for the glass beaker (Fig. 3.8)(Fig 3.9).

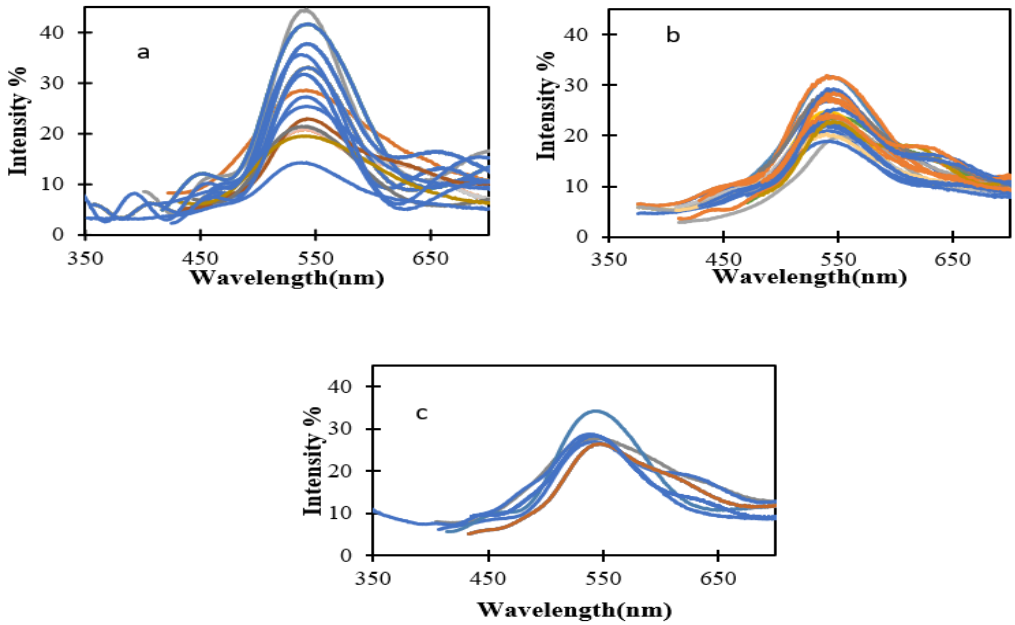

Figure 3. 8. The reflective spectra of colloidal crystal obtained from solutions in different container materials at 70°C:(a) polyethylene, (b)Teflon, (c)glass.

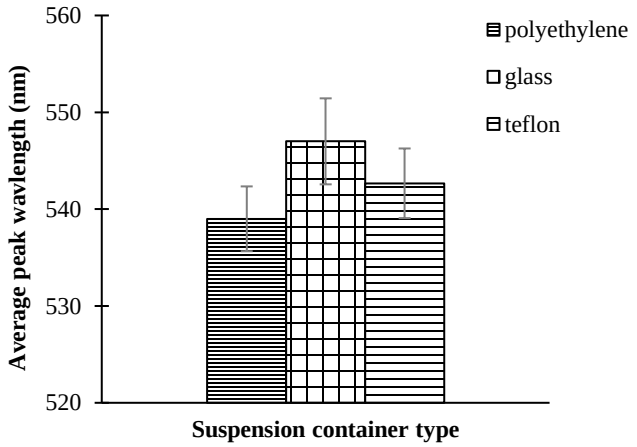

Figure 3. 9. The average peak wavelength for the colloidal crystal obtained in containers of different materials.

The results demonstrated that using polyethylene and Teflon vials lowered the interaction between the colloidal particles and the container walls, as a result, the nanoparticle concentration was maintained fixed in the suspension and therefore created samples with precisely controlled thickness. On the other hand, the glass vial showed less uniform peak properties in terms of a wider peak shape and lower consistent peak wavelength. Silica particles were attracted and deposited on the wall surface as the solvent evaporated, in a similar process to the deposition on the glass slide. This led to colloidal particles been removed from the suspension, and thus a reduction of the particle volume fraction. Since the colloidal crystal thickness is related to the concentration of particles in the suspension from which is grown, the above-mentioned effect led to a continuous decrease in available particles and consequent thinner crystal as the deposition progressed (Jiang et al.,) as shown in (Eq. 3-1). The results showed that colloidal crystals should be fabricated using container materials that minimize interactions between particles and container walls to avoid undesirable loss of particles by adsorption to the container walls and variations in the suspension volume fraction.

3.5.2.1.3. Effect of Arrangement of Heating elements

The heat distribution effect on the colloidal crystal fabrication was explored employing two different heated plate configurations to heat the container containing the particle suspension. The results revealed that type 1 heater had a better impact on the colloidal crystal formation with an average peak wavelength λmax of 541±3.9 nm, while type 2 the new flat heater had an average peak wavelength λmax of 546±4.2 nm. The reflectance of crystals produced with heater type 2 was higher than those fabricated using heater type1, the peaks were wider and had a lower reproducibility (Fig. 3.10 and Fig. 3.11).

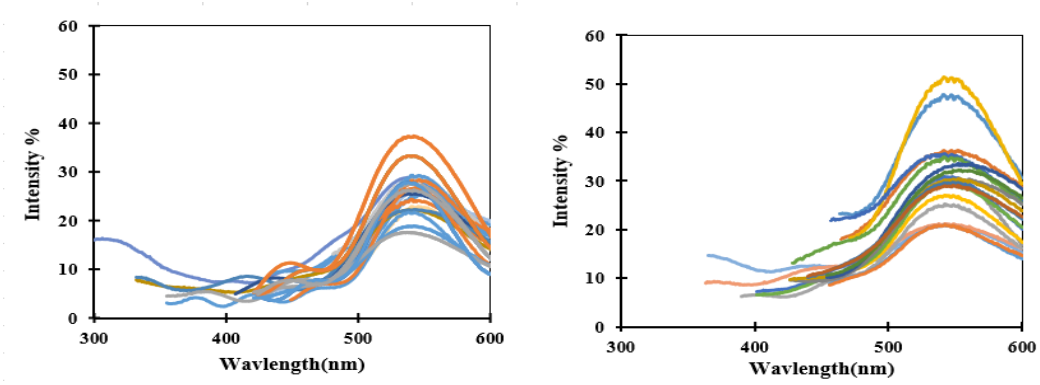

Figure 3. 10. The optical reflectance of the colloidal crystal deposition using different heating elements:(a)Type 1,(b)Type 2. Temperature 70 °C, Teflon beaker.

Using the type 1 heater, a balance between the evaporation rate and the withdrawal rate of the substrate was afforded, and thus more uniform quality of particle arrays was yielded. It is assumed that the solvent evaporation rate under both heater configurations was under the steady-state condition inside the chamber, as some of the solvent vapors were running out persistently. The equilibrium state reactions can be assumed to be a higher-level condition between the liquid-gas phase, in case of the colloidal assembling chamber was closed perfectly, and both phases reached the saturation concentration.

Therefore, the enthalpy of evaporation can change according to the applied temperature from a specific heating configuration. However, the rapid heat transfer was stimulated while using the heater type 2, and that may have induced faster evaporation, and thus faster influx rate of the colloids through the meniscus region, and lower quality of particles arrays film.

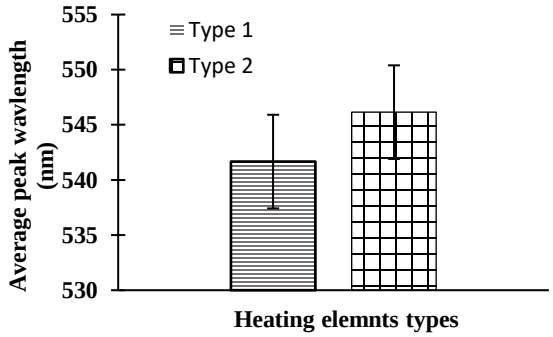

Figure 3. 11. The average peak wavelength of the colloidal crystal obtained from different arrangement of heating elements.

Comparing the heating elements type 1 and type 2, type 1 has shown a preferable performance in the matter of lower standard deviations of the average peak wavelengths, also type 1 created a better quality of colloidal crystal deposition, via good heat distribution inside the deposition chamber.

3.5.2.2 Optimization of the polymerization: Time of polymerization reaction

The molecularly imprinted polymers (MIPs) were optimized by investigating different times of the polymerization reaction. The optical response of the fabricated films showed that the 3 hrs time of polymerization reaction had several advantages over 4 hrs (Fig 3.12 a,b). First, the Bragg diffraction peak wavelength λmax of different MIPs at 3 hours had about 14% higher intensity than those that were subjected to UV-light for 4 hours, and

more consistent reflection spectra, with an average peak wavelength at 416± 9 nm for 3 hrs, and 433±11 nm for 4 hrs reaction time (Fig. 3.13). Besides, the shorter time yielded a uniform film quality, a very narrow peak at 3hrs, while a wider peak at 4 hrs, and no shoulders. An increase in the time of the UV polymerization reaction leads to an increase in the reaction temperature, more radicals generated by the initiator, and thus faster reaction rate, and slower termination rate, all of which contribute to the formation of highly cross-linked, random polymers (Cáceres et al., 2018). All of that, have demonstrated that 3 hrs reaction time can form higher efficiency of imprinting films than at 4 hrs.

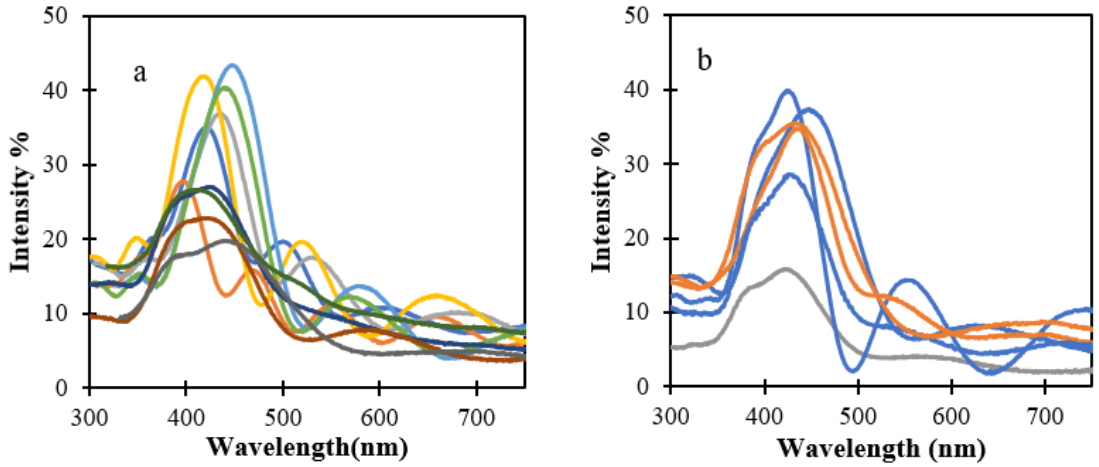

Figure 3. 12. The optical reflectance of the fabricated MIPs after polymerization :(a) after 3hrs, (b)after 4 hrs.

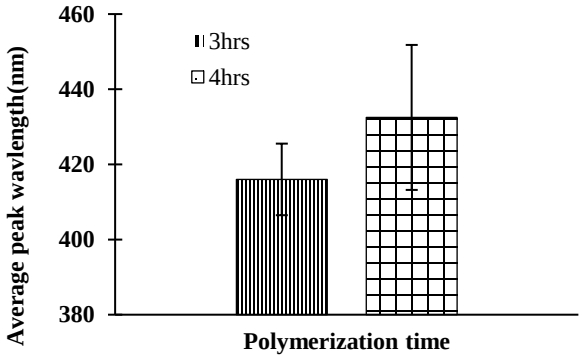

Figure 3. 13. The average peak wavelength of MIP films versus different times of polymerization reaction

.

The results from this investigation showed that 3 hrs time of polymerization reaction time is better than 4 hrs for the MIPs fabrication process, as it appeared to be optimum to control the formation of the radical by the initiator, furthermore, the rection termination time, thus more uniform film quality, and minimum damage to the fabricated film.

3.5.2.3 Optimization of the silica particle etching step: Time in Hydrofluoric Acid bath

The removal of the silica NPs from the molecularly imprinted polymers (MIPs), was optimized by investigating the immersion time of the MIPs in the hydrofluoric acid bath: 24 hrs, 36 hrs, and 48 hrs. Figure 3.14. revealed a good consistency in peak wavelength values in the UV-visible range, with an average of 427±19 nm at 36 hrs bath time in HF. For a time in HF of 36 hrs, the silica particles removed from the polymer films lead to a shrinkage in the imprinted cavities and cause a volume change in the hydrogel film porosity resulting in the significant change of the Bragg diffraction peak (Chen et al., 2019). On the other hand, 24 and 48 hrs times showed lower wavelength shifts (Fig. 3.15) with average values of 443±23 nm and 428±24 nm at 24 hrs and 48 hrs, respectively, which reflect lower removal of the silica particles from the films. Although the time 48 hrs also demonstrated a shift toward lower wavelengths values, it was discarded as a good option because after visual inspection, the film appeared to be damaged.

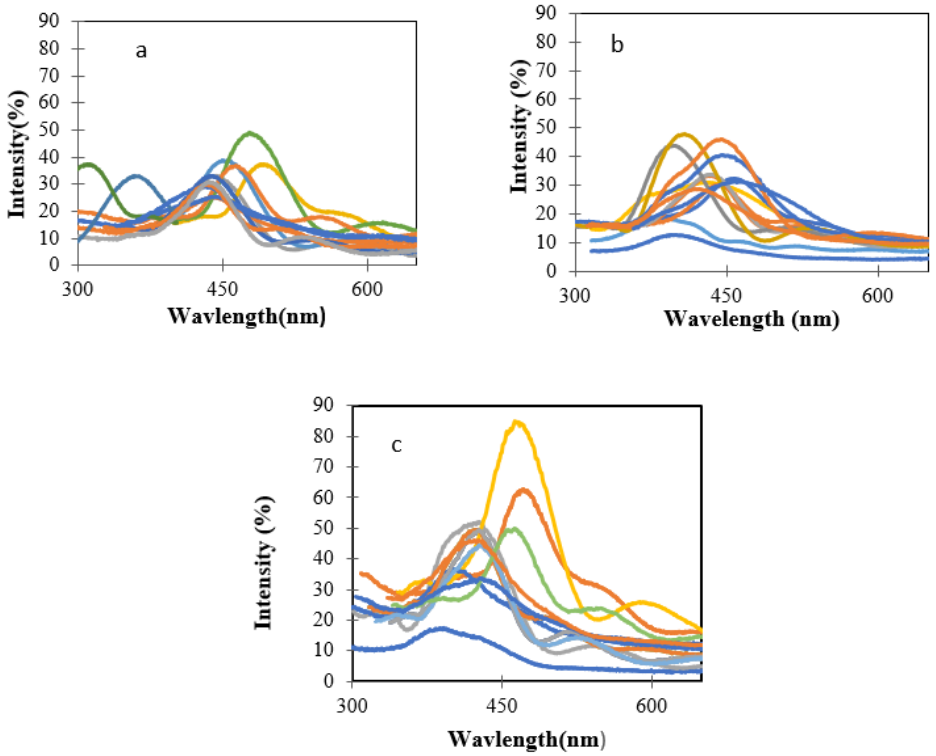

Figure 3. 14. The optical reflectance of the fabricated MIPs after immersion in 5% hydrofluoric acid for different times :(a) at 24hrs, (b)at 36 hrs,(c) at 48 hrs.

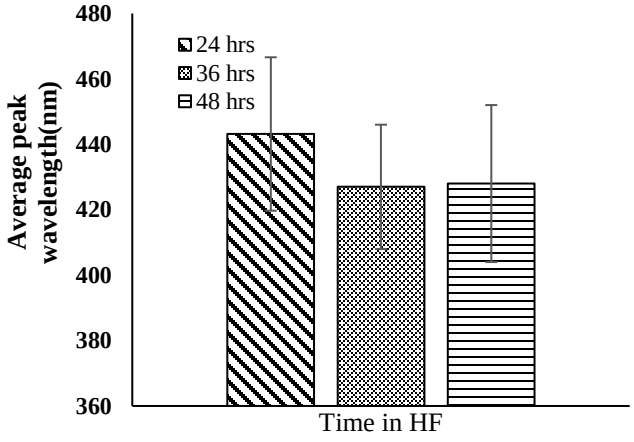

Figure 3. 15. The average peak wavelength of MIP films vs. time in 5% HF bath.

The results showed that 36 hrs time in HF suspension is superior to 24, and 48 hrs, as it demonstrated higher shift values toward the lower wavelengths, thus better removal of silica particles without producing damage to the polymer film. Therefore, 36 hrs can be determined as the optimum time to perform a full detach of silica NPs from the fabricated films after polymerization.

3.5.2.4 Optimization of the target elution step

3.5.2.4.1. Effect of the solvent composition (Acetic Acid: Ethanol ratio)

Figure 3.16 a,b,c showed the optimization results of the target analyte elution from the prepared polymer molecule template. Three different washing ratios of acetic acid: ethanol at 1:9 (1 mL AA + 9 mL ethanol), 1: 5.67 (1.5 mL AA + 8.5 mL ethanol), and 1:2.33 (3 mL AA + 7 mL ethanol)volume in volume were tested (Fig 3.17). The results of the reflectance spectra of the films with washing ratio (1:9) (Fig. 3.16 a)showed a shift toward shorter wavelength of visible spectra region (350-450), with an average λmax value of 395±15 nm, which reflects the removal of the analyte from the binding sites and the shrinking of the hydrogel film (Zhou et al., 2012). (1.5:8.5) washing ratio, the spectra had an average λmax of 414±19 (Fig. 3.16 b), but with poor quality of optical response in terms of a wide peak shape, undefined maximum reflectance, and slightly damaged film. With increasing ratio of acetic acid: ethanol up to 3:7, the films appeared to be totally damaged and detached from the slides. The optical response was inspected, and it appeared that the average wavelength reached to be (408±28 nm) with deteriorated peak shapes(Fig 3.16 c).

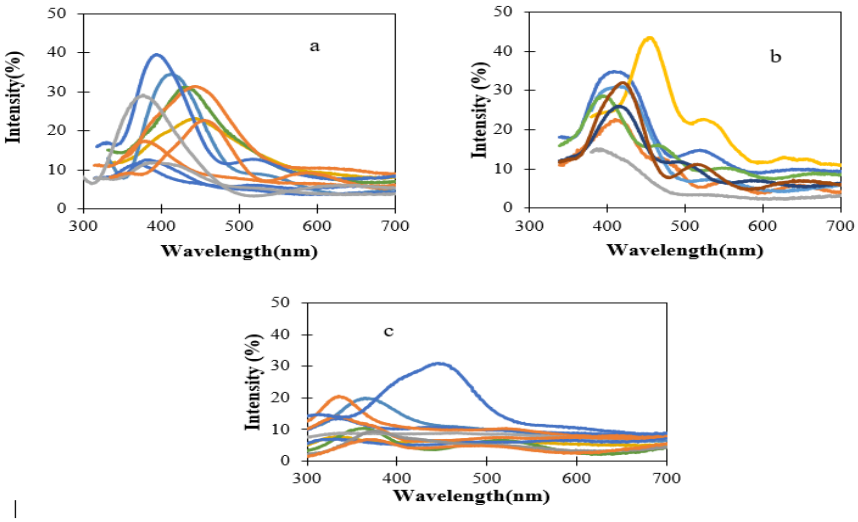

Figure 3. 16. The optical reflectance of the fabricated MIPs with different washing ratios of (Acetic acid: Ethanol v:v) :(a) 1:9, (b) 1.5:8.5,(c) 3:7 .

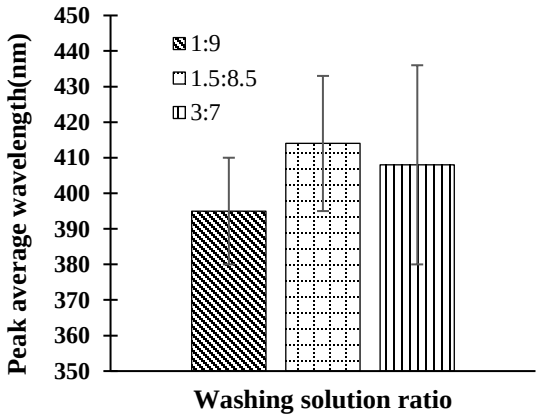

Figure 3. 17. The average peak wavelength of MIP films vs. different solvent composition (Acetic Acid: Ethanol ratio).

The ratio of 1:9 of ethanol/acetic acid solution has revealed higher removal of the analyte particles than 1.5:8.5, and 3:7 ratios, with the higher shift toward lower wavelengths along with maintaining the quality of fabricated films.

3.5.2.4.2. Effect of the washing time

Different washing times were investigated for the removal of the target analyte from imprinted polymer films, UV-vis reflectance spectra were recorded after washing the film with 1:9 (v: v) acetic acid: ethanol solutions, for 3 hours and 4 hours, both with the replacement of clean solutions every 30 min. The shift in peak wavelength was measured and checked every 30 min during the experiments. The results of Figure 3.18 a,b, and Figure 3.19 showed that the 3 hrs washing time had higher elution efficiency of the target molecules from the MIPs matrix. No further shift toward shorter wavelength value was detected beyond 3hrs with an average final λmax of 390±21 nm. This can be explained by the change in Bragg diffraction due to the progesterone molecules extraction from the nanocavities and consequent shrinking of the hydrogel film, which reached the maximum limit when all the progesterone was removed. Figure 3.18 b showed that washing time 4hrs had a decrease in wavelength shift with an average value of 405±29 nm. This result can be attributed to at this washing time the film excessive exposure to the acetic acid and ethanol solution which caused damage to the film cavities and made the hydrogel film nanopores wider (Ričanyová et al., 2010). This effect was reflected on the detected Bragg diffraction peaks signal and led to the shift back to higher wavelengths.

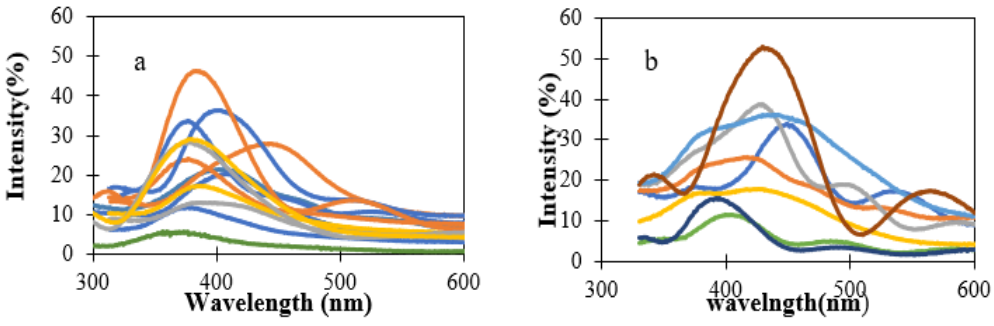

Figure 3. 18. The optical reflectance of the fabricated MIPs after different washing times :(a) 3 hrs, (b) 4 hrs.

After investigating the results of the optimization of the washing time, it can be concluded that 3 hrs achieved high analyte removal, without causing any excessive damage to the film.

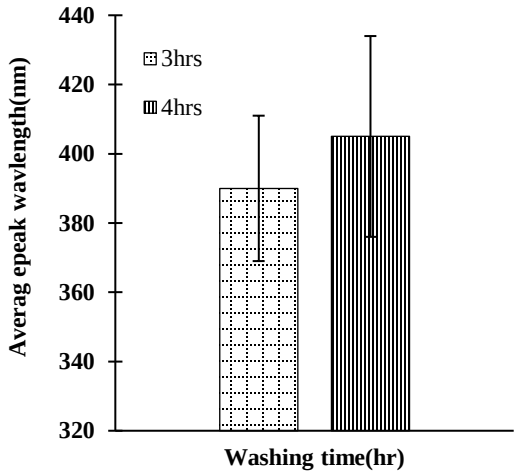

Figure 3. 19. the average peak wavelength of MIP films vs. different washing times.

3.6. Conclusion

This study highlighted the influence of the optimization factors of molecularly imprinted polymer fabrication. The colloidal crystal fabrication showed good results at all temperatures investigated. Lower surface interaction was yield using polyethylene container type. A good balance between the evaporation rate and the withdrawal rate of the substrate was afforded using the Type 1 heater element. However, the reflectance of crystals produced with heater 2 was higher than those fabricated using heater type 1; the peaks were wider and had a lower reproducibility. On the other hand, shorter polymerization reaction time allowed the control of the formation of the radical by the

initiator, furthermore, reduced the damage in the fabricated MIPs. The wavelength shift values have revealed that time 36 hrs is the optimum time to perform a full detach of silica NPs from the fabricated films after polymerization. The results of the optimization of the target elution step: the solvent composition (Acetic Acid: Ethanol ratio) with washing ratio (1:9), had higher removal of the analyte from the binding sites than other ratios, without causing any damage to the film. The progesterone molecules extraction from the nanocavities and consequent shrinking of the hydrogel film had reached the maximum limit at 3 hrs washing time, represented by a higher shift toward shorter wavelength. Overall, the optimal conditions for the synthesis of MIPs for PG were defined following experimental design, which helped to avoid all unfavorable conditions that would produce damaged or faulty MIPs, and therefore reduce a large number of syntheses.

Chapter 4. Detection of Progesterone in Aqueous Samples by Molecularly Imprinted Photonic Polymers

4.1 Introduction

Progesterone is a naturally occurring estrogenic compound in the cholesterol-long biosynthetic pathway. The average level of progesterone produced by women daily during their monthly cycle is about 20–25 mg, and increases to 300–400 mg daily during pregnancy(Ričanyová et al., 2010). In addition, synthetic progesterone has been extensively used in human and veterinary therapies as growth promoters in cattle (Fent, 2015), as contraceptive pills, to promote regular menstrual cycles, to treat abnormal uterine bleeding, control the symptoms of menopause, and prevent endometrial cancer (Golovko et al., 2018). Large amounts of steroid hormones, as for example progesterone, testosterone, and estradiol, are released into surface waters, causing adverse biological effects both on humans and wildlife; commonly large quantities of progestonic entities are excreted through urine. The primary cause of the occurrence of progesterone and other endocrine disrupting chemicals in the environment is the release of untreated or partially treated effluents from the wastewater plants (WWTPs)(Kumar et al., 2015). Concentrations reported in surface waters ranged from 5 to 199 ng $L^{-}1$, and over 6,300 ng L^{-1} in waste stabilization ponds (Wasps) (Kambale et al., 2019).

High performance liquid chromatography (HPLC) with variety of detectors including ultraviolet−visible (UV−visible), diode array, fluorescence, and mass spectroscopy allows for the measurement of progesterone down to 0.04−2.01 ng L^{-1} in environmental waters, 0.08−2.84 ng g^{-1} in soils, 26−175 ng g^{-1} in sewage sludge and

140−410 ng L^{-1} in wastewater(X. Huang et al., 2008). Other methods have also been applied, combining adsorption or concentration media and analytical techniques: LC mass spectroscopy (LC-MS)(Tomšíková et al., 2012), HPLC with diode-array detection (HPLC-DAD) (X. Huang et al., 2008). Some of these methods require significant pretreatment steps, expensive, time-consuming, and not easily accessible. Consequently, there is a need for simple and reliable method for the analysis of progesterone that will facilitate the detection and monitoring of this hormone in natural waters (Chang et al., 2011).

Molecularly imprinted polymers (MIP) fabrication process include the spatial allocation of the target molecules via a careful design polymerization and creating a complementary binding nanocavities, a subsequent target removal and allowing the "key-lock" principle similar to enzymes rebinding mechanism, with high affinity to the target molecules(Alvarez-Lorenzo, 2013). MIPs have been reported for the detection of hormones and other endocrine disrupting chemicals in water (Cáceres et al., 2018), molecular imprinting-based solid-phase extraction (MI-SPE) has provided a powerful way to improve the recognition selectivity and detection sensitivity for chemo/bioanalysis in complex matrices(Arabi, Ostovan, Bagheri, Guo, Wang, et al., 2020), hydrophilic molecularly imprinted nanospheres (MINs) utilized as dispersant sorbent in matrix solid phase dispersion (MSPD) for the extraction of rhodamine B (RhB) as the illogical food additive dye from different foodstuffs, followed by HPLC analysis(Arabi, Ostovan, Bagheri, Guo, Li, et al., 2020),and a specific recognition and extraction of the blood pressure regulating drugs valsartan (VAL) and losartan (LOS) using water compatible hollow porous molecularly imprinted nanospheres (HP-MINs)(Gholami et al., 2019). The high sensitivity and selectivity has been achieved applying a combination of diverse

nanomaterials, sophisticated, complex sensing and manufacturing processes. Photonic MIPs are label free sensors that combine non-covalent imprinting and colloidal crystal used as templates to produce optically active thin films (Casis et al., 2014). Their simple operation makes them ideal candidates for field measurements or for point of care biomedical applications. However, their optical properties have shown to be very sensitive to the fabrication parameters, which resulted in variability between manufacturing batches. An enhanced control in the multi-step fabrication process and a full understanding of the effect of the parameters involved are highly needed but still lacking.

The objective of this work was to fabricate a photonic molecularly imprinted sensor for the detection of progesterone in aqueous media and to optimize the control in the fabrication processes by a systematically investigation of selected factors in the colloidal crystal formation, polymerization reaction, etching, and the target elution processes, mainly temperature, humidity and colloid concentration during crystal growth, polymerization and acid bath time, and elution solution formulation in order to enhance both the morphological and chemical binding properties of the MIP.

We fabricated and tested a MIP capable of selectively recognizing progesterone in water samples. The label free-photonic MIP displayed shifts of the peak wavelength (λ_{max}) of their reflectance spectra driven by the selective rebinding of the progesterone molecules (Han et al., 2020; Z. Lin et al., 2020). The capture and detection of progesterone in test samples was investigated via equilibrium and kinetics tests. Subsequently, the effect of potential background interference, such as presence of dissolved salts and their selectivity in the presence of other steroid hormones with the similar chemical structure was evaluated, through experiments and computational methods.

4.2 Methods and Materials

4.2.1 Materials

Monodispersed silica particles with a diameter of 300 nm were obtained from Pinfire - Gems & Colloids (Frankfurt, Germany) and characterized by electron microscopy in a FEI Quanta 600 FEG Environmental Scanning Electron Microscopy,(Thermo Fisher Scientific,Hillsboro, OR, USA)(https://www.thermofisher.com/us/en/home.html).Ethanol (99.5%, 200 proof), acrylic acid (AA) (99%), ethylene glycol dimethacrylate (EGDMA) (98%), methanol (99%), HPLC-grade progesterone standard, and 2,2'-azobisisobutyronitrile (AIBN) (98%) were purchased from Sigma-Aldrich(St. Louis, MO, USA).(https://www.sigmaaldrich.com/united-states.html). Progesterone (PG) (98%) was purchased from Cayman Chemical (Ann Arbor, MI, USA)(https://www.caymanchem.com) and used in the MIP fabrication process. Hydrofluoric acid (HF) (49%) and acetic acid(HAc) (96%) were supplied by Fisher, (Fair Lawn, NJ, USA) (https://www.fishersci.com). A Thermo Scientific™ Barnstead™ E-Pure™ Ultrapure Water Purification System (Waltham, MA, USA). was used to high purity (Type I) water (18.2 MΩ.cm at 25 ^{0} C). All chemicals were reagent grade and used as received without further purification.

4.2.2 MIP Fabrication

The sensor fabrication process involved the deposition of silica nanoparticles to form colloidal crystals, the infiltration of the crystal structure by the pre-polymerization solution, polymerization, SiO_2 removal by HF, and elution of the target with a solvent (Fig. 4.1). A 1.3% volume fraction suspension of SiO_2 in ethanol(4 g) in 150 ml, the suspension was stirred at 600 rpm for 1 h and then sonicated for another hour. this

process was repeated three more times. Clean glass slides were inserted vertically into the suspension and removed by a step motor in a custom-made chamber that allows for the control of the slide removal velocity and temperature during the deposition (Fig.4.1 a). The step motor was operated at a constant speed of 0.14 mm/min and the temperature was maintained at 70 ±0.1 °C with a heated plated, controlled by an OMEGA a proportional–integral–derivative controller (PID) temperature controller CND3 series(Fig.4.1 b).

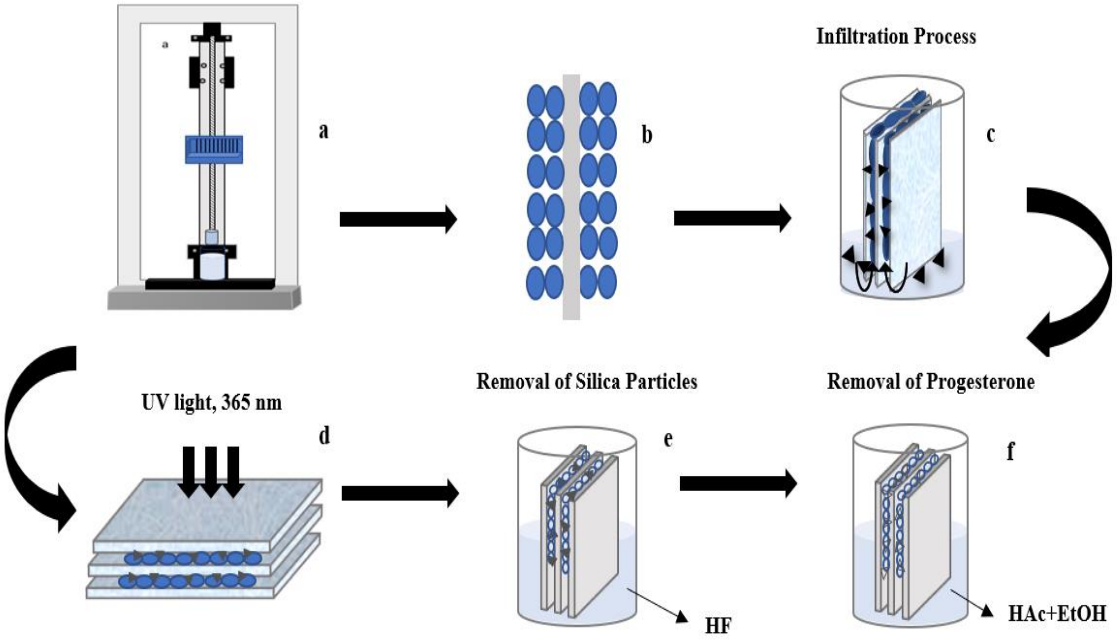

Figure 4. 1. Schematic representation of the MIPs fabrication process: (a) silica deposition machine; (b) colloidal crystal formation; (c) infiltration process; (d) polymerization reaction; (e) silica particles etching; (f) target elution.

The pre-polymerization solution was fabricated as follows: 62.9 mg of PG was dissolved in 1 ml ethanol and AA (439 µl) was added; the mixture was left for 12 h at 4 ^{o}C to allow the complexation of the target with monomer via hydrogen bonding to proceed

before addition of 302 µl of the crosslinker EGDMA, resulting in a molar ratio of 1:32:8 (PG:AA:EGMDA). Finally, 12 mg of AIBN was added as initiator. The optimum template-functional monomer-cross-linker molar ratio was chosen based on results from our previous studies; minimum resistance was provided using AA, it showed high penetration of the solution and diffusion of the target due to its hydrophilicity, while the polymer was cross-linked to a degree that it produced a connected matrix but still allowed some flexibility for the chains to swell/shrink upon binding/eluting of the target(Dai & Fidalgo de Cortalezzi, 2019; Kadhem et al., 2018). A PMMA slide was placed on each side of the glass slide and one end of this "sandwich"-type structure was allowed to contact the pre-polymerization solution and infiltrated the colloidal crystal by capillary forces (Fig.4.1 c). The assembly was irradiated with UV light at λ= 365 nm for the polymerization reaction to proceed for 3 h (Fig.4.1d). The glass slides and SiO_2 particles were etched in 5% HF for 36 hours, followed by extensive rinsing with deionized water (Fig.4.1 e). In the last step, the target was eluted by washing the polymeric film with a 1:9 (v:v) HAc: EtOH solution, with replacement of solution every 30 min for a total of 3 hours, and final rinse with ethanol in order to remove the HAc residues from the slides. (Fig. 4.1 f). Non-imprinted polymeric (NIPs) films were fabricated as controls following the same steps as MIPs except for the addition of PG. Further fabrication details are added to the supplementary information section.

4.3 Characterization

The colloidal crystals and polymeric films were imaged to investigate the particle or pore size and morphology by a FEI Quanta 600 FEG (Thermo Fisher Scientific, Hillsboro, OR, USA) Environmental Scanning Electron Microscopy (SEEM). Samples

were attached to stubs with conductive carbon tape and sputter with a thin layer of gold (1.5–3.0 nm) using an Emitech K575x sputter coater (Quorum Technologies Ltd., Ashford, Kent, UK). The images were analyzed using ImageJ software version 1.50 (National Institutes of Health, NIH). At least 3 different images for over 300 particles were measured.

A Zetasizer Nano ZS instrument (Malvern Instruments) was used to investigate the silica particle size distribution in the suspension by Dynamic Light Scattering (DLS). At least 3 suspensions of silica nanoparticles were prepared independently with a concentration of 10 mg/L.

Attenuated-total-reflectance-Fourier Transformed Infrared Spectroscopy (ATR-FT-IR)was used to investigate the chemical structure of the material, and the spectra of the polymeric films were collected using a Nicolet 4700 FT-IR (Thermo Electron Corporation, Waltham, Massachusetts, U.S.A), between the wavelengths of 4000–400 cm^{-1}.

The equilibrium swelling experiments were performed on NIPs in phosphate buffer at two pHs (4 and 7), at 25 C. The polymers were swollen in solutions for 48 h at room temperature to reach equilibrium, and the degree of swelling was determined gravimetrically. The percentage of swelling ratio (SR) was evaluated from the following expression 4.1.

$$SR = (m_s - m_d) / m_d \qquad (4.1)$$

where m_s is the mass of the swollen film at equilibrium and m_d the mass of the lyophilized films.

The optical response of the sensor was assessed by recording the reflectance spectrum before and after incubation in PG solutions, and the λ_{max} were connected with sample test concentration(see the Supplementary information).

In the kinetics experiments, the MIPs were first immersed in DI water for 20 minutes and then incubated under gently shaking in a 20 μg L^{-1} PG solution; slides were removed from the solution and reflectance spectra recorded every 2 min during at least 12 minutes. Equilibrium rebinding experiments were conducted in PG solutions of variable concentrations, from 1–100 μg L^{-1}. In a typical experiment, MIPs were first immersed in DI water for 12 minutes and then the films were incubated in 25 ml of each PG solution using a shaker (orbital shaker, Cole-Parmer, IL, US) to facilitate the transport of the target molecule from the bulk solution into the porous film. After equilibrium was assumed, the slides were removed and rinsed with DI water and their reflectance spectra recorded.

The effect of ionic strength on the sensor response was investigated by the incubation in PG standard solutions with a background ionic strength of 150 mM as NaCl. This level of IS is representative of some industrial wastewater or brines, high salinity groundwater or physiological conditions, as the sensor may be applied in the detection of PG in body fluids. To investigate the recognition ability of the MIPs film and NIPs film, a group of selected structurally similar compounds were selected: estradiol, hydrocortisone, and dehydroepiandrosterone-sulfate (Figure S.4.1 Supplementary data). The sensor response to a concentration 5 μg L^{-1} of the analog compounds was compared to that corresponding to PG. The measurements were repeated at least 5 times with different sensors for each hormone in the study. The concentration of all test solutions were validated

by HPLC MS/MS. The analytical methods and the standard solutions preparation are in ESM(see the supplementary data).

The sensor was tested in real water samples collected from wetlands near Columbia, Missouri, and tap water at the University of Missouri (coming from Water Treatment Plant with Columbia Utilities) that were spiked with PG. Immediately after collection, the sampled water was characterized by pH, conductivity and total organic carbon (TOC) measurements using a Shimadzu TOC-VCPN analyzer. The MIP-sensor were first immersed in clean water for approximately 12 minutes and the initial diffraction peak measured; secondly, the sensors were dipped in the spiked solutions, let to equilibrate for 12 minutes and rinsed with DI before reading wavelength shift. PG concentrations were determined by the optical response as established by the Bragg equation that relates the diffraction peak (λ_{max}) for the polymer. Sensor measurements were validated by analytical determinations of the PG concentrations in the samples, by Liquid Chromatography Triple Quadrupole Mass Spectrometry (LC-MS/MS)). The experiments were conducted in triplicate.

The electrostatic potential calculations were performed using Gaussian 09W software, applying the density functional theory (DFT) method with the hybrid Becke, three-parameter, Lee–Yang–Parr functional (B3LYP) and Pople's basis set 6-311G (2d,p)(Azofra et al., 2013; Krishnakumar & Balachandran, 2005; H. Lin et al., 2008). No symmetry constrain were imposed; potential energy surface minima were verified by vibrational frequencies (Azofra et al., 2013). Solvent effects were included using SMD continuum solvation model(Azofra et al., 2013). The molecular electrostatic potential mapped onto the isodensity surfaces was visualized using Gauss View 6(Kolar et al., 2019)

and the quantitative analysis of molecular surfaces were performed using Multiwfn 3.8(J. Zhang & Lu, 2021).

4.4. Results and Discussion

4.4.1 Characterization of silica particles and films

The size of the silica particles was measured by DLS measurements. The results showed that the Z- average hydrodynamic diameter was 375±7 nm, with a polydispersity index of 0.012. The results are in general good agreement with nominal values as reported by the manufacturer, since DLS commonly overestimates particle size due to the effect of the solvent on the hydrodynamic diameter.

Figure 4.2 shows the morphology of the colloidal crystals and the molecular imprinted polymeric films. Figure 4.2 a,b shows the top and cross-sectional view of the colloidal crystals structure. Particle size measurements from the SEM images yielded a size distribution of the particles, with an average radius of 232±27 nm. Since the packing structure of a colloidal crystal is considered the crucial factor that determines its functioning in the optical application, the desirable thickness of the colloidal crystals film thickness was achieved by controlling the particle concentration in the suspension. A relationship was established between the thickness of the crystals and the volume fraction of particle suspension (P. Jiang et al., 1999) as shown in Equation 4.2:

$$K = \frac{\beta L \emptyset}{0.605 d(1-\emptyset)} \quad (4.2)$$

where K represents the number of layers, β is proportion of the particle velocity in solution to fluid velocity (assumed to be 1), L is meniscus height, d is the diameter of the particle, and Ø is the particle volume fraction in the solution. The calculated number of layers

according to equation 1, with L± = 3500 μm =0.013,β= 1, and d =232 nm, was 328 layers. However, the number of layers observed in the SEM images was about 13-15 layers. Since Equation 4-2 was derived for colloidal crystals fabricated by evaporation of ethanol at room temperature with a fixed vertical substrate (P. Jiang et al., 1999), it is not unexpected that it did not provide a very accurate prediction their thickness under the conditions of the current study, as it overestimated the number of layers obtained. However, the inverse relationship between the particle volume fraction Ø and the number of layers K was still valid. Fig 4.2 c, d show the porous structure of the imprinted film after the removing of the silica. The surface porosity of the polymer afforded higher surface area and more available binding sites.

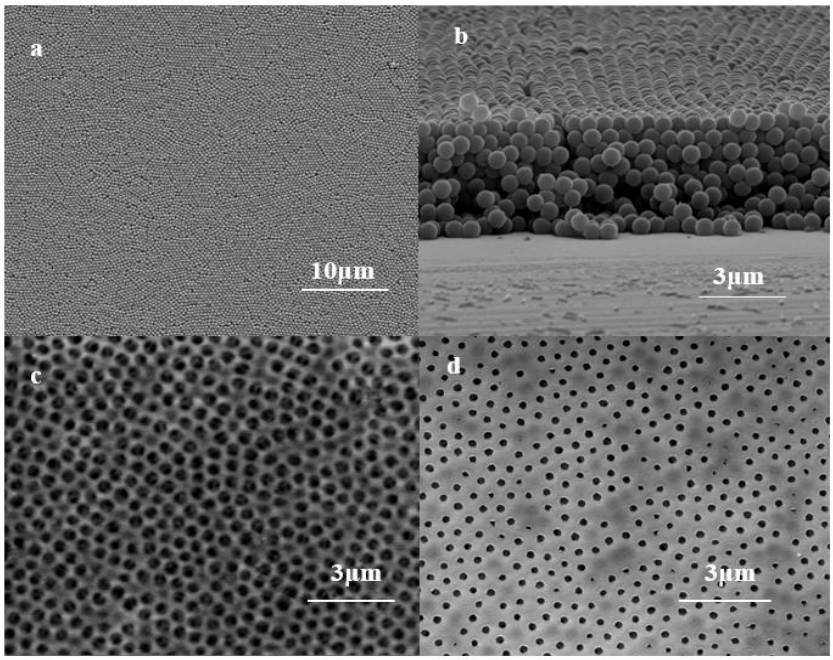

Figure 4. 2. SEM image of silica particles: (a) colloidal crystal top layer; (b) colloidal crystal cross section; (c) polymer structure; (d) surface porosity.

The bond between the chemical functional groups of the polymer and the PG molecule was investigated by ATR- FTIR. Spectra for MIP films before and after PG removal as well as NIPs were obtained (Figure 4.3). Different absorption bands appeared for MIPs after PG removal compared to the MIPs before target removal and the NIPs. The ATR-FT-IR spectrum displayed a peak at 3000 cm^{-1} corresponding to O-H group, in the range 2500–3500 cm^{-1} of the characteristic profile of the carboxylic acids; this peak observed in the MIP film after target removal. Additionally, the peak at 1750 cm^{-1} is related to carbonyl group (C=O) of the monomer, which can be evidence of a total removal of the PG target from the MIP film. The non-covalent binding of the PG with the polymer before the washing process inhibited the absorption by the functional groups involved, while after PG removal, those groups were free to interact with the incident light and showed stronger adsorption bands [22].

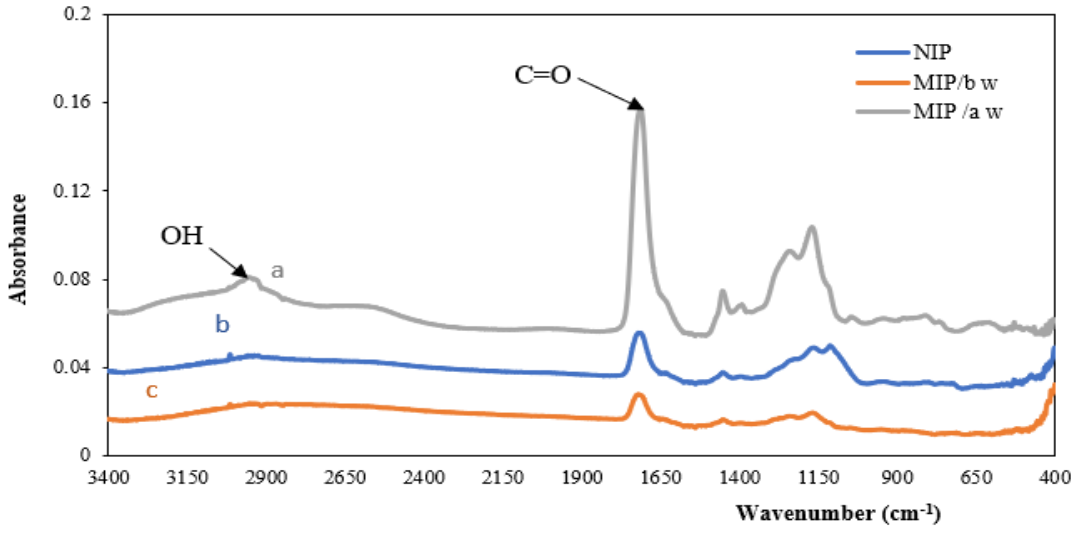

Figure 4. 3. ATR-FT-IR spectra of different films: (**a**) MIP after progesterone removal; (**b**) NIP; (**c**) MIP before progesterone removal.

The SR % of hydrogel film depends on the cross-linking and charge densities of the polymer network. High degree of the swelling translates into a larger variation in the photonic crystal structure, which, in turn, is associated with a more significant optical response. AA films presented high swelling ratio at neutral pH than at acidic pH (Figure 4.4). At the higher pH, the carboxyl group is deprotonated to a higher extent, leading to electrostatic repulsion that causes the swelling ratio to be outweighed. On the other hand, at low pH value when carboxyl groups present in the polymer reduce the repulsive interactions between the polymer chains, resulting in less swelling, where AA expected to be present in its ionic form, with pKa of 4.26.

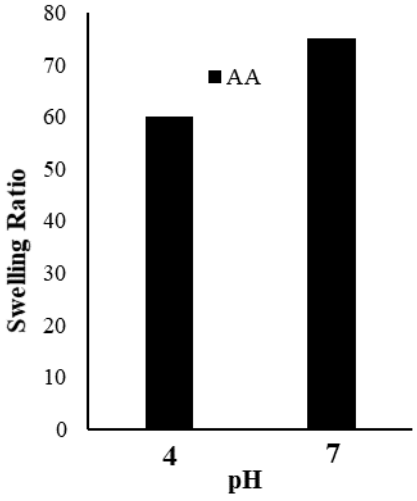

Figure 4. 4. Swelling ratio (%SR) variations of AA films with pH.

4.4.2 Analysis of manufacturing parameters

The colloidal crystal formation was investigated at 50±0.1 and 70±0.1 °C in order to investigate the effect of temperature on the uniformity and film thickness, and thus the diffraction properties of the opal films,(see Fig S.4.2 in the supplementary data)(P. Jiang et al., 1999). However, the crystal deposition at temperature 70°C was preferred for lower standard deviation values and the faster crystal formation.

Another variables were investigated in the photonic film fabrication: time in hydrofluoric acid bath, elution time and solution concentration. (S. Chen et al., 2019). The 36 hr time was superior to 24hr as it demonstrated higher shift values, evidencing better removal of silica particles without producing damage to the polymer film that was observed after 48 hrs immersion in the HF bath. In addition, three different washing ratios of acetic acid: ethanol (v:v) were considered for the PG removal. The results showed a maximum shift toward shorter wavelength of visible spectra region to an average of 395±15 nm of the reflectance spectra with washing ratio (1:9) (Figure S.4.2 c), which reflects the removal of the analyte from the binding sites and the shrinking of the hydrogel film (Zhou et al., 2012).Besides, the results showed that 3 hrs washing time had high efficiency of target molecules elution from the MIPs matrix. Longer times proved to be excessive exposure to the acetic acid and ethanol solution, as the 4 hour washing time caused damage to the film polymeric structure (Ričanyová et al., 2010) and led to the shift back to higher wavelengths (Fig. S. 4.2d Supplementary data)

4.4.3. Kinetics and Equilibrium of binding

The kinetics experiment of PG rebinding to the MIPs showed a progressive shift in the peak wavelength of the reflectance spectrum that leveled off after about 12 minutes, calculated as the average time of 6 different MIPs tested; the peak wavelength remained stable for the remainder of the experiment (Fig. S4.3, Supplementary materials). The adsorption of PG into the imprinted sites involves the transport of the molecule form the bulk of the solution to the binding site and the adsorption step. The porous morphology of the sensor is expected to provide numerous binding sites close to the polymer-liquid interface, which can be reached relatively fast, and other sites inside the polymer matrix. The utility of the latter for sensing is limited by the diffusion step of the molecules through the solid, which is much slower than the movement through the liquid in the pores. Gently mixing was applied during incubation in this work, to accelerate the transport of PG molecule through the porosity, leading to shorter equilibration times that those previously reported (Kadhem et al., 2018).

The equilibrium incubation experiments showed a gradual shift to higher wavelengths in the peak of the reflection spectra with increasing concentration of PG solutions; the shift was measurable after exposures to concentrations as low as 1 $\mu g\ L^{-1}$. Ten MIP films were tested in each solution; the average and standard deviation of the observed shifts are shown in Fig. 4.5 a. The photonic properties of the MIPs changed with the amount of the rebinding of PG molecules, which in turn can be correlated with the peak wavelength of the reflection spectrum; increasing the concentration of the target in the incubation solutions produced a shift of the peak to a longer wavelength [22- 24]. Moreover, the shift observed after exposing the NIPs to the PG solutions was much lower,

which revealed some degree of non-specific adsorption occurred in the NIP films, that can be interpreted as background or noise for the technique.

Fig. 4.5 b shows the result of the observed reflection spectra of the MIPs incubated in solutions of different concentration of PG. A noticeable decrease in λ_{max} intensity appeared with increasing PG concentrations. This can be attributed to uneven swelling of the porous hydrogel during rebinding, producing an uneven deformation of the structure that reduced its photonic characteristics. However, peak wavelength values could be identified for each case, with no negative effect over the sensor performance.

The MIP sensor was able to detect concentrations of PG from 1 –100 μg L^{-1} (Fig. 4.5). The detection limit (LOD) was determined to be 0.5 μg $L^{-1,}$ LOD was calculated as the concentration resulting from three times the standard deviation of 5 independent measurement of the blank (3σ criterion) (standard deviation measured on wavelength = 4.9 nm) (S/N=3)(Kasambala et al., 2019).The limit of quantification (LOQ) was determined to be 2 μg L^{-1}; it was calculated as ten times the standard deviation of 5 independent measurement of the blank (10 σ criterion) (standard deviation measured on wavelength = 9.5 nm) (S/N=10). The MIP exhibited relatively a linear response with concentration, between 1 – 20 μg L^{-1}, but flatten to a plateau as it approached saturation for higher concentrations. A larger total diffraction peak shift denoted a much stronger binding affinity of PG to the MIP than NIP. The same manufacturing protocol was carefully followed in the fabrication of all MIP sensors. However, the high standard deviation of the measurement values in (Fig. 4.5 a) evidenced variations in films, possibility due to differences in binding cavities in the polymeric structures and degradation or unreacted compounds that act as contaminants of solutions during sensor use. Generally, the

affordability, ease of fabrication and use make MIPs an ideal technology for on-site screening and/or quantification of PG in water. Although film reproducibility was improved by the analysis of parameter presented in this study, more work is needed in the control of the fabrication process that will enhanced the accuracy of the technology(Kadhem et al., 2021). A comparison of the sensor developed in this work with others reported in the literature evidences its shortcomings. For example, MIP based sensors for progesterone combined with surface plasmon resonance, gas chromatography-flame ionization or HPCL achieved LODs of 8.8×10^{-12} ng/mL(Nawaz et al., 2020), 1.1×10^{-4} ng/mL (Nezhadali et al., 2016) (Cáceres et al., 2018) for the first, and second, third case respectively. These values are much lower than the one reported in this work; however, a direct comparison with these methods ignores the pros of our proposed sensor. Optical and in particular photonic sensors, have the advantage of being simpler, since they are label-free and do not require complex analytical equipment to read their responses, which can be particularly important for in situ measurements.

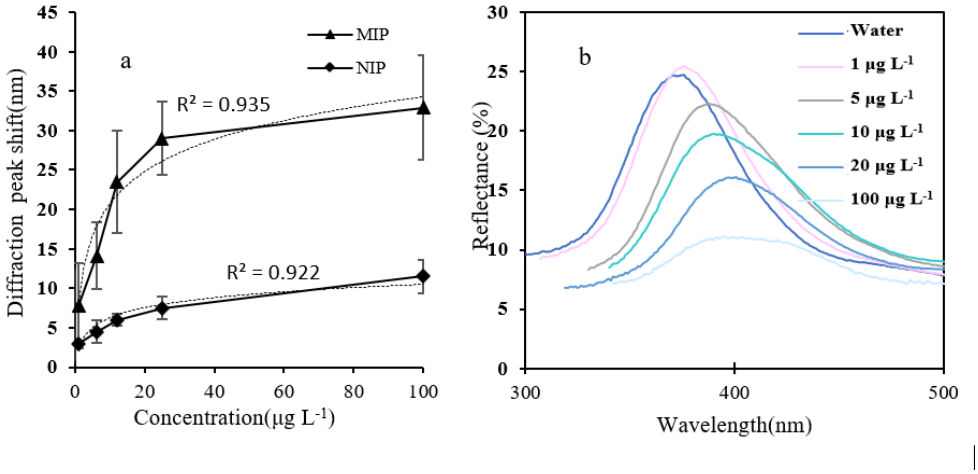

Figure 4. 5. Optical response of MIPs sensors after incubation at various concentration of PG aqueous solutions: (a) diffraction peak shift; (b) reflectance spectra. The standard deviation and mean average are calculated based on the measurements of at least ten individual MIPs sensors for each concentration (sample volume = 25 mL, incubation time = 12 min, temperature= 25°C, n=10).

4.4.4 Effect of Ionic Strength

The variation of sample characteristics (i.e. ionic strength) might affect the sensor response in the form of peak wavelength shift not associated with PG rebinding (W. Chen et al., 2016). The ionic strength (IS) of the test solution may affect the sensor response in two main ways: first, the addition of charged ions would results in the compression of the electric double layer at the polymer-solution interface and a decrease in the electrostatic repulsive forces of the surfaces within the pore structure, which contribute to less swelling under similar rebinding conditions; second; the influence of salt ions on the MIP binding affinity under the Hofmeister effect. The MIPs were applied to the quantification of PG in standard aqueous solutions with a background ionic strength of 150 mM NaCl concentration (Fig. 4.6). While the average peak wavelength shift at each PG concentration was similar to the deionized water solutions, much less variability at 150 mM IS was observed in the readings of different sensor. The responses resulted in lower standard deviations, narrower peaks, higher reflectance intensity and more consistent responses of the polymer hydrogel film other than for the deionized water solution.

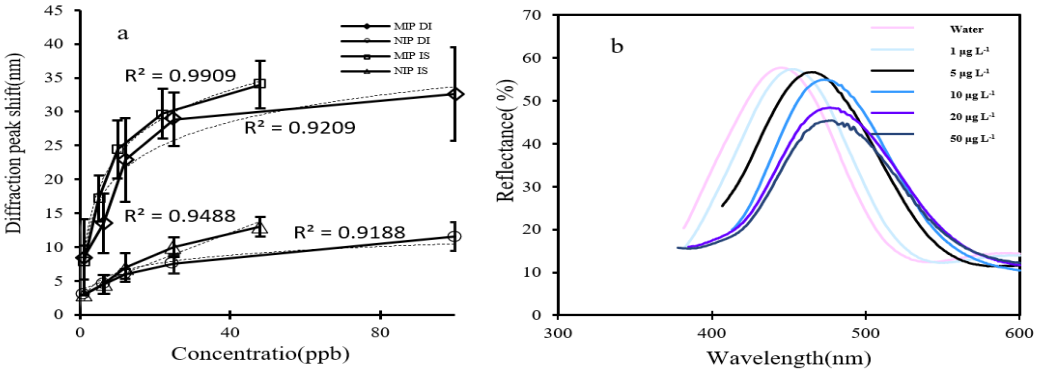

Figure 4. 6. Optical responses of the MIPs sensors after incubation at various concentration of PG aqueous solutions, 150 mM NaCl. The standard deviation and mean average are calculated based on the

measurements of at least ten individual MIPs sensors for each concentration:(a) diffraction peak shift; (b) reflectance spectra (sample volume = 25 mL, incubation time = 12 min, temperature= 25°C, n=10).

The larger peak shift hints to an enhanced binding efficiency of the MIPs after incubation in IS solutions [24–26] with respect to that observed in deionized (DI) water solutions (Fig. 4.6 a). This can be related to the effect of IS on the hydrogel swelling degree (J. Huang et al., 2008) as well as the increased non-specific adsorption and interaction with compounds promoted by the IS. This enhanced optical response of MIPs IS with suggested that the second effect is more likely and pronounced than the first one in this case, which can be explained by the solvation energy disparities between the kosmotropic salt ions and the neighboring water molecules. The observation follows the mechanism of the Hofmeister series of cations, especially being the sodium the most kosmotropic cation. The kosmotropic ions presence can increase of the general cohesiveness of the solution by the solvation energy, as well as the hydrogen bonding between PG and the polymer, thus decreasing the interference from the water molecules in the recognition nanocavities.

4.4.5 Effect of analog compounds

The selected analog compounds are steroid hormones, naturally synthetized from the cholesterol molecule and have chemical structures similar to PG. Other compounds can potentially be adsorbed into the imprinted cavities, if they have comparable molecular size and similar functional groups, and as a result hinder the correct determination of PG by the MIPs. Consequently, the binding affinity of the MIPs for PG might be affected significantly by the presence of the analogue hormones, and the sensor optical response as well. The binding affinity depends mainly on the size and shape of the target molecule, as well as the degree of interaction of binding sites. The target preferentially occupied the

imprinted cavities within the hydrogel film due to the congruent shape, size, and interaction sites with the formed binding sites.

The PG MIPs were incubated in 5 μg L^{-1} solutions of each one of the chemicals and the results are shown in Fig. 4.7. As expected, the MIPs showed the highest response towards the PG hormone with a peak wavelength shift of 12±3.5 nm due to the affinity of the PG to the imprinted nanocavities within the film. Incubation of the film in the 17-β estradiol solution produced a shift of 6±2.5 nm, about half of the target molecule. Estradiol is the closest to PG in chemical structure of all tested compounds, slighter smaller with some differences in functional groups two hydroxyl groups in lieu of ketone groups. Hydrocortisone solutions yielded a shift of 4.7± 3.2 nm; although hydrocortisone shares many structural and functional groups characteristics with PG, the results suggested that the additional carbon in the C17 chain effectively decreased the binding affinity to the PG-imprinted sites. On the other hand, the DHEA-S test solution gave the lowest wavelength shift value with 2.7±2 nm. The presence of the sulfate group attached from C3 appeared to produce a steric hindrance to the rebinding and lowered the binding affinity within the film. Meanwhile, a minimum response towards the adsorption solutions without specific binding cavities, and thus, one type of non-specific adsorption interaction showed by the NIPs, due to the general attraction between the polymer surface material and the compounds. The selectivity of NIPs was evaluated as an average diffraction peak shift as 1.1 ,1.3 1.19, and 1.2 nm for progesterone, 17β-estradiol, hydrocortisone and Dehydroepiandrosterone sulfate, respectively. Although the sensor response was significantly higher for PG than for the other molecules, the results indicated that a similar but smaller molecule may be able to bind to a significant degree and produce a false reading of PG concentration. The binding

affinity of different analogues towards the MIP and NIP film reveled that the specific binding sites is the key for the recognition of the template molecule.

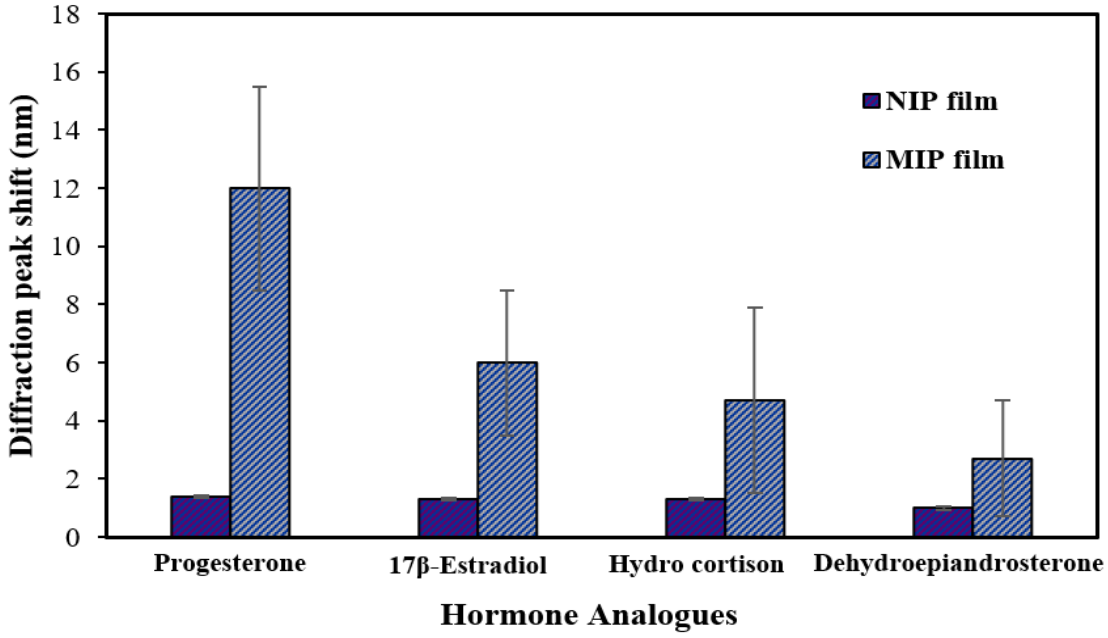

Figure 4. 7. The diffraction peak shift of the MIPs and NIPs when incubated in progesterone and 3potential interfering compounds (17β-Estradiol, Hydrocortisone, Dehydroepiandrosterone sulfate), (sample volume = 25 mL, incubation time = 12 min, solution concentration=5 μg L^{-1} , temperature =25°C, n=5).

In order to compare the molecular shape, size and electrostatic potential values of the selected hormones, the molecular electrostatic potential surface, which is a plot of electrostatic potential (ESP) mapped onto the iso-electron density surface, was calculated (see Fig.S 4.3 Supplementary data)(Boufas et al., 2014). Regions with most negative and most positive electrostatic surface potentials are colored with red and blue, respectively. In addition, quantitative analyses were performed, and the calculated parameters are presented in Table S 4.2 Supplementary data. The only molecule that is smaller than progesterone is the estradiol, and, consequently, it the only one that can fit in all cavities imprinted by progesterone in MIP sensors (see table S.4.2). This is because its aromatic ring that makes planar that part of the molecule, as it can be appreciate in the side-view in

Fig. S.3. Although its smaller size, the estradiol exhibited less interference that could be expected (Figure 4.7); the observation can be explained comparing the ESP distribution on the iso-electron density surface and the polarity of the molecule. Estradiol surface is dominated by nonpolar interactions (62.3% of its area is nonpolar) and is the hormone with the smaller molecular polarity index. In addition, the top-view in Figure S 4.3 shows that the ESP distribution on both hormones is quite different. These factors make it difficult for estradiol to interact with the functional groups imprinted in the cavities by progesterone. On the other hand, hydrocortisone and DHEA-S has more similar ESP distribution on the iso-electron density surface and polarity. However, the volume of these hormones is larger than progesterone and therefore, they cannot fit in all cavities imprinted in MIP sensors. This is in agreement with the low interference by these molecules observed in the assays.

4.4.6 Analytical applications in natural water samples

In the composition of complex real natural water samples, there may be challenging components and characteristics, such as, pH, dissolved solids and natural organic compounds. To further test the applicability of the sensor, the MIPs films were used for the determination of PG concentrations in two types of real waters: natural water samples obtained from creeks near Columbia, MO (Glendale Rd & Maupin Rd) and tap water from the laboratory at the University of Missouri. The collected samples were spiked with PG and its concentration measured by the newly fabricated sensor and compared to Liquid Chromatography Triple Quadrupole Mass Spectrometry (LCMS/MS), which were considered the true concentration values. The corresponding analysis results are listed in Table 4.1. Both the natural water and tap water had a neutral pH. The IS of the tap water was much higher than the natural water samples, and it was expected to have some effects

on the sensor performance. The TOC level of the natural water was higher than tap water due to the existence of dissolved NOM.

The readings by the MIP sensor in tap water were closer to the true values than in natural water samples. The matrix complexity results in a higher chance of block the cavities or the surfaces of sensor films. Still, the values in both tap and wetlands were reasonably close to the LCMSMS measured PG concentrations. The sensor underestimated the PG concentration in the high PG level natural water samples: the TOC content in in natural water and possible contributions of other unknown pollutants and particulate matter that can cause interference with the sensor performance may have affected the measurements, while tap water constitutes a much simpler and well-known matrix. IS did not show results in negative effects in the measurements, as demonstrated by the good readings obtained for the tap water samples. The MIPs results revealed satisfactory recognition ability towards the analyte, and a promising performance in challenging, unknown natural water samples.

Table 4. 1 Measuring of PG in real water samples and their physicochemical characteristics.

Sample	Sensor measured PG concentration (μgL^{-1})	Stdev	Error (%)	LC-MS/MS measured PG concentration (μgL^{-1})	pH	IS (mM)	TOC (ppm)
Glendale Rd	17.75	0.56	27.4	13.9	7.45	2.3184	4.287
	8.2	0.42	5.6	8.6			
Maupin Rd	20.1	0.35	17.1	24.2	7.13	1.016	2.212
	8.05	0.21	23.3	10.5			
Tap	19.4	0.78	17.1	23.0	7.2	13.8	N/D

4.5. Conclusions

Molecularly imprinted polymeric films were fabricated with highly ordered 3D-structures that conferred them photonic properties. Analysis of the manufacturing parameters showed that a temperature of 70°C for the colloidal crystal fabrication, 36 hrs. etching time and a 1:9 (v/v) Acetic Acid: Ethanol ratio for 3 hrs. yielded the best results. High quality colloidal crystals were obtained in a custom-made equipment, and the following steps in the fabrication process are capable of automatization through a similar approach. This would not only result in higher throughput in manufacturing but also significant reduction in waste, minimizing chemical consumption and waste production, addressing one of the main drawbacks of MIP technology. However, variability still remained high, as evidenced by the error bars in the calibration curves, and more research is needed to improve the polymerization and target removal steps of the manufacturing process. The sensors demonstrated high response after exposures to concentrations down to 1 $\mu g\ L^{-1}$ and 12 min equilibrium time, with LOD 0.5 μgL^{-1}. Significant improvement in the response was observed by the incubation in standard aqueous solutions with a background 150 mM NaCl, with much less variability in sensor response and slightly higher wavelength shifts at each concentration tested. Moreover, the developed sensor was successfully applied to detect progesterone in the presence of complex matrices, in both natural water and tap water samples, with errors between 1-27%, which suggest the use of the sensor to quantify PG at low concentrations or as a screening tool for the presence of PG in natural water. Furthermore, higher affinity for PG in the presence of other steroid hormones (structural analogues),was illustrated the good recognition of the MIPs, that proved via the computed

surface electrostatic potentials and the ability to form bonds with the polymer functional groups. Appreciable advantage exhibited with higher specificity of MIPs films over NIPs films toward PG hormone with other structurally related analogues.This work has shown the potential for photonic MIPs in environmental applications. The use of the sensor is straightforward and fast, while it is capable to differentiate hormones with similar structures to PG. Moreover, the sensor can find uses in biomedical applications, as for example blood analysis, where several hormones are expected to be present in the sample. However, hormone concentrations can vary widely and expected levels of each hormone concentration at any given time for one individual are rarely similar, which will impact possible interference effect. In those cases, background information about the sample, such as individual gender, age, medical conditions, should be part of the interpretation of the sensor response.

Chapter 5: Progesterone Detection and Quantification in Dairy Cows using Molecularly Imprinted Photonic Sensors

5.1. Introduction

Progesterone has a substantial role in the reproductive health, such as regulating the estrous cycle time-length, maintaining pregnancy (Ab et al., 2017). In veterinary medicine, progesterone measurements have helped to improve fertility, used to assess the reproductive status of the cow and to diagnose pregnancy (Blavy et al., 2016). The progesterone and the estrous cycle are the cornerstone of dairy cattle reproduction. Progesterone (PG) is the key sex hormone responsible on reproductive events associated with establishment and pregnancy maintenance through its effect on the uterine endometrium, where lower fertility rates are related to reduced PG concentrations during growth of the ovulatory, and thus lower pregnancy rates in cattle (Lonergan & Sánchez, 2020).

Progesterone occurs naturally during the cows estrous cycle. After ovulation, at the beginning of the cycle, follicular cells will luteinize and become a functional corpus luteum. This corpus luteum secretes progesterone until about day 16 of the cycle. If pregnancy did not occur the corpus luteum will regress between day 16-20 of the cycle and the cow will come back in heat and ovulate to start the cycle all over again. If pregnancy occurs, the corpus luteum will be retained and will continue to secrete progesterone throughout pregnancy.(Senger, 1997).

Many of studies have investigated different methods to monitor PG in cows in different media such as milk (Samsonova et al., 2018) (Blavy et al., 2016),blood (Lasheen et al.,

2018), urine (Volkery et al., 2012), and saliva (Ab et al., 2017) . The efficacy of biotechnologies for synchronization of estrus in cattle is fundamentally dependent on the PG quantitation in biologic fluids. This analysis is largely been performed via the radioimmunoassay (RIA), which, and despite the risk accompanied with handling radioactive materials, is relatively simple, rapid, sensitive, and easy. However, number of studies have reported that RIA lacks specificity for steroids with several interferences and severe matrix effects. In addition, at low concentration of steroids, the used antibodies in the RIA can cross-react during the recognition in complex biological fluids (Fernandes et al., 2011; Stanczyk et al., 2007). Other studies proposed using a biosensor as an immunosensor (Gillis et al., 2006; Koelsch et al., 1994), that use a specific antibody–antigen interaction as its recognition element. These techniques are typically fast and sensitive, but their main problem is the high cost. Other analytical techniques such as liquid chromatography coupled with mass spectrometry (LC–MS/MS)(Fernandes et al., 2011), high-performance liquid chromatography (HPLC) (Sudeshna et al., 2013) and gas chromatography–mass spectrometry (GC-MS) (Janssens et al., 2016) have been applied to PG detection. The limit of detection of progesterone using a GC–MS approach in single-ion mode is 5 μg/l, and the for LC–MS is 0.4–20 μg/l (Díaz-Cruz et al., 2003). Although, these techniques are perfectly suitable for detection low levels of PG regarding the high accuracy and specificity, they are too expensive for routine analysis, and require time-consuming and complicated sample pretreatment (Posthuma-Trumpie et al., 2009). Although different biofluids can be used for PG analysis, we focus in this work on plasma and whole blood samples. Milk, urine and saliva don't have the exact circulation measurements of PG hormone; plus, less interference can be observed with other

analogues, as opposed to blood. In blood, the prevailing profile of progesterone is 98% bound to plasma proteins (Bolaji, 1994). In saliva, only the 2% fraction of free progesterone is available, whereas in milk, the progesterone is concentrated in the fat fraction(Roelofs et al., 2006). For the above-mentioned aspects, it is extremely desirable to develop a method that enables for easier, cost saving, and faster detection of progesterone in blood. MIPs sensors can provide reliable results, are low cost, fast, do not require a second analytical step, and therefore are more practical in environmental and medical fields, such as sensing different application hormones (Kadhem et al., 2021).

The proposed photonic sensors are inverse opals with three-dimensional structures elaborated from the self -assembly of photonic colloidal crystals(opals) templates, using a nano-spheres with a dielectric properties (Waterhouse & Waterland, 2007). Photonic crystals (PhCs) sensing technique is based on adjusting the structural color in a specific environment via different design of its chemical components (Fan et al., 2021).

The main objective of this work is to investigate the adequacy of the molecular imprinted sensor in the analysis of progesterone hormone level in cow's blood, since this detection technique has the potential to afford fast, cheap and useful results. The experimental work is aimed towards a better understanding of recognition ability of molecular imprinted photonic sensors toward PG target, testing the sensor in plasma and whole blood samples of different animals and evaluating the binding affinity of MIPs with interference existence of other steroid hormones (structural analogues). The outcome of this project will contribute to the optimization of the animal production operation, monitoring the reproductive PG hormone levels of the herd with photonic MIPs sensors.

In this chapter the sensors described in Chapter 5 were used in a biomedical application such as the blood analysis to detect the concentration of progesterone in dairy cattle. Cow blood samples were collected and tested by the sensors and validating methods. The results were compared to show the accuracy of our results and the applicability of the sensors to this particular problem.

5.2. Methods and Materials

5.2.1. Materials

Ethanol (99.5%, 200 proof), acrylic acid (AA) (99%), ethylene glycol dimethacrylate (EGDMA) (98%), 2,2'-azobisisobutyronitrile (AIBN) (98%), methanol (99%) and HPLC- grade progesterone standard were purchased from Sigma-Aldrich (St. Louis, MO, USA). Progesterone (98%) was purchased from Cayman Chemical (Ann Arbor, MI, USA). Sodium acetate (NaAc), hydrofluoric acid (HF) (49%) and acetic acid (96%) were supplied by Fisher (Fair Lawn, NJ, USA). All chemicals were reagent grade and used as received without further purification. Ultra-pure water (18.2 MΩ.cm at 25 ^{0}C) was obtained from a Thermo Scientific™ Barnstead™ E-Pure™ Ultrapure Water Purification System (Waltham, MA, USA).

Monodispersed silica particles with a diameter of 300 nm were obtained from Pinfire - Gems & Colloids (Frankfurt, Germany). A poly (methyl meth-acrylate) PMMA Plexiglass plastic slides and glass microscope slides, both with dimensions (1 X 13 X 76) mm, were purchased from ePlastics (San Diego, CA, USA) and Fisher Scientific (Pittsburgh, PA, USA), respectively.

5.2.2. Synthesis of Molecularly Imprinted Photonic Hydrogel

The MIP fabrication process involves the following steps: the deposition of silica nanoparticles to form colloidal crystals; addition of PMMA support slides on top of colloidal crystals; infiltration of the crystal structure by the pre-polymerization solution; UV polymerization; silica particle removal by immersion in HF; and elution of the target with a suitable solvent. The steps are described in more detail in the following paragraphs.

In order to obtain a stable suspension to be used in the colloidal crystal fabrication, 4 g of SiO_2 particles were suspended in 150 ml of ethanol, mixed and stirred at 300 rpm at approximately 24 h. The colloidal crystals were created by dipping a batch of 4 clean microscope glass slides with dimensions 1x13x76 mm vertically into different container vials that was explained before in previous part, containing variable volume fraction suspension of SiO_2 particles in ethanol; the controlled velocity motor was used to remove the slides from the suspension. The photonic crystal templates were fabricated under controlled temperature 70 °C with a deviation of ±0.1 degree, and the relative humidity was measured accordingly. The slides were moved upwards from the suspension with a specified motor velocity 0.139 mm/min, for approximately 3-4 h, accompanied by the volatilization of ethanol, resulting in the self-assembling of the particles forming crystals (0.104 mm/min) on both sides of the glass slides.

The pre-polymerization solution was prepared as follows: 62.9 mg of progesterone as the target, dissolved in 1 ml ethanol; the functional monomer AA (439 µl) was added, and the mixture was left for 12 h at controlled temperature of 4 ^{o}C to allow the complexation with monomer via hydrogen bonding to proceed. Then, 302 µl of the crosslinker EGDMA were added, which corresponds to a molar ratio of target: functional monomer: crosslinker

of 1:32:8. Finally, 12 mg of AIBN was added as initiator. PMMA plastic slides were placed on both sides of glass slide surface with colloidal crystals nanospheres, holding them together firmly forming a “sandwich”-type structure. The polymerization solution was allowed to rise by capillary forces via one end of the "sandwich”-type structure until the solution penetrated all the void volume of the colloidal crystals. The polymerization reaction proceeded inside the colloidal crystal voids under UV light at λ= 365 nm for 3 h at room temperature. The non-imprinted polymers (NIPs) were fabricated as a control with the same steps as MIPs except for the addition of progesterone. The colloidal crystal template, i.e. silica particles, was eliminated by immersion in 5% HF for 36 hours, followed by rinsing with deionized water exhaustively. In the last step, the target was eluted by washing the inverse opal film with different ratios 1:9 (v:v) of acetic acid: ethanol solutions, with replacement of solution every 30 min for a total of 3 h, and the final wash was with ethanol solution only, in order to remove the acetic acid residues from the slides.

5.2.3 Blood samples preparation

Blood samples are collected from the median coccygeal vein or artery into evacuated tubes containing K3 EDTA (Becton Dickinson Vacutainer Systems, Franklin Lakes, NJ, USA). Samples collected in 5 specific days based on the PG hormone levels during the estrous cycle of the cow.

All samples are centrifuged at 1200× *g* for 20 min at 4 ◦C, and plasma collected and stored at –20 °C. Progesterone concentrations are determined by duplicate in 100 μl aliquots of plasma using a commercially available progesterone kit (MP Biomedical, Santa Ana, CA) following manufacturer instructions. Inter- and intraassay coefficients of variation are 1.97% and 1.33%, respectively. Data of circulating progesterone

concentrations are analyzed by analysis of variance (ANOVA) for repeated measures using MIXED procedure. The models included the effects of SCR class, the day of sample collection, the interaction between SCR class and day of sample collection, and the random effect of heifer nested within SCR class.

The whole blood samples were treated with NaAc solution in order to release the bound hormone from the globulin. The dissolution buffer (0.5 mol/L NaAc, pH 5.5) was prepared by dissolving 10.25 g sodium acetate into 200 mL of DI water, stirring the solution and mixing until completely dissolved and adjusting pH to 5.5 (±0.1) with diluted acetic acid (*Division of Laboratory Sciences | CDC*, 2021).

5.2.4 Blood samples analysis with MIPs

To investigate practical application of PG sensors and evaluating the MIPs ability of capturing the free and total PG levels in cow's blood, 5- 6 days of the estrous cycle of three different animals were tested. Equilibrium rebinding experiments were conducted in PG solutions. In a typical experiment, MIPs were first immersed in DI water for 12 minutes and then the films were incubated again for 12 min in 25 ml of each sample (whole blood, plasma, and Na Ac treated whole blood). After equilibrium, the slides was removed. The sensor was carefully rinsed with ultrapure water and its reflectance spectrum recorded with a UV-spectrophotometer. From the relation between peak wavelength shift and concentration as determined in Chapter 4, the PG concentrations were estimated. In this work, previously obtained calibration curves obtained via incubation in PG standard solutions with a background ionic strength of 150 mM as NaCl were used, as this condition corresponds to typical physiological levels of ionic strength. All experiments were

conducted in at least triplicate. The MIP measurements were compared to the commercial PG immunoassay kit results.

5.3 Results and Discussion

5.3.1 Free and protein-bound progesterone

Cow's blood and plasma samples analysis

The MIP sensors were applied to the measurement of non-bound and protein-bound PG in blood and plasma serum. Biologically active steroids are transported in the blood by albumin, sex hormone-binding globulin (SHBG), and corticosteroid-binding globulin (CBG). These plasma proteins also regulate the non-protein-bound or 'free' fractions. A progesterone has an affinity to bind cortisol binding globulin and albumin. To assess the total PG, NaAc was added to release the bound fraction of PG from the globulin. A dissociation of the analyte from binding proteins, and extraction of the analyte form the sample matrix took place with adding the NaAc solution to the whole blood samples.

MIPs results were compared with commercial PG kit based results as shown in Fig 5.1 for **cow 1**. After the MIPs incubation in whole blood samples, a gradual shift to higher wavelengths starts in day 0 and continues until day 18. For the initial day of the estrous cycle, no peak shift was displayed in the tested MIPs in the case of the day 0 sample which translates in a concentration of PG of 0 ppb (non-detect). The LH hormone starts to release in day 0, which in turn induces ovulation and releases the egg, and the progesterone level is expected to be very low. The peak wavelength shift reached 17.5±4 nm at day 5, which corresponds to 5.3 ppb, and continued to increase up to 52.2±3.4 nm at day 10, where the PG level reached the maximum in blood. A decreasing trend in PG concentration was

measured until day 18, when the peak wavelength shift reached 34.2± 3.1 nm. This shift exceeds the range of the proposed calibration curve; an extrapolation of the fitted curve estimates the concentration to be 47 ppb. According to Fig 5.1 a, plasma samples showed similar scenario, the shift started with 0 nm at day 0 and continued to increase up to 56±4.5 nm at day 18, which is over the range for the calibration curve. The commercial PG kit test results followed the same trend that detected by MIP sensor in the whole blood samples without treatment and are assumed to be non-bound PG compounds. The measurements revealed that the minimum concentration at day 0 with 2.7 ppb, and highest level at day 10 with 7.7 ppb. The total PG was also examined in blood samples with adding NaAc buffer solution. The results showed higher levels of total PG concentration than a detected level of PG, before adding NaA reaching 60 ±4.5 nm shift and over range concentration at day 10 of the cycle (Fig. 5.1 a and b).The shift values were elevated with the increased percentage for days 1-18 during the estrous cycle with values 198.5,156,71.8,14.9, 11.5, and 12.5 % for **cow 1** samples.

In Fig 5.2 the MIPs binding affinity to whole blood and NaAc added are investigated in **cow 2** samples. The MIPs incubation in whole blood samples, revealed a gradual shift to higher wavelengths in the peak of the reflection spectra λ_{max} with during the estrous cycle up to day 14. The measured shift of PG in blood sample started at 5± 3.9 nm and concentration 1.2 ppb at day 0. In day 0, the LH hormone is started to release, thus the progesterone level stated to decrease became very low, and the cycle became in follicular phase. After day 0 the wavelength shift increased to 16±5.4 nm at day 6, with 6.7 ppb and continued to increase up to 54±5.5 nm at day 14, where the PG level reached the maximum in blood and the cycle starts the luteal phase with over range concentration, and after then

started to decrease until it the minimum level at day 19, it reached to 15±3.9 nm wavelength shift and 5 ppb concentration.

In plasma samples, it can clearly be seen that the shift started with 0 nm at day 0 and continued to increase up to 44±6.3 nm at day 14, and then started to decrease until it the minimum level at day 19, it reached to 17±5.7 nm wavelength shift, with 5.2 ppb concentration. The PG kit test result followed the same trend with MIPs test results for the PG in the blood samples, with minimum concentration value at day 0, then reach maximum at day 14 with concentration 9.8 ppb and starts again to decrease at day 19 when reaches to 0.6 ppb. Both MIPs and commercial PG kits test results were in agreement in evaluating the PG levels trend during the estrous cycle and the pregnancy profile of cow, however, there was discrepancy in evaluating the exact concentrations of free PG during the cycle.

The MIPs were also incubated in blood samples with NaAc buffer solution, the results reveled a slightly higher levels of total PG concentration than a free PG (Fig. 5.2). The detected concentration started at 7.5 ppb at day 0 with 19±2.9 nm shift, then increased to be over range concentrations at days 6,9, and 14 with shift reached up to until 91±5.6 nm. There is an obvious increment in the shift wavelength from those observed in the whole blood samples. This increase in released progesterone hormone from the globulin was added to the PG compound in the sample and represented as the total progesterone. Moreover, high progesterone concentration in sample boosted MIPs binding affinity. The increase percentage in PG levels between the supposed to be non-bound and bound compound reached 280,162.5,45.9,68.5 and 120 % for cow 2 samples after treatment with NaAc. These results reflecting MIPs measurements are correlated to biological aspect in previous articles, that only a small fraction of steroid hormone is the biologically active

component and is generally considered to be circulated free or unbound to plasma proteins hormone is (Hammond, 2016).

The binding affinity of the MIP to PG in **cow 3** samples was investigated in plasma and blood and compared to the RIA results (Fig. 5.3). After the incubation of MIP in whole blood samples, the measured shift of PG started at 6±1.2 nm and concentration 1.3 ppb at day 0. After day 0, the peak wavelength shift increased to 24±1.5 nm at day 6 with 11ppb and to 46± 3 nm at day 14, where the PG level reached the maximum in blood and the cycle starts the luteal phase with over range concentration. Then, a decreasing phase started until the minimum level at day 19 was reached of 15±3.5 nm (shift) and 5 ppb concentration. For plasma samples, the shift started at 0 nm for day 0 and increased up to 41±2.7 nm at day 14, following a and decrease until the minimum level in day 19 of 13±3 nm peak wavelength shift and 4.5 ppb concentration. Fig 5.3 a,b reveled higher levels of total PG concentration after the MIPs are incubation in whole blood samples pretreated with NaAc, the detected concentration started at 10 ppb at day 0 with 23±2.1 nm shift, then increased to be over range concentrations starting at 6,9, through day 14 with shift reached up to until 88.5±7.7 nm, and 28 ppb at day 18. The shifts for cow 3 samples for days 1-19 during the estrous cycle were slightly increased with the percentage with values 33.3,8.5,4.9,4.1, and 13.7%. The measured results are assuming that the MIPs have captured only free compound in cow 3 samples. As only a small fraction (6-13%) of the total progesterone in plasma is in the unbound form, and this fraction increases with the increase in total progesterone (BATRA et al., 1976).

Overall, the overestimation of progesterone hormone levels given by the MIP sensors can be explained by interferences of other circulating hormones that have an affinity for MIP

film due to the similarities in chemical structure to the progesterone, that made facilitate the binding to the progesterone-specific sensor cavities, as studied in previous chapter (ch.4 , section 4.4.5 Effect of analog compounds).

The molecules smaller than progesterone, can fit in all cavities imprinted by progesterone in MIP sensors. One of the nominated hormone molecules that cam interfere with MIPs performance in capturing PG target in whole blood and plasma samples is estrogen. Estrogen concentrations in blood are expected to show fluctuations through the estrous cycle, with significant decrease from day '0' to day 10 with a significant rise on day 15 ,and increase trend from day 15 to subsequent estrus day '00'(Naik et al., 2013). The estrogen level (ng/ml) in cows during estrus cycle is higher than PG ,it can reach on '0' day to (20.24) and decrease up to 15th days (12.36) and again gradually increase to a level of 22.58 on day '00'. While PG concentration increases significantly from day '0' to day 9-14, and decreases thereafter up to day 18-19, remaining low from day 20 to subsequent estrus day '00'.

On the other hand, the expected available hormones during the estrous cycle are serum steroid hormone and sex hormone-binding globulin (SHBG), and a consecutive change in the concentration might be accompanied with PG concentration change. The actual values are tested in (ng/ml) for testosterone, 5a-dihydrotestosterone (5a-DHT), pregnenolone, serum estradiol-17β, and estrogen during the luteal phase, and are as follows, 0.0037, 0.0355, 0.276, 0.003381, and 0.0089 respectively. While during the Follicular phase the concentration are 0.00446, 0.188, 0.2106, 0.0037, and 0.0089 (Vesanen et al., 1990).From the results in the mentioned article it can be illustrated that these hormones can cause some

interface to the MIP binding affinity toward PG compounds, although they are available in low concentration levels in whole blood samples.

The high shift values of MIPs compared to the commercial PG kit results can be clarified from a different perspective: first, the interferences of the other hormones which showed that the free progesterone will be increased extremely even with a very low concentration of hormones interferences. Second, the higher amount of total progesterone, appeared when the sensors were incubated in NaAc samples, and this may be either detect directly by sensor or release and transfer to free progesterone and increased the reading.

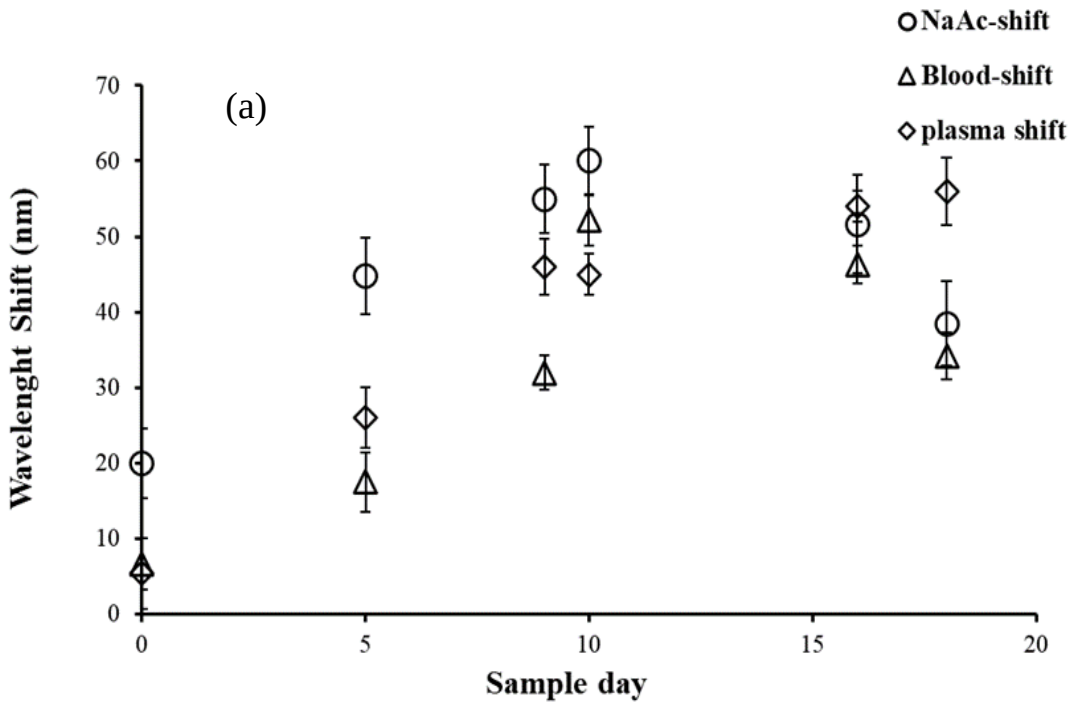

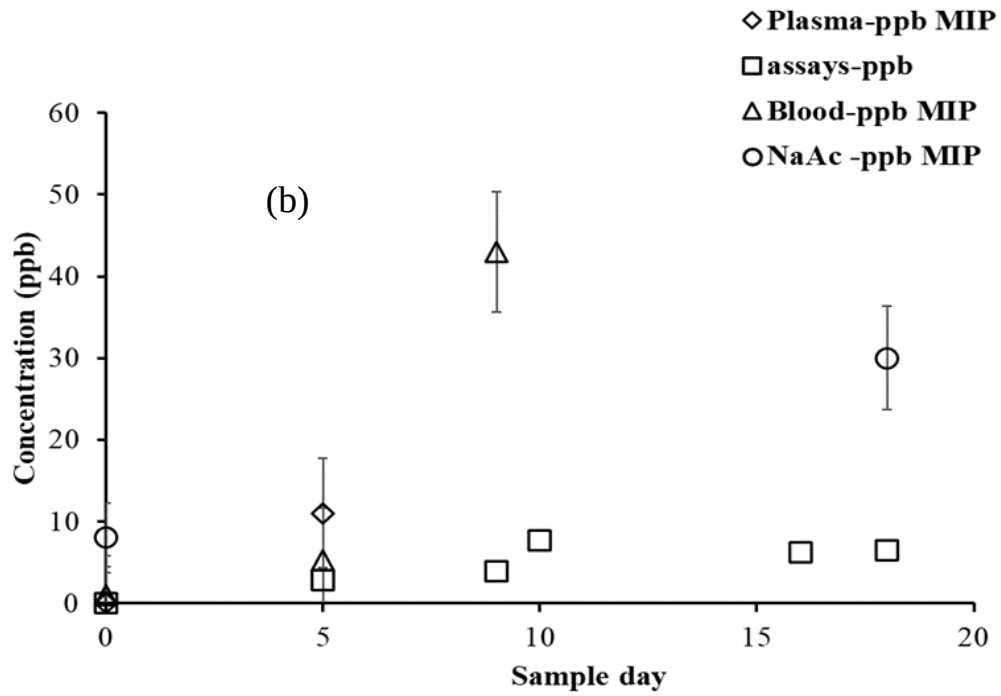

Figure 5. 1. Progesterone levels in blood for animal 1 during the estrous cycle (a) sensor wavelength shift , (b) PG concentration.

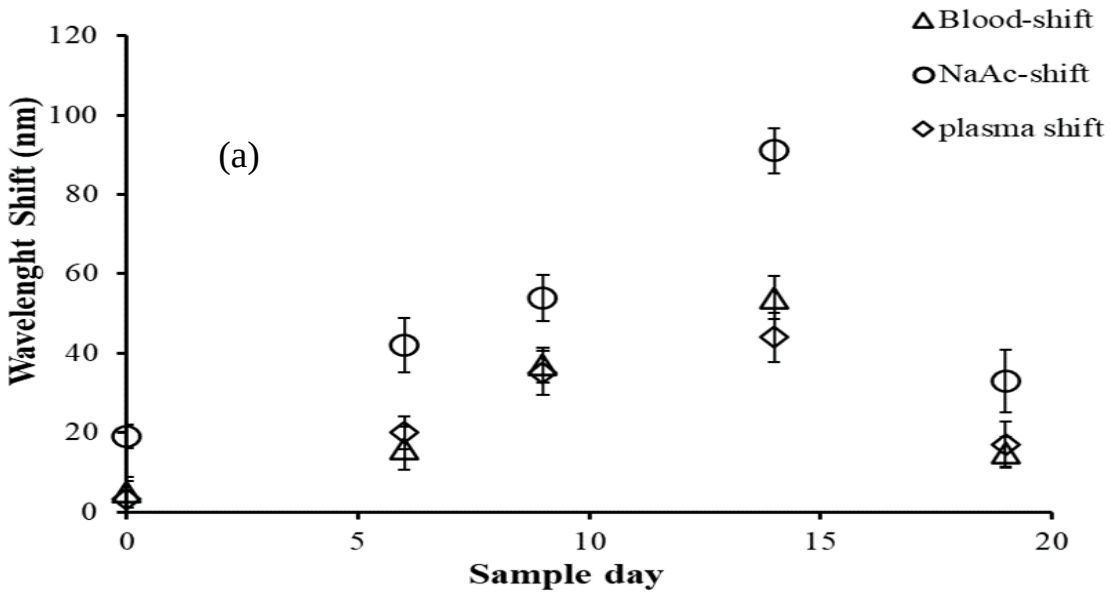

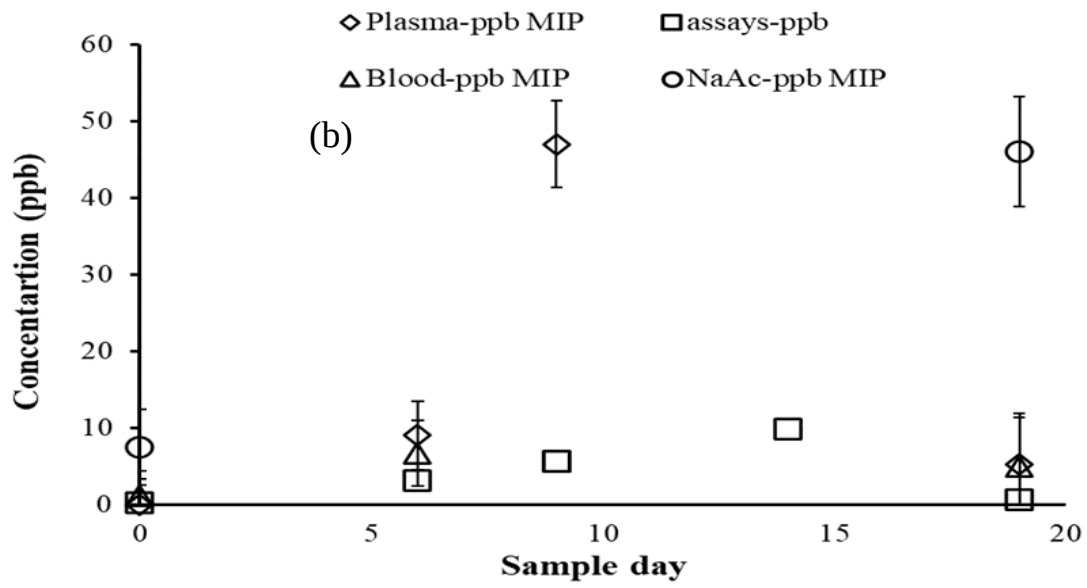

Figure 5. 2. Progesterone levels in blood for animal 2 during the estrous cycle (a) sensor wavelength shift , (b) PG concentration

.

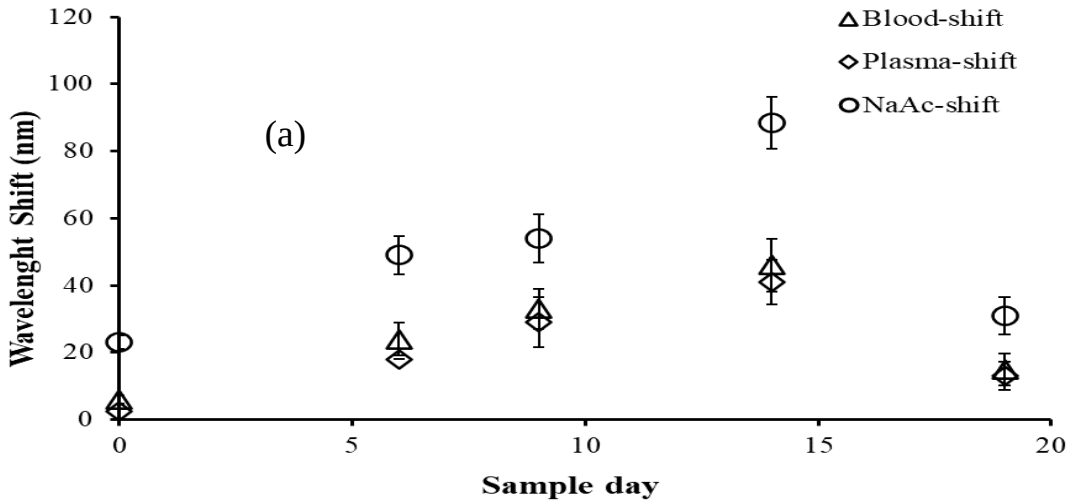

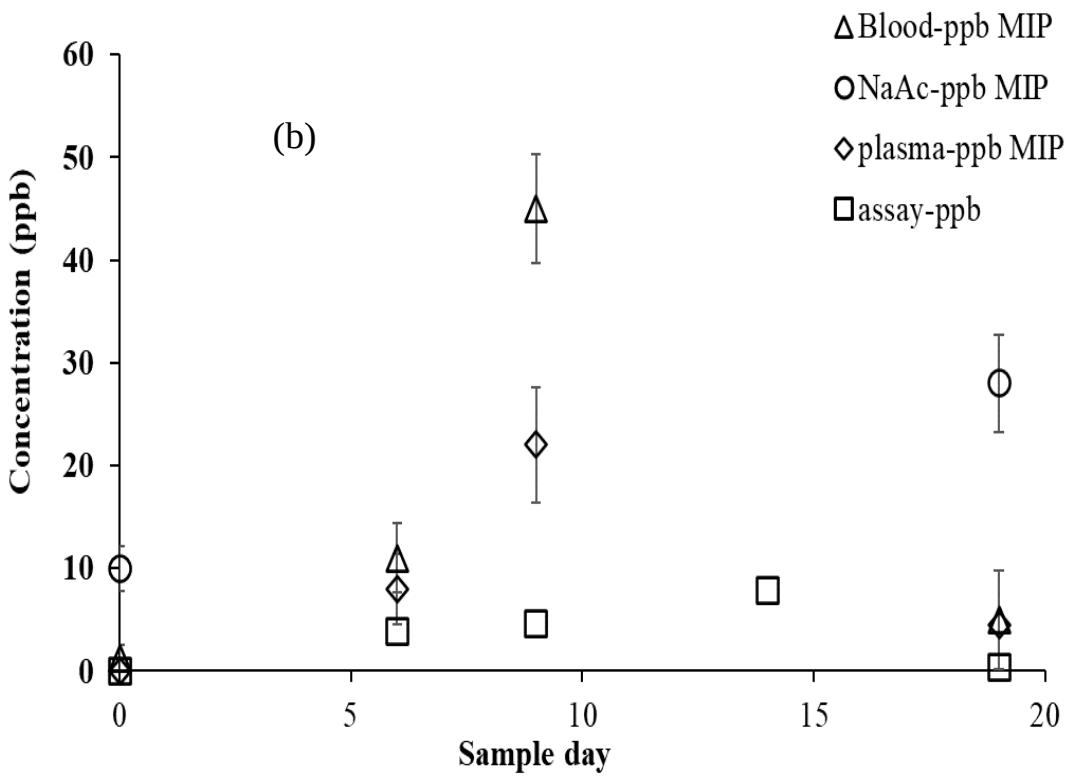

Figure 5. 3. Progesterone levels in blood for animal 3 during the estrous cycle (a) sensor wavelength shift , (b) PG concentration.

5.4 Conclusion

In this work, a technique based on photonic crystal and molecularly imprinted polymer was employed for the analysis of free and total progesterone in plasma and blood samples. The interference effect with other hormones on the MIPs binding affinity was analyzed via the results, when compared to the RIA concentration. The results revealed that the hormones that have a similar structure and functional group affected progesterone detection even with a lower concentration, however, the MIPs sensors had the ability on diagnosis the pregnancy profile of different animals, via evaluating the progesterone concentration levels during the estrous cycle. Overall, if these limitations are overcome, the sensors can be considered a very applicable screening tool to be used in the field.

Chapter 6. Conclusions and Future Study

In first work, a mixing of particles of different sizes and chemical compositions have significantly led to a variation in pore size, surface area, and pore volume. Th pore size of different deposition didn't change with pH values; oppositely, the particle size effect was apparent in various mixing ratios. On account of adding some features to final ceramics a loss in porosity was apparent in mixing particle depositions. The DLVO theory correctly predicted the interactions between the particles at different pH values.

In another study we highlighted the influence of the optimization factors of molecularly imprinted polymer fabrication. The colloidal crystal fabrication showed good results at all temperatures investigated. Lower surface interaction was yield using polyethylene container type. On the other hand, shorter polymerization reaction time allowed the control of the formation of the radical by the initiator, furthermore, reduced the damage in the fabricated MIPs. The wavelength shift values have revealed that time 36 hrs is the optimum time to perform a full detach of silica NPs from the fabricated films. The solvent composition with washing ratio (1:9), had higher removal of the analyte from the binding sites, without causing any damage to the film. The progesterone molecules extraction from the nanocavities and consequent shrinking of the hydrogel film had reached the maximum limit at 3 hrs washing time, represented by a higher shift toward shorter wavelength. Overall, the optimal conditions helped to avoid all unfavorable conditions that would produce damaged or faulty MIPs, and therefore reduce a large number of syntheses.

MIPs were investigated by equilibrium binding, swelling ratio, kinetics experiments, and UV- visible spectra to investigate Bragg diffraction peak shift that occurs with the

rebinding at different progesterone concentrations in deionized water and 150 mM NaCl solutions. The sensors demonstrated high response after exposures to concentrations down to 1 μg L^{-1} and 12 min equilibrium time, with LOD 0.5 μgL^{-1}. Significant improvement in the response was observed by the incubation in standard aqueous solutions with a background 150 mM NaCl. Moreover, the developed sensor was applied to detect progesterone in the presence of complex matrices, in both natural and tap water samples, with errors between 1-27%, which suggest the use of the sensor to quantify PG at low concentrations or as a screening tool for the presence of PG in natural water. Furthermore, higher affinity for PG in the presence of other steroid hormones (structural analogues),was illustrated and proved via the computed surface electrostatic potentials and the ability to form bonds with the polymer functional groups. This work has shown the potential for photonic MIPs in environmental applications. The use of the sensor is straightforward and fast, while it is capable to differentiate hormones with similar structures to PG.

Finally, MIPs were employed to investigate in the analysis of progesterone hormone, both free and total compounds. The interference effect with other hormones on the MIPs binding affinity was analyzed via the results, when compared to the RIA concentration. The results revealed that the progesterone detection can be affected by the hormones that have a similar structure and functional group even with a lower concentration, however, the MIPs sensors had the ability on diagnosis the pregnancy profile of different animals, via evaluating the progesterone concentration levels during the estrous cycle. Overall, if these limitations are overcome, the sensors can be considered a very applicable screening tool to be used in the field. More intensive and expanded research is requisite for the detection of progesterone sensors in whole blood solutions either in human or animals. Besides, a comprehensive

study for the natural, synthetic, and environmental chemicals for binding by progesterone sensor taking in consideration different anticipated interferences.

References

A, Alagarasi,. (2011). Chapter—INTRODUCTION TO NANOMATERIALS. (n.d.).

Ab, M., Af, H., Sc, R., G, G., Dt, T., G, D., G, A., B, G., & Cr, H. (2017). Serum, milk, saliva and urine progesterone and estradiol profiles in crossbred (Zebu x Holstein Friesian) dairy cattle. *Animal Husbandry, Dairy and Veterinary Science*, *1*(3). https://doi.org/10.15761/AHDVS.1000118

Abdin, M. J., Altintas, Z., & Tothill, I. E. (2015). In silico designed nanoMIP based optical sensor for endotoxins monitoring. *Biosensors and Bioelectronics*, *67*, 177–183. https://doi.org/10.1016/j.bios.2014.08.009

Ali, A., Zafar, H., Zia, M., Ul Haq, I., Phull, A. R., Ali, J. S., & Hussain, A. (2016). Synthesis, characterization, applications, and challenges of iron oxide nanoparticles. *Nanotechnology, Science and Applications*, *9*, 49–67. https://doi.org/10.2147/NSA.S99986

Alvarez-Lorenzo, C. (2013). *Handbook of Molecularly Imprinted Polymers*. Smithers Rapra.

Amin, M. T., Alazba, A. A., & Manzoor, U. (2014). A Review of Removal of Pollutants from Water/Wastewater Using Different Types of Nanomaterials. *Advances in Materials Science and Engineering*, *2014*, 1–24. https://doi.org/10.1155/2014/825910

An, L., Pang, Z., & Guo, Y. (2015). Synthesis of magnetic molecular imprinted silica spheres for recognition of ciprofloxacin by metal-coordinate interaction. *Journal of Sol-Gel Science and Technology*, *76*(1), 36–42. https://doi.org/10.1007/s10971-015-3747-8

Annamma, K., & Mathew, B. (2011). Design of 2, 4-Dichlorophenoxyacetic Acid Imprinted Polymer with High Specificity and Selectivity. *Materials Sciences and Applications*, *2*. https://doi.org/10.4236/msa.2011.23017

Arabi, M., Ostovan, A., Bagheri, A. R., Guo, X., Li, J., Ma, J., & Chen, L. (2020). Hydrophilic molecularly imprinted nanospheres for the extraction of rhodamine B followed by HPLC analysis: A green approach and hazardous waste elimination. *Talanta*, *215*, 120933. https://doi.org/10.1016/j.talanta.2020.120933

Arabi, M., Ostovan, A., Bagheri, A. R., Guo, X., Wang, L., Li, J., Wang, X., Li, B., & Chen, L. (2020). Strategies of molecular imprinting-based solid-phase extraction prior to chromatographic analysis. *TrAC Trends in Analytical Chemistry*, *128*, 115923. https://doi.org/10.1016/j.trac.2020.115923

Arancibia-Miranda, N., Baltazar, S. E., García, A., Muñoz-Lira, D., Sepúlveda, P., Rubio, M. A., & Altbir, D. (2016). Nanoscale zero valent supported by Zeolite and Montmorillonite: Template effect of the removal of lead ion from an aqueous solution. *Journal of Hazardous Materials*, *301*, 371–380. https://doi.org/10.1016/j.jhazmat.2015.09.007

Azofra, L. M., Alkorta, I., & Elguero, J. (2013). Theoretical study of the mutarotation of erythrose and threose: Acid catalysis. *Carbohydrate Research*, *372*, 1–8. https://doi.org/10.1016/j.carres.2013.01.013

BATRA, S., BENGTSSON, L. P., GRUNDSELL, H., & SJöBERG, N.-O. (1976). Levels of Free and Protein-Bound Progesterone in Plasma During Late Pregnancy. *The Journal of Clinical Endocrinology & Metabolism*, *42*(6), 1041–1047. https://doi.org/10.1210/jcem-42-6-1041

Bell, G. M., Levine, S., & McCartney, L. N. (1970). Approximate methods of determining the double-layer free energy of interaction between two charged colloidal spheres. *Journal of Colloid and Interface Science*, *33*(3), 335–359. https://doi.org/10.1016/0021-9797(70)90228-6

Berg, J. C. (2010). *An Introduction to Interfaces & Colloids: The Bridge to Nanoscience*. World Scientific.

Bernstein, R., Kaufman, Y., & Freger, V. (2013). Membrane Characterization. In *Encyclopedia of Membrane Science and Technology* (pp. 1–41). American Cancer Society. https://doi.org/10.1002/9781118522318.emst063

Blavy, P., Derks, M., Martin, O., Höglund, J. K., & Friggens, N. C. (2016). Overview of progesterone profiles in dairy cows. *Theriogenology*, *86*(4), 1061–1071. https://doi.org/10.1016/j.theriogenology.2016.03.037

Bolaji, I. i. (1994). Sero-salivary progesterone correlation. *International Journal of Gynecology & Obstetrics*, *45*(2), 125–131. https://doi.org/10.1016/0020-7292(94)90119-8

Boufas, W., Dupont, N., Berredjem, M., Berrezag, K., Becheker, I., Berredjem, H., & Aouf, N.-E. (2014). Synthesis and antibacterial activity of sulfonamides. SAR and DFT studies. *Journal of Molecular Structure*, *1074*, 180–185. https://doi.org/10.1016/j.molstruc.2014.05.066

Busch, K., & John, S. (1999). Liquid-Crystal Photonic-Band-Gap Materials: The Tunable Electromagnetic Vacuum. *Physical Review Letters*, *83*(5), 967–970. https://doi.org/10.1103/PhysRevLett.83.967

Butt, H.-J., & Kappl, M. (2018). *Surface and Interfacial Forces*. John Wiley & Sons.

Cáceres, C., Bravo, C., Rivas, B., Moczko, E., Sáez, P., García, Y., & Pereira, E. (2018). Molecularly Imprinted Polymers for the Selective Extraction of Bisphenol A and Progesterone from Aqueous Media. *Polymers*, *10*(6). https://doi.org/10.3390/polym10060679

Cacho, C., Turiel, E., Martin-Esteban, A., Pérez-Conde, C., & Cámara, C. (2004). Characterisation and quality assessment of binding sites on a propazine-imprinted polymer prepared by precipitation polymerisation. *Journal of Chromatography B*, *802*(2), 347–353. https://doi.org/10.1016/j.jchromb.2003.12.018

Cargnello, M. (2019). Colloidal Nanocrystals as Building Blocks for Well-Defined Heterogeneous Catalysts. *Chemistry of Materials*, *31*(3), 576–596. https://doi.org/10.1021/acs.chemmater.8b04533

Casis, N., Busatto, C. A., Fidalgo, M. M., Ravaine, S., & Estenoz, D. A. (2014). *Molecularly imprinted hydrogels from colloidal crystals for the detection of progesterone*. https://doi.org/10.1002/pi.4851/abstract

Chang, H., Wan, Y., Wu, S., Fan, Z., & Hu, J. (2011). Occurrence of androgens and progestogens in wastewater treatment plants and receiving river waters: Comparison to estrogens. *Water Research*, *45*(2), 732–740. https://doi.org/10.1016/j.watres.2010.08.046

Chen, S., Sun, H., Huang, Z., Jin, Z., Fang, S., He, J., Liu, Y., Zhang, Y., & Lai, J. (2019). The visual detection of anesthetics in fish based on an inverse opal photonic crystal sensor. *RSC Advances*, *9*(29), 16831–16838. https://doi.org/10.1039/C9RA01600G

Chen, W., Meng, Z., Xue, M., & Shea, K. (2016). Molecular imprinted photonic crystal for sensing of biomolecules. *Molecular Imprinting*, *4*, 1–12. https://doi.org/10.1515/molim-2016-0001

Cherian, A., Benny, L., George, A., Sirimahachai, U., Varghese, A., & Hegde, G. (2022). Electro fabrication of molecularly imprinted sensor based on Pd nanoparticles decorated poly-(3 thiophene acetic acid) for progesterone detection. *Electrochimica Acta*, *408*, 139963. https://doi.org/10.1016/j.electacta.2022.139963

Corsi, I., Winther-Nielsen, M., Sethi, R., Punta, C., Della Torre, C., Libralato, G., Lofrano, G., Sabatini, L., Aiello, M., Fiordi, L., Cinuzzi, F., Caneschi, A., Pellegrini, D., & Buttino, I. (2018). Ecofriendly nanotechnologies and nanomaterials for environmental applications: Key issue and consensus recommendations for sustainable and ecosafe nanoremediation. *Ecotoxicology and Environmental Safety*, *154*, 237–244. https://doi.org/10.1016/j.ecoenv.2018.02.037

Dai, J. (2017). *Molecularly imprinted polymers and their application as environmental sensors* [Thesis, University of Missouri--Columbia]. https://mospace.umsystem.edu/xmlui/handle/10355/66722

Dai, J., & Fidalgo de Cortalezzi, M. (2019). Influence of pH, ionic strength and natural organic matter concentration on a MIP-Fluorescent sensor for the quantification of DNT in water. *Heliyon*, *5*(6), e01922. https://doi.org/10.1016/j.heliyon.2019.e01922

Deng, R., Yue, J., Qu, H., Liang, L., Sun, D., Zhang, J., Liang, C., Xu, W., & Xu, S. (2018). Glucose-bridged silver nanoparticle assemblies for highly sensitive molecular recognition of sialic acid on cancer cells via surface-enhanced raman scattering spectroscopy. *Talanta, 179*, 200–206. https://doi.org/10.1016/j.talanta.2017.11.006

Díaz-Cruz, M. S., López de Alda, M. J., López, R., & Barceló, D. (2003). Determination of estrogens and progestogens by mass spectrometric techniques (GC/MS, LC/MS and LC/MS/MS). *Journal of Mass Spectrometry, 38*(9), 917–923. https://doi.org/10.1002/jms.529

Dimitrov, A. S., & Nagayama, K. (1996). Continuous Convective Assembling of Fine Particles into Two-Dimensional Arrays on Solid Surfaces. *Langmuir, 12*(5), 1303–1311. https://doi.org/10.1021/la9502251

Division of Laboratory Sciences | CDC. (2021, December 20). https://www.cdc.gov/nceh/dls/index.html

Duan, H., Li, L., Wang, X., Wang, Y., Li, J., & Luo, C. (2016). CdTe quantum dots@luminol as signal amplification system for chrysoidine with chemiluminescence-chitosan/graphene oxide-magnetite-molecularly imprinting sensor. *Spectrochimica Acta Part A: Molecular and Biomolecular Spectroscopy, 153*, 535–541. https://doi.org/10.1016/j.saa.2015.09.016

Elimelech, M., Jia, X., Gregory, J., & Williams, R. (1998). *Particle Deposition and Aggregation: Measurement, Modelling and Simulation*. Elsevier.

Esawi, A. M. K., Morsi, K., Sayed, A., Taher, M., & Lanka, S. (2010). Effect of carbon nanotube (CNT) content on the mechanical properties of CNT-reinforced

aluminium composites. *Composites Science and Technology*, *70*(16), 2237–2241. https://doi.org/10.1016/j.compscitech.2010.05.004

Fan, J., Qiu, L., Qiao, Y., Xue, M., Dong, X., & Meng, Z. (2021). Recent Advances in Sensing Applications of Molecularly Imprinted Photonic Crystals. *Frontiers in Chemistry*, *9*, 665119. https://doi.org/10.3389/fchem.2021.665119

Fent, K. (2015). Progestins as endocrine disrupters in aquatic ecosystems: Concentrations, effects and risk assessment. *Environment International*, *84*, 115–130. https://doi.org/10.1016/j.envint.2015.06.012

Fernandes, R. M. T., Gomes, G. C., Porcari, A. M., Pimentel, J. R. V., Porciúncula, P. M., Martins-Júnior, H. A., Miguez, P. H. P., da Costa, J. L., Amaral, P. H., Perecin, F., Meurer, E. C., Furtado, P. V., Simas, R. C., Eberlin, M. N., Ferreira, C. R., & Madureira, E. H. (2011). LC-MS/MS quantitation of plasma progesterone in cattle. *Theriogenology*, *76*(7), 1266-1274.e2. https://doi.org/10.1016/j.theriogenology.2011.05.033

Fu, F., Dionysiou, D. D., & Liu, H. (2014). The use of zero-valent iron for groundwater remediation and wastewater treatment: A review. *Journal of Hazardous Materials*, *267*, 194–205. https://doi.org/10.1016/j.jhazmat.2013.12.062

Garciagarcia, S., Wold, S., & Jonsson, M. (2009). Effects of temperature on the stability of colloidal montmorillonite particles at different pH and ionic strength. *Applied Clay Science*, *43*(1), 21–26. https://doi.org/10.1016/j.clay.2008.07.011

Gholami, H., Ghaedi, M., Ostovan, A., Arabi, M., & Bagheri, A. R. (2019). Preparation of hollow porous molecularly imprinted and aluminum(III) doped silica nanospheres for extraction of the drugs valsartan and losartan prior to their

quantitation by HPLC. *Mikrochimica Acta, 186*(11), 702. https://doi.org/10.1007/s00604-019-3794-x

Gillis, E. H., Traynor, I., Gosling, J. P., & Kane, M. (2006). Improvements to a surface plasmon resonance-based immunoassay for the steroid hormone progesterone. *Journal of AOAC International*, *89*(3), 838–842.

Golovko, O., Šauer, P., Fedorova, G., Kroupová, H. K., & Grabic, R. (2018). Determination of progestogens in surface and waste water using SPE extraction and LC-APCI/APPI-HRPS. *Science of The Total Environment*, *621*, 1066–1073. https://doi.org/10.1016/j.scitotenv.2017.10.120

Gregory, J. (1975). Interaction of unequal double layers at constant charge. *Journal of Colloid and Interface Science*, *51*(1), 44–51. https://doi.org/10.1016/0021-9797(75)90081-8

Gregory, J. (1981). Approximate expressions for retarded van der waals interaction. *Journal of Colloid and Interface Science*, *83*(1), 138–145. https://doi.org/10.1016/0021-9797(81)90018-7

Griffete, N., Frederich, H., Maître, A., Ravaine, S., Chehimi, M. M., & Mangeney, C. (2012). Inverse Opals of Molecularly Imprinted Hydrogels for the Detection of Bisphenol A and pH Sensing. *Langmuir*, *28*(1), 1005–1012. https://doi.org/10.1021/la202840y

Guzmán-Verri, G. G., & Voon, L. C. L. Y. (2007). Electronic structure of silicon-based nanostructures. *Physical Review B*, *76*(7), 075131. https://doi.org/10.1103/PhysRevB.76.075131

Hammond, G. L. (2016). Plasma steroid-binding proteins: Primary gatekeepers of steroid hormone action. *The Journal of Endocrinology*, *230*(1), R13-25. https://doi.org/10.1530/JOE-16-0070

Han, S., Jin, Y., Su, L., Chu, H., & Zhang, W. (2020). A two-dimensional molecularly imprinted photonic crystal sensor for highly efficient tetracycline detection. *Analytical Methods*, *12*(10), 1374–1379. https://doi.org/10.1039/D0AY00110D

He, Y. T., Wan, J., & Tokunaga, T. (2008). Kinetic stability of hematite nanoparticles: The effect of particle sizes. *Journal of Nanoparticle Research*, *10*(2), 321–332. https://doi.org/10.1007/s11051-007-9255-1

He, Z., Lyu, Z., Gu, Q., Zhang, L., & Wang, J. (2019). Ceramic-based membranes for water and wastewater treatment. *Colloids and Surfaces A: Physicochemical and Engineering Aspects*, *578*, 123513. https://doi.org/10.1016/j.colsurfa.2019.05.074

Ho, N. F. H., & Higuchi, W. I. (1968). Preferential Aggregation and Coalescence in Heterodispersed Systems. *Journal of Pharmaceutical Sciences*, *57*(3), 436–442. https://doi.org/10.1002/jps.2600570314

Hogg, R., Healy, T. W., & Fuerstenau, D. W. (1966). Mutual coagulation of colloidal dispersions. *Transactions of the Faraday Society*, *62*, 1638. https://doi.org/10.1039/tf9666201638

Huang, J., Hu, X., Zhang, W., Zhang, Y., & Li, G. (2008). PH and ionic strength responsive photonic polymers fabricated by using colloidal crystal templating. *Colloid and Polymer Science*, *286*(1), 113–118. https://doi.org/10.1007/s00396-007-1775-9

Huang, X., Yuan, D., & Huang, B. (2008). Determination of steroid sex hormones in urine matrix by stir bar sorptive extraction based on monolithic material and liquid chromatography with diode array detection. *Talanta*, *75*(1), 172–177. https://doi.org/10.1016/j.talanta.2007.10.052

Iskandar, F. (2009). Nanoparticle processing for optical applications – A review. *Advanced Powder Technology*, *20*(4), 283–292. https://doi.org/10.1016/j.apt.2009.07.001

Israelachvili, J. N. (2011). *Intermolecular and surface forces. [Electronic resource]: With applications to colloidal and biological systems.* (MU Online; 3rd. ed.). Academic Press; MERLIN. http://proxy.mul.missouri.edu/login?url=http://search.ebscohost.com/login.aspx?direct=true&AuthType=ip,cookie,url,uid&db=cat04885a&AN=merlin.b8333744&site=eds-live&scope=site

Janssens, G., Mangelinckx, S., Courtheyn, D., De Kimpe, N., Matthijs, B., & Le Bizec, B. (2016). The use of gas chromatography–mass spectrometry/combustion/isotope ratio mass spectrometry to demonstrate progesterone treatment in bovines. *Journal of Chromatography A*, *1449*, 129–140. https://doi.org/10.1016/j.chroma.2016.04.074

Jiang, P., Bertone, J. F., Hwang, K. S., & Colvin, V. L. (n.d.-a). *Single-Crystal Colloidal Multilayers of Controlled Thickness*. 9.

Jiang, P., Bertone, J. F., Hwang, K. S., & Colvin, V. L. (n.d.-b). *Single-Crystal Colloidal Multilayers of Controlled Thickness*. 9.

Jiang, P., Bertone, J. F., Hwang, K. S., & Colvin, V. L. (1999). Single-Crystal Colloidal Multilayers of Controlled Thickness. *Chemistry of Materials*, *11*(8), 2132–2140. https://doi.org/10.1021/cm990080+

Jiang, S., Peng, Y., Ning, B., Bai, J., Liu, Y., Zhang, N., & Gao, Z. (2015). Surface plasmon resonance sensor based on molecularly imprinted polymer film for detection of histamine. *Sensors and Actuators B: Chemical*, *221*, 15–21. https://doi.org/10.1016/j.snb.2015.06.058

Kadhem, A. J., Gentile, G. J., & Fidalgo de Cortalezzi, M. M. (2021). Molecularly Imprinted Polymers (MIPs) in Sensors for Environmental and Biomedical Applications: A Review. *Molecules (Basel, Switzerland)*, *26*(20), 6233. PubMed. https://doi.org/10.3390/molecules26206233

Kadhem, A. J., Xiang, S., Nagel, S., Lin, C.-H., & Fidalgo de Cortalezzi, M. (2018). Photonic Molecularly Imprinted Polymer Film for the Detection of Testosterone in Aqueous Samples. *Polymers*, *10*(4), 349. https://doi.org/10.3390/polym10040349

Kalecki, J., Cieplak, M., Dąbrowski, M., Lisowski, W., Kuhn, A., & Sharma, P. S. (2020). Hexagonally Packed Macroporous Molecularly Imprinted Polymers for Chemosensing of Follicle-Stimulating Hormone Protein. *ACS Sensors*, *5*(1), 118–126. https://doi.org/10.1021/acssensors.9b01878

Kar, G., Chander, S., & Mika, T. S. (1973). The potential energy of interaction between dissimilar electrical double layers. *Journal of Colloid and Interface Science*, *44*(2), 347–355. https://doi.org/10.1016/0021-9797(73)90226-9

Karnik, B. S., Baumann, M. J., Masten, S. J., & Davies, S. H. (2006). AFM and SEM characterization of iron oxide coated ceramic membranes. *Journal of Materials Science*, *41*(20), 6861–6870. https://doi.org/10.1007/s10853-006-0943-5

Kasambala, H. R., Rwiza, M. J., & Mdegela, R. H. (2019). Levels and distribution of progesterone in receiving waters and wastewaters of a growing urban area. *Water Science and Technology*, *80*(6), 1107–1117. https://doi.org/10.2166/wst.2019.350

Kempe, H., & Kempe, M. (2010). Influence of salt ions on binding to molecularly imprinted polymers. *Analytical and Bioanalytical Chemistry*, *396*(4), 1599–1606. https://doi.org/10.1007/s00216-009-3329-0

Kibechu, R. W., Mamo, M. A., Msagati, T. A. M., Sampath, S., & Mamba, B. B. (2014). Synthesis and application of reduced graphene oxide and molecularly imprinted polymers composite in chemo sensor for trichloroacetic acid detection in aqueous solution. *Physics and Chemistry of the Earth, Parts A/B/C*, *76–78*, 49–53. https://doi.org/10.1016/j.pce.2014.09.008

Koelsch, R. K., Aneshansley, D. J., & Butler, W. R. (1994). Milk Progesterone Sensor for Application with Dairy Cattle. *Journal of Agricultural Engineering Research*, *58*(2), 115–120. https://doi.org/10.1006/jaer.1994.1041

Kolar, P., Classen, J., & Hall, S. G. (2019). Physicochemical data of p-cresol, butyric acid, and ammonia. *Data in Brief*, *26*, 104356. https://doi.org/10.1016/j.dib.2019.104356

Krishnakumar, V., & Balachandran, V. (2005). Analysis of vibrational spectra of 5-fluoro, 5-chloro and 5-bromo-cytosines based on density functional theory

calculations. *Spectrochimica Acta Part A: Molecular and Biomolecular Spectroscopy*, *61*(5), 1001–1006. https://doi.org/10.1016/j.saa.2004.05.044

Kumar, V., Johnson, A. C., Trubiroha, A., Tumová, J., Ihara, M., Grabic, R., Kloas, W., Tanaka, H., & Kroupová, H. K. (2015). The Challenge Presented by Progestins in Ecotoxicological Research: A Critical Review. *Environmental Science & Technology*, *49*(5), 2625–2638. https://doi.org/10.1021/es5051343

Kundu, S., Wang, Y., Xia, W., & Muhler, M. (2008). Thermal Stability and Reducibility of Oxygen-Containing Functional Groups on Multiwalled Carbon Nanotube Surfaces: A Quantitative High-Resolution XPS and TPD/TPR Study. *The Journal of Physical Chemistry C*, *112*(43), 16869–16878. https://doi.org/10.1021/jp804413a

Lasheen, M. E., Badr, H. M., Kandiel, M. M. M., Abo El-Maaty, A. M., Samir, H., Farouk, M., & Eldawy, M. H. (2018). Predicting early pregnancy in Egyptian buffalo cows via measuring uterine and luteal blood flows, and serum and saliva progesterone. *Tropical Animal Health and Production*, *50*(1), 137–142. https://doi.org/10.1007/s11250-017-1413-6

Lee, R., Stack, K., Richardson, D., Lewis, T., & Garnier, G. (2012). Multi-salt coagulation of soft pitch colloids. *Colloids and Surfaces A: Physicochemical and Engineering Aspects*, *409*, 74–80. https://doi.org/10.1016/j.colsurfa.2012.06.005

Lee, W.-C., Cheng, C.-H., Pan, H.-H., Chung, T.-H., & Hwang, C.-C. (2008). Chromatographic characterization of molecularly imprinted polymers. *Analytical and Bioanalytical Chemistry*, *390*(4), 1101–1109. https://doi.org/10.1007/s00216-007-1765-2

Li, C., Sun, W., Lu, Z., Ao, X., & Li, S. (2020). Ceramic nanocomposite membranes and membrane fouling: A review. *Water Research*, *175*, 115674. https://doi.org/10.1016/j.watres.2020.115674

Lin, H., Wu, D., Liu, L., & Jia, D. (2008). Theoretical study on molecular structures, intramolecular proton transfer reaction, and solvent effects of 1-phenyl-3-methyl-4-(6-hydro-4-amino-5-sulfo-2,3-pyrazine)-pyrazole-5-one. *Journal of Molecular Structure: THEOCHEM*, *850*(1), 32–37. https://doi.org/10.1016/j.theochem.2007.10.011

Lin, Z., Li, L., Fu, G., Lai, Z., Peng, A., & Huang, Z. (2020). Molecularly imprinted polymer-based photonic crystal sensor array for the discrimination of sulfonamides. *Analytica Chimica Acta*, *1101*, 32–40. https://doi.org/10.1016/j.aca.2019.12.032

Liu, Y., Bao, J., Zhang, L., Chao, C., Guo, J., Cheng, Y., Zhu, Y., & Xu, G. (2018). Ultrasensitive SERS detection of propranolol based on sandwich nanostructure of molecular imprinting polymers. *Sensors and Actuators B: Chemical*, *255*, 110–116. https://doi.org/10.1016/j.snb.2017.08.018

Lonergan, P., & Sánchez, J. M. (2020). Symposium review: Progesterone effects on early embryo development in cattle. *Journal of Dairy Science*, *103*(9), 8698–8707. https://doi.org/10.3168/jds.2020-18583

Lu, H., Wang, J., Stoller, M., Wang, T., Bao, Y., & Hao, H. (2016). An Overview of Nanomaterials for Water and Wastewater Treatment. *Advances in Materials Science and Engineering*, *2016*, 1–10. https://doi.org/10.1155/2016/4964828

Luo, S., Thomas, J., Guo, H., Liao, W., Lee, M., & Lin, H. (2017). Electrosynthesis of Nanostructured, Imprinted Poly(hydroxymethyl 3,4-ethylenedioxythiophene) for the Ultrasensitive Electrochemical Detection of Urinary Progesterone. *ChemistrySelect*, *2*, 7935–7939. https://doi.org/10.1002/slct.201701469

Mohamed, M. A., Jaafar, J., Ismail, A. F., Othman, M. H. D., & Rahman, M. A. (2017). Chapter 1—Fourier Transform Infrared (FTIR) Spectroscopy. In N. Hilal, A. F. Ismail, T. Matsuura, & D. Oatley-Radcliffe (Eds.), *Membrane Characterization* (pp. 3–29). Elsevier. https://doi.org/10.1016/B978-0-444-63776-5.00001-2

Mukherjee, B., & Weaver, J. W. (2010). Aggregation and Charge Behavior of Metallic and Nonmetallic Nanoparticles in the Presence of Competing Similarly-Charged Inorganic Ions. *Environmental Science & Technology*, *44*(9), 3332–3338. https://doi.org/10.1021/es903456e

Muldarisnur, M., & Marlow, F. (2010). Opal Films Made by the Capillary Deposition Method: Crystal Orientation and Defects. *The Journal of Physical Chemistry C*, *115*. https://doi.org/10.1021/jp108975p

Nagarajan, R., & Hatton, T. A. (Eds.). (2008). *Nanoparticles: Synthesis, Stabilization, Passivation, and Functionalization* (Vol. 996). American Chemical Society. https://doi.org/10.1021/bk-2008-0996

Naik, B., A.V.N, S. K., & Bramhaiah, K. (2013). *ESTROGEN AND PROGESTERONE HORMONE LEVELS IN PUNGANUR CATTLE*. https://doi.org/10.9790/2380-0255053

Nawaz, T., Ahmad, M., Yu, J., Wang, S., & Wei, T. (2020). The biomimetic detection of progesterone by novel bifunctional group monomer based molecularly imprinted

polymers prepared in UV light. *New Journal of Chemistry*, *44*(17), 6992–7000. https://doi.org/10.1039/C9NJ06387K

Nezhadali, A., Es'haghi, Z., & Khatibi, A. (2016). Selective extraction of progesterone hormones from environmental and biological samples using a polypyrrole molecularly imprinted polymer and determination by gas chromatography. *Analytical Methods*, *8*(8), 1813–1827. https://doi.org/10.1039/C5AY02174J

Overbeek, J. T. G., & Jonker, G. H. (1952). *Colloid Science Edited by HR Kruyt: Contributors-GH Jonker, J. Th. G. Overbeek*. Elsevier.

Posthuma-Trumpie, G. A., van Amerongen, A., Korf, J., & van Berkel, W. J. H. (2009). Perspectives for on-site monitoring of progesterone. *Trends in Biotechnology*, *27*(11), 652–660. https://doi.org/10.1016/j.tibtech.2009.07.008

Prádanos, P., Rodriguez, M. L., Calvo, J. I., Hernández, A., Tejerina, F., & de Saja, J. A. (1996). Structural characterization of an UF membrane by gas adsorption-desorption and AFM measurements. *Journal of Membrane Science*, *117*(1), 291–302. https://doi.org/10.1016/0376-7388(96)00081-6

Ričanyová, J., Gadzała-Kopciuch, R., Reiffova, K., Bazel, Y., & Buszewski, B. (2010). Molecularly imprinted adsorbents for preconcentration and isolation of progesterone and testosterone by solid phase extraction combined with HPLC. *Adsorption*, *16*(4), 473–483. https://doi.org/10.1007/s10450-010-9265-7

Rodrigues, S. M., Demokritou, P., Dokoozlian, N., Hendren, C. O., Karn, B., Mauter, M. S., Sadik, O. A., Safarpour, M., Unrine, J. M., Viers, J., Welle, P., White, J. C., Wiesner, M. R., & Lowry, G. V. (2017). Nanotechnology for sustainable food

production: Promising opportunities and scientific challenges. *Environmental Science: Nano*, *4*(4), 767–781. https://doi.org/10.1039/C6EN00573J

Roelofs, J. B., Van Eerdenburg, F. J. C. M., Hazeleger, W., Soede, N. M., & Kemp, B. (2006). Relationship between progesterone concentrations in milk and blood and time of ovulation in dairy cattle. *Animal Reproduction Science*, *91*(3), 337–343. https://doi.org/10.1016/j.anireprosci.2005.04.015

Sajanlal, P. R., Sreeprasad, T. S., Samal, A. K., & Pradeep, T. (2011). Anisotropic nanomaterials: Structure, growth, assembly, and functions. *Nano Reviews*, *2*. https://doi.org/10.3402/nano.v2i0.5883

Samsonova, J. V., Safronova, V. A., & Osipov, A. P. (2018). Rapid flow-through enzyme immunoassay of progesterone in whole cows' milk. *Analytical Biochemistry*, *545*, 43–48. https://doi.org/10.1016/j.ab.2018.01.011

Schenkel, J. H., & Kitchener, J. A. (1960). A test of the Derjaguin-Verwey-Overbeek theory with a colloidal suspension. *Transactions of the Faraday Society*, *56*(0), 161–173. https://doi.org/10.1039/TF9605600161

Senger, P. L. (1997). Pathways to Pregnancy and Parturition. *Undefined*. https://www.semanticscholar.org/paper/Pathways-to-Pregnancy-and-Parturition-Senger/0b5a4430e5965f97a12702e48c6539721ed20b2f

Shenhar, R., Norsten, T. B., & Rotello, V. M. (2005). Polymer-Mediated Nanoparticle Assembly: Structural Control and Applications. *Advanced Materials*, *17*(6), 657–669. https://doi.org/10.1002/adma.200401291

Siegel, R. W., Hu, E., Cox, D. M., Goronkin, H., Jelinski, L., Koch, C. C., Mendel, J., Roco, M. C., & Shaw, D. T. (1999). *Nanostructure Science and Technology:*

R&D Status and Trends in Nanoparticles, Nanostructured Materials, and Nanodevices. Springer Netherlands. https://doi.org/10.1007/978-94-015-9185-0

Singh, D., Bhat, R., Dervash, M., Qadri, H., Mehmood, M., Hamid Dar, G., Hameed, M., & Rashid, N. (2020). *Wonders of Nanotechnology for Remediation of Polluted Aquatic Environs* (pp. 319–339). https://doi.org/10.1007/978-981-13-8277-2_17

Singh, S., Kumar, V., Romero, R., Sharma, K., & Singh, J. (2019). *Applications of Nanoparticles in Wastewater Treatment* (pp. 395–418). https://doi.org/10.1007/978-3-030-17061-5_17

Sole, R. D., Luca, A. D., Catalano, M., Mele, G., & Vasapollo, G. (2007). Noncovalent imprinted microspheres: Preparation, evaluation and selectivity of DBU template. *Journal of Applied Polymer Science*, *105*(4), 2190–2197. https://doi.org/10.1002/app.26208

Stanczyk, F. Z., Lee, J. S., & Santen, R. J. (2007). Standardization of steroid hormone assays: Why, how, and when? *Cancer Epidemiology, Biomarkers & Prevention: A Publication of the American Association for Cancer Research, Cosponsored by the American Society of Preventive Oncology*, *16*(9), 1713–1719. https://doi.org/10.1158/1055-9965.EPI-06-0765

Sudeshna, T., Anand, K., & Medhamurthy, R. (2013). Analysis of 20alpha-hydroxysteroid dehydrogenase expression in the corpus luteum of the buffalo cow: Effect of prostaglandin F2-alpha treatment on circulating 20alpha-hydroxyprogesterone levels. *Reproductive Biology and Endocrinology*, *11*(1), 1–10. https://doi.org/10.1186/1477-7827-11-111

Sun, N., & Walz, J. Y. (2001). A Model for Calculating Electrostatic Interactions between Colloidal Particles of Arbitrary Surface Topology. *Journal of Colloid and Interface Science*, *234*(1), 90–105. https://doi.org/10.1006/jcis.2000.7248

Sun, Z., Song, G., Du, R., & Hu, X. (2017). Modification of a Pd-loaded electrode with a carbon nanotubes–polypyrrole interlayer and its dechlorination performance for 2,3-dichlorophenol. *RSC Advances*, *7*(36), 22054–22062. https://doi.org/10.1039/C7RA02515G

Tamime, R., Wyart, Y., Siozade, L., Baudin, I., Deumie, C., Glucina, K., & Moulin, P. (2011). Membrane Characterization by Microscopic and Scattering Methods: Multiscale Structure. *Membranes*, *1*(2), 91–97. https://doi.org/10.3390/membranes1020091

Tomšíková, H., Aufartová, J., Solich, P., Nováková, L., Sosa-Ferrera, Z., & Santana-Rodríguez, J. J. (2012). High-sensitivity analysis of female-steroid hormones in environmental samples. *TrAC Trends in Analytical Chemistry*, *34*, 35–58. https://doi.org/10.1016/j.trac.2011.11.008

Vasapollo, G., Sole, R. D., Mergola, L., Lazzoi, M. R., Scardino, A., Scorrano, S., & Mele, G. (2011). Molecularly imprinted polymers: Present and future prospective. *International Journal of Molecular Sciences*, *12*(9), 5908–5945. https://doi.org/10.3390/ijms12095908

Velev, O. D., Jede, T. A., Lobo, R. F., & Lenhoff, A. M. (1998). Microstructured Porous Silica Obtained via Colloidal Crystal Templates. *Chemistry of Materials*, *10*(11), 3597–3602. https://doi.org/10.1021/cm980444i

Vesanen, M., Isomaa, V., Bolton, N. J., Alanko, M., & Vihko, R. (1990). Bovine Steroid Hormone and SHBG Concentrations Postpartum and during the Oestrous Cycle. *Acta Veterinaria Scandinavica*, *31*(4), 459–469. https://doi.org/10.1186/BF03547529

Volkery, J., Gottschalk, J., Sobiraj, A., Wittek, T., & Einspanier, A. (2012). Progesterone, pregnanediol-3-glucuronide, relaxin and oestrone sulphate concentrations in saliva, milk and urine of female alpacas (Vicugna pacos) and their application in pregnancy diagnosis. *Veterinary Record*, *171*(8), 195–195. https://doi.org/10.1136/vr.100393

Vukovic, I., Brinke, G. ten, & Loos, K. (2013). Block copolymer template-directed synthesis of well-ordered metallic nanostructures. *Polymer*, *54*(11), 2591–2605. https://doi.org/10.1016/j.polymer.2013.03.013

Wang, L.-Q., Lin, F.-Y., & Yu, L.-P. (2012). A molecularly imprinted photonic polymer sensor with high selectivity for tetracyclines analysis in food. *The Analyst*, *137*(15), 3502. https://doi.org/10.1039/c2an35460h

Wang, Z., Wei, Y.-M., Xu, Z.-L., Cao, Y., Dong, Z.-Q., & Shi, X.-L. (2016). Preparation, characterization and solvent resistance of γ-Al2O3/α-Al2O3 inorganic hollow fiber nanofiltration membrane. *Journal of Membrane Science*, *503*, 69–80. https://doi.org/10.1016/j.memsci.2015.12.039

Waterhouse, G. I. N., & Waterland, M. R. (2007). Opal and inverse opal photonic crystals: Fabrication and characterization. *Polyhedron*, *26*(2), 356–368. https://doi.org/10.1016/j.poly.2006.06.024

Wiese, G. R., & Healy, T. W. (1970). Effect of particle size on colloid stability. *Transactions of the Faraday Society*, *66*, 490. https://doi.org/10.1039/tf9706600490

Wu, Z., Tao, C., Lin, C., Shen, D., & Li, G. (2008). Label-Free Colorimetric Detection of Trace Atrazine in Aqueous Solution by Using Molecularly Imprinted Photonic Polymers. *Chemistry – A European Journal*, *14*(36), 11358–11368. https://doi.org/10.1002/chem.200801250

Xue, J.-Q., Li, D.-W., Qu, L.-L., & Long, Y.-T. (2013). Surface-imprinted core–shell Au nanoparticles for selective detection of bisphenol A based on surface-enhanced Raman scattering. *Analytica Chimica Acta*, *777*, 57–62. https://doi.org/10.1016/j.aca.2013.03.037

Zekić, E., Vuković, Ž., & Halkijevic, I. (2018). Application of nanotechnology in wastewater treatment. *Gradjevinar*, *70*, 315–323. https://doi.org/10.14256/JCE.2165.2017

Zhang, J., & Lu, T. (2021). Efficient evaluation of electrostatic potential with computerized optimized code. *Physical Chemistry Chemical Physics*, *23*(36), 20323–20328. https://doi.org/10.1039/D1CP02805G

Zhang, W. (2014). Nanoparticle Aggregation: Principles and Modeling. In D. G. Capco & Y. Chen (Eds.), *Nanomaterial: Impacts on Cell Biology and Medicine* (pp. 19–43). Springer Netherlands. https://doi.org/10.1007/978-94-017-8739-0_2

Zhang, Y., Fu, M., Wang, J., He, D., & Wang, Y. (2012). Photonic crystal heterostructures fabricated by TiO2 and ZnO inverse opals using colloidal crystal

template with single kind of microspheres. *Optical Materials*, *34*(11), 1758–1761. https://doi.org/10.1016/j.optmat.2012.04.014

Zhou, C., Wang, T., Liu, J., Guo, C., Peng, Y., Bai, J., Liu, M., Dong, J., Gao, N., Ning, B., & Gao, Z. (2012). Molecularly imprinted photonic polymer as an optical sensor to detect chloramphenicol. *The Analyst*, *137*(19), 4469. https://doi.org/10.1039/c2an35617a

Zou, D., Qiu, M., Chen, X., & Fan, Y. (2017). One-step preparation of high-performance bilayer α-alumina ultrafiltration membranes via co-sintering process. *Journal of Membrane Science*, *524*, 141–150. https://doi.org/10.1016/j.memsci.2016.11.025

VITA

Sally M Qasim was born on Nov. 23rd in Baghdad, Iraq. In 2003 she received a degree in Bachelor of Science majoring in Environmental Engineering, from the University of Technology, Baghdad, Iraq. She completed her master's degree in Environmental Engineering in the same university in 2007. Afterward, Sally worked with one of the famous companies in engineering consultant, she was testing, analyzing, evaluating the water and wastewater samples in research lab,researching and collecting data through different techniques and procedures. Her great ambition pushed sally to resume her study and get an admission to the PhD program in the University of Missouri in August 2017 in the Civil and Environmental Engineering Department. During her Ph.D. study, she focused on the detection of contaminants in water. Sally proposed a novel sensor to detect the progesterone hormone in aqueous and whole blood samples by using molecularly imprinted polymer.